Institut für Technische Chemie
Lehrstuhl II

New composite material based on silsesquioxane polymers and nanoporous particles for low-κ dielectric application

Ruo Qing Su

Vollständiger Abdruck der von der Fakultät für Chemie der Technischen Universität München zur Erlangung des akademischen Grades eines

Doktors der Naturwissenschaften (Dr. rer. nat.)

genehmigten Dissertation.

Vorsitzender:		Univ.-Prof. Dr. K. Köhler
Prüfer der Dissertation:	1.	Univ.-Prof. Dr. J.A. Lercher
	2.	Univ.-Prof. Dr. Dr. h. c. St. Vepřek

Die Dissertation wurde am 08.06.2004 bei der Technischen Universität München eingereicht und durch die Fakultät für Chemie am 13.07.2004 angenommen.

to Xiaoning Wu
to my parents

Don't seriously try to make it out of anything else if it has a chance of working with silicon.

Jerry Woodal

Curriculum Vitae

Ruo Qing Su was born on the 11th of July 1971 in Shanghai, China. In 1989 she graduated from high school and started her Bachelor of S.D. in Chemical Engineering at the Shanghai University of Science and Engineering. After moving to Germany she began her Diplom Study in Chemistry at Technische Universität München (TUM) in November 1994. In August 2000 she finished her study with the Diploma project entitled "*Catalyzed intramolecular hydroamination of alkenes and alkynes with late transition metals*" which she had done at the Institute of Technical Chemistry under supervision of Prof. J.A. Lercher.

After graduation as Diplom Chemiker (Univ.) in October 2000 Ruo Qing Su worked as a Ph.D. student in the workgroup of Prof. J.A. Lercher. The work involved the development of new porous material with ultra low dielectric constant for the semiconductor industry. The project was embedded in an interdisciplinary cooperation of five research groups and was supported by Deutsche Forschungsgemeinschaft. The results of her research on the development on new composite material based on silsesquioxane polymers and nanoporous materials for low-κ dielectric application are described in this thesis.

Acknowledgment

This dissertation was carried out in the time from October 2000 until March 2004 at Institut für Technische Chemie, Lehrstuhl II under the supervision of Prof. Johannes A. Lercher. This project was financially supported by Deutsche Forschungsgemeinschaft (DFG) under project No. 395.

First of all, I am very much indebted to Johannes for trusting me with this interesting project to do new work at the interface between chemistry and material science for semiconductor applications and the chance to learn managing. I am grateful for these experiences, which have certainly influenced my own life in a significant way. Also I have to express my gratitude to my assistant-promoter Dr. Thomas E. Müller being always calm, helpful and positive about our research efforts for his credible help and all kinds of discussion we had during my whole Ph.D., also for his help during the correction of this thesis. Dr. P. Härter and Dr. A. Jentys are thanked for scientific discussions and remarks.

In this regard, a special word of gratitude to Dr. G. Zadrozna for the synthesis of her "nanoparticles", which became an important element of this study. I am also thankful for the discussions on the properties and characterisation of nanoporous materials. To my other colleagues (present and past) in the TC II group I thank: Alex H., Christian S., Iker Z., Hiroaki T., Christian W., Peter S., Toshi N., Maria B., Stephan G., Andreas F., Josef F., Philipp H., for the nice office atmosphere and the fellowship at work and during the social events; Jan-Olaf B., Renate S. for the help with experimental and non-experimental problems. I thank Jochen P., Oriol J. and Adam C. for all the moments we shared inside the lab; Hendrik D. and Alexander G. for the help with the IR measurements, also Florencia W. for the TEM measurements. My Chinese colleagues Xuebing Li and Shourong Zheng thank you for the nice discussions in and outside the lab.

I also thank the other people: Frau Schüler und Frau Herrmann for efficiently resolving all kinds of office and financial matters; Andreas M. for his support on computer & software; Martin N. for SEM measurements and AAS analytics and Xaver H. for BET measurements and other experimental support.

And now it is turn to the colleagues in the other institutes at TUM. Dipl.-Ing. R. Emling and Dipl.-Ing. J. Gstöttner from Institute for Technical Electronics, thank you for the cooperation in the CMP experiment and FIB measurement; Dr. M. Hanzlik (Dept. of electron microscopy) for introducing me into TEM measurement; Dr. J. Prochazka (Institute for Chemistry of Inorganic Materials) for discussions and practical help.

Last, but not least Xiaoning, my loving husband, I thank you for all your love and understanding, without you being by my side it would have been very difficult to finish thesis. Also I would like to thank my parents for their deep love und encouragement in all situations of my life.

Table of Contents

Chapter 1

General introduction

In this chapter, the state of the art for materials with low dielectric constant for highly integrated electrical circuits is presented.

1.1 General introduction on low dielectric constant materials for IC applications

Integrated circuits (IC) have achieved progressively higher device densities and speeds over the past 30 years since Moore's Law predicted a doubling in device density every 18 months. In his original paper, [1] Moore observed an exponential growth in the number of transistors per integrated circuit and predicted that this trend will continue. Currently several millions and in the near future billions of transistors are integrated on a microchip. This is accomplished by shrinking the size of transistors, the distance between them, and by increasing the number of layers in a microchip (Figure 1.1). These improvements have considerably reduced the time it takes for electrical signals to travel within integrated circuits as the length of the connecting lines between transistors is reduced. However, as integrated circuit miniaturization continued to be well below the quarter micron level (< 250 nm) in the quest for greater efficiency and higher speed, the resistance and capacitance of the various interconnects on a chip rather than the transistors themselves become the limiting factor causing IC to slow down and preventing them from operating at low voltages. In other words, the stringent performance requirement of Moore's law continues to push the fabrication technology for integrated circuits to reduce not only gate delays but also back-end-of-the-line (BEOL) delays. Improving the BEOL delay requires a change in the materials such that the metal has a maximum conductivity and the insulator has a minimum dielectric constant.

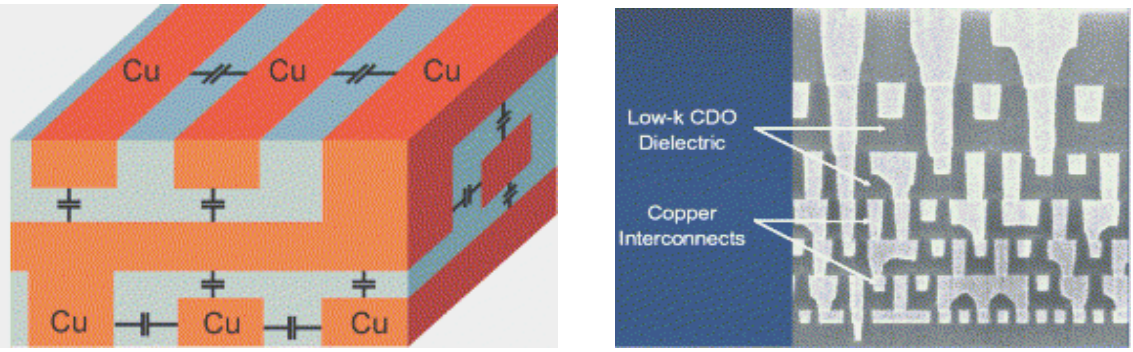

Figure 1.1 Cross section of a typical interconnect for the 90 nm node technology.

As integrated circuits shrink, the room available for the material insulating the wires is reduced. If insulation is inadequate, the current that carries signals on the chip "leaks," causing signal confusion or "cross-talk". This lowers the reliability of the logic, memory, or processing functions, which are executed by the integrated circuit. Figure 1.2 shows a

schematic illustration of typical elements in multilevel interconnects, where *P* represent the line pitch, *W* the width, *S* the line spacing, and *T* the line thickness. The thickness of the dielectric material above and below the interconnect is equal. The time, which is related to the resulting signal delay, is given by $\tau = RC$ and is called the RC–time delay, where R is the line resistance and C the line capacitance of the structure used. A simple first order model can be used to estimate the RC delay (Eq. 1.1).[2] The increase in the number of metal layers to meet the wiring requirements due to scaling presents additional concerns in terms of manufacturing yield and cost for future interconnects.

$$RC = 2\rho\varepsilon\varepsilon_0\left(\frac{4L^2}{P^2}+\frac{L^2}{T^2}\right) \qquad \text{Eq. 1.1}$$

ρ: metal resistivity; ε_0: vacuum permittivity; ε: relative dielectric constant of the insulating material; *L*: length of the interconnect line; *P*: line pitch; *T* line thickness.

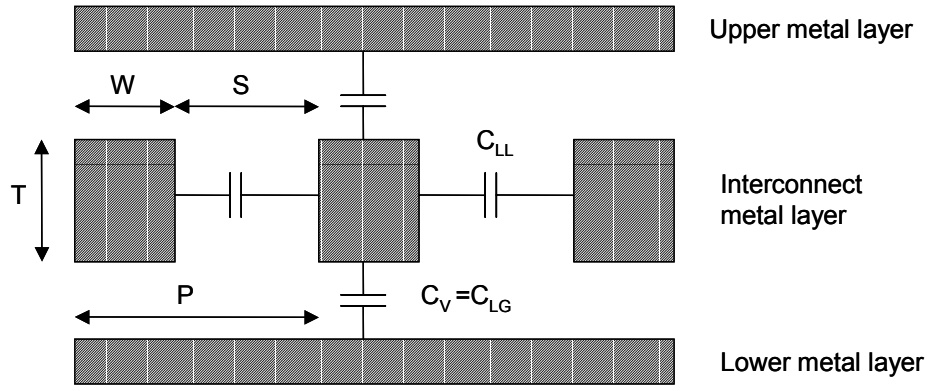

Figure 1.2 Schematic diagram of a typical interconnect element

The combination of aluminium alloys with SiO_2 dielectrics has been the preferred choice of materials for interconnect systems since the dawn of the integrated circuit (IC) era. These materials were convenient to process using mature subtractive etch processes for metal line patterning. In addition, they were compatible with the fabricated devices and presented no significant performance worries. However, as ICs have relentlessly marched down the path towards smaller geometries in the pursuit of increased speed and integration density, the Al/SiO_2 interconnect system itself has become a limiting factor. To address the problems mentioned above, new materials with lower resistivity and dielectric constant for use as metal lines and interlayer dielectric materials (LID), respectively, are intensively investigated. Recently this led to the announcement of Cu interconnect metallization.[3,4] The low

resistivity of Cu with 1.9 $\mu\Omega cm^{-1}$ which compares with 3.0 $\mu\Omega cm^{-1}$ for Al, can be used to improve the RC delay. An acute point for using Cu in scaling is that not only the width but also the thickness of the interconnect line can be reduced. The latter effectively lowers the line-to-line coupling capacitance, reducing the crosstalk noise and power dissipation, while improving the RC delay. At sub 250 nm features and below, the capacitance of interconnects is dominated by the line-to-line capacitance, contributing almost 90 % of the total capacitance. [5] By scaling the Cu thickness down to the point where the resistance equals that of a similar Al line, the capacitance of the interconnect can be reduced by approximately 20 to 25% and crosstalk by 15%. This is equivalent to changing SiO_2 with $\kappa = 4.0$ to a new material with much lower dielectric constant ($\kappa < 2.0$).

1.2 Future challenges for ILD materials in interconnect processes

The implementation of low–κ materials was first identified as a key enabling technology for the development of on–chip interconnects in the 1994 National Technology Roadmap for Semiconductors. Several years later this effort became part of an international activity with the major global regions participating in the definition of a roadmap, which is now called the International Technology Roadmap for Semiconductor (ITRS). In the 1997 implementation the requirement of ILD materials with κ value of 2.0-2.5 in 2001 was highlighted. [7a] As this was not achieved, the roadmap was revised in 1999 with an effective κ value of 2.7-3.5 in 2001 for the 180 nm technology node. [7b] This was not fulfilled until 2000 when IBM announced the combination of Cu interconnects for the 130 nm node with SiLK ™, which was developed by the Dow Chemical Company with a κ value of about 2.7. [7c] At this time, there is intensive effort in the industry to develop new Cu / ultra low-κ (ULK) interconnects on the basis of porous dielectric material with κ value of about 2.2. The main challenges in the interconnect roadmap of 2001 ITRS with respect to dielectric constant material are summarised in Table 1.1.

Table 1.1 2001 ITRS Interconnect Technology Requirements

Year of first production shipment	2001	2002	2003	2004	2005	2008	2011	2014
Technology node ½ Pitch (nm)	130				100	70	50	35
Number of metal levels – logic	7	7–8	8	8	8–9	9	9–10	10
Interlevel metal insulator – κ_{eff}	3.3	2.9	2.5	2.5	1.9	1.6	< 1.6	< 1.3
Interlevel metal insulator – κ_{bulk}	2.9	2.7	2.0	1.8	1.3	1.3	< 1.3	1.1
Barrier/cladding thickness (nm)	14	13	12	11	10	7	5	4
Effective conductor resistivity (μW/cm)	2.2	2.2	2.2	2.2	2.2	2.2	< 1.8	< 1.8
Number of metal levels – DRAM	3	3–4	4	4	4	4	4	4
Effective conductor resistivity – DRAM	3.3	3.3	3.3	3.3	2.2	2.2	2.2	2.2
Interlevel metal insulator – DRAM κ_{eff}	4.1	3.5	3.5	3.5	2.7	2.7	2.3	2.0

Solution exists Solution being pursued No known solution

In addition to a low dielectric constant, candidates for intra- and interlevel dielectrics must satisfy a large number of diverse requirements in order to be successfully integrated in the IC manufacturing process. Typical requirements include high thermal (up to 400°C) and mechanical stability, good adhesion to the other interconnect materials (copper, capping layer), resistance to processing chemicals, low moisture absorption, and low cost. [6] In recent years there have been widespread efforts to develop low–κ materials that can simultaneously satisfy all of these requirements.

Thermal stability is one of the most important requirements for ILD materials to withstand the elevated processing temperatures that can occur during interconnect processing. In general, the thermal stability is limited to the curing temperature of about 400°C in future interconnect processing. The thermal expansion coefficient (CTE) of ILD materials is equally important. Thermal stress results from CTE mismatches between the different materials which are included in interconnect structures. SiO_2 is a good material in this case, which has a CTE of 0.5 ppm/°C, whereas that of Cu is 16.5 ppm/°C. [14] The CTE of many organic dielectrics exceeds 50 ppm/°C. In combination with Cu wires the high CTE it can lead to highly stressed interconnect structures during thermal processing, which results in a significant reliability concern.

Mechanical strength is a further requirement as the structural integrity of the interconnect can be compromised if the film cannot withstand stresses which occur during processing. The elastic, or Young's, modulus (E) is often used as an indication of mechanical stability of ILD materials. The E modulus of most organic and inorganic low-κ dielectric

candidates is at least one order of magnitude lower than that of standard SiO_2 films with a modulus of 59 GPa. Unfortunately, Cu does not form volatile compounds with reactive gases. Thus, to form the Cu wiring in the dielectrics, the damascene process was developed. Trenches are prepared in the dielectric film by lithographic patterning and plasma etching. The trenches are subsequently filled with Cu, and the wiring inside the dielectric is defined by removing the excess Cu with chemical mechanical polishing (CMP). As a consequence, the dielectrics must withstand mechanical stresses during the polishing process. In Li *et al.* [43] the CMP feasibility of a low-κ material was related to its mechanical properties (see Fig. 1.3). Young's modulus (E) larger than 4 GPa and hardness (H) larger than 0.5 GPa can be required to pass conventional CMP.

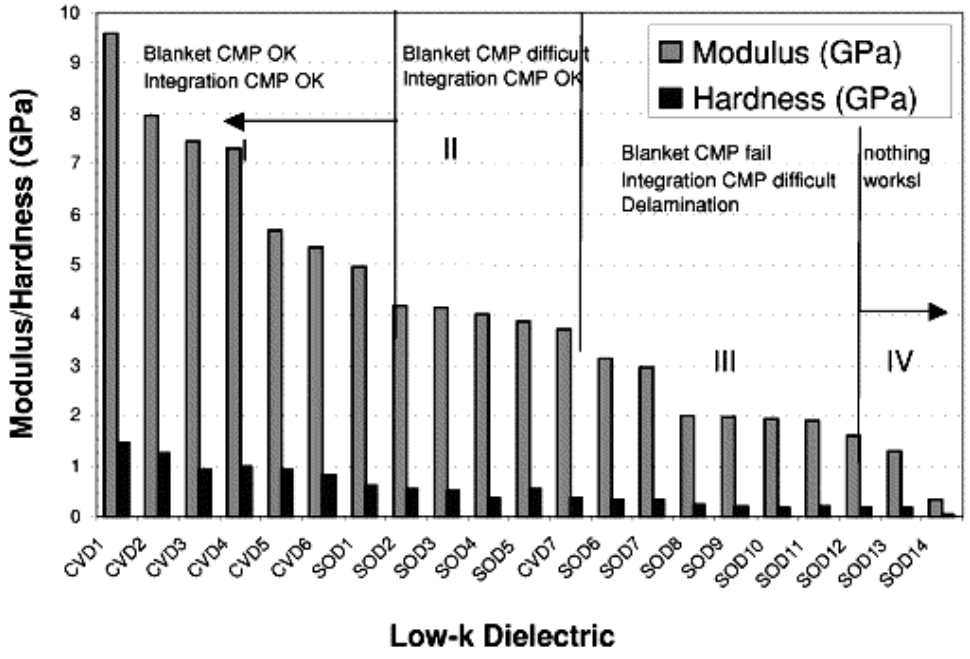

Figure 1.3 Correlation between Young's modulus and CMP feasibility

Adhesion strength is determined by chemical binding at the metal/ILD interface and the energy dissipation from mechanical interaction between the metal and ILD. Scherban reported a correlation between adhesion and CMP. Adhesion energies larger than 5 J/m^2 are required for CMP. [44] Again, typical ULK adhesion energies presented by other research groups are at the same level or even lower (about 2 J/m^2) than this specification. [45,46] Moreover a ULK material must be hydrophobic. Water has extremely polar O-H bonds and a dielectric constant close to 80. Even a small amount of adsorbed water significantly increases

the overall κ value. This is especially important for porous materials with a large surface area, where water can potentially be absorbed. Therefore the ideal porous material has a closed pore system. Simultaneously, a porous ULK material must withstand other processing chemicals in the etching steps (e.g. during the use of oxygen plasma) and cleaning steps (washing with organic solvents and water).

In recent years, the back-end ITRS roadmap was re-adjusted year to year, revealing the difficulties of integrating new types of ILD materials in the integration. Integration of low-κ material is intimately related with the optimisation between different tradeoffs, in particular material properties, device architectures, and process flows. The major driving forces for future integrated low-κ material are dielectric constant, process cost and process reliability/robustness. The ultimate solution for any particular node will be determined by the best compromise between these 3 factors.

1.3 Low–κ dielectric materials

1.3.1 Dielectric constant and chemical compounds

Dielectric constant κ (also called relative permittivity ε_r) is the ratio of the permittivity of a substance (ε) to that of vacuum (ε_0). Any material contains polar components, which are represented as dipoles (e.g. polar chemical bonds). The dipoles align with an external electric field, adding the electric field of every dipole to the external field. As the result, a capacitor with a dielectric medium other than vacuum will hold more electric charges at a certain applied voltage, in other words, its capacitance will be higher. The dipole formation is the sum of electric polarization (displacement of electrons), distortion polarization (displacement of ions and atoms), or orientation polarization (displacement of molecules) in an alternating electric field (see Figure 1.4). All three components contribute to the κ value and should be minimised for optimum performance. In general, all materials with a dielectric constant lower than 4.0 are called low dielectrics and those with a dielectric constant below 2.0 ultra-low dielectrics.

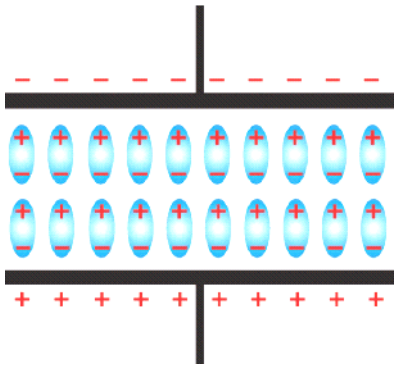

Figure 1.4 Schema of a capacitor

Typical electronic polarizabilities and the associated bond enthalpies are shown in Table 1.2. [9,10] The values indicate that a single C-C bond has the lowest electronic polarizability, making aliphatic hydrocarbons potential candidates for low dielectrics. Conversely, materials containing a large number of carbon double and triple bonds can be expected to have a large polarization due to the increased mobility of the π electrons. Additionally, conjugated carbon double bonds in aromatic structures are a common source of extensive electron delocalization leading to high electronic polarizability. The nuclear dielectric response results from polarization due to both permanent and transition dipoles in the material. The response is often dominated by polar substituents, such as hydroxyl and carbonyl groups, which can increase the orientational component of the polarizability. However, there is a trade-off in achieving a low dielectric constant and high bond strength, as the less polarizable single bonds are among the weakest, while the double and triple bonds have much higher bond enthalpies.

Table 1.2 Electronic polarizability and bond enthalpies

Bond	Polarizability ($Å^3$)	Bond enthalpy (kcal/mol)
C–C	0.531	83
C–F	0.555	116
C–O	0.584	84
C–H	0.652	99
O–H	0.706	102
C=O	1.020	176
C=C	1.643	146
C≡C	2.036	200
C≡N	2.239	213

The dielectric constant is determined not only by the type of atoms and bonds, but also by the atom and bond densities. The material density can be lowered by using lighter atoms and by incorporating more free space around the atoms. Therefore, the lower dielectric constant of organic polymers relative to SiO_2 is partly due to the lighter carbon and hydrogen atoms in comparison to silicon and oxygen atoms, and to the low packing density of most polymer chains relative to the cross-linked silica network. Likewise, the incorporation of light, space-occupying groups such as H or CH_3 into the silica network can significantly lower the material density, and therefore, the dielectric constant of materials such as spin-on glasses (SOG) relative to dense oxides. [11-13] Thus, the κ value is strongly dependent on chemical structure and density. [14-16]

1.3.2 Candidates for low-κ materials

The following is a brief discussion of some low–κ materials which are intensively investigated for ILD applications. Table 1.3 lists a number of key dielectric materials and the corresponding deposition methods which are suitable for technology nodes smaller than 100 nm. [17] The chemical structures of the ILD materials are shown in Table 1.3c.

Since ILD materials need to be used as thin films, the preparation involves either spin coating or chemical vapour deposition (CVD). Spin coating is a simple and effective process to deposit films from highly viscous precursor solutions on a substrate. After the deposition of the layer a curing process is necessary to remove the solvent. Compared with this, CVD results in inherent cleanliness and minimal waste production, because of the absence of solvents in the process. However, spin coating has a planarizing property, while the vapour-deposition process results in conformal coverage of the topography. Any protrusion or step present at the film surface before deposition would also be present with almost the same topography after the film deposition from the gas phase. In contrast, after spin coating the film shows in a smoother (or almost planar) surface, which is highly desirable.

Table 1.3 a Candidates for ILD materials for < 100 nm node (ITRS 2001)

Potential candidates	Dielectric constant κ	Deposition methods
Polyimides	3.1-3.4	spin-on
Poly (aryl ethers) (PAE)	2.8-3.0	spin-on
Hydrogen silsesquioxane (HSQ)	2.8-3.0	spin-on
Black Diamond ™ (SiCOH) [1]	2.7-3.3	CVD
Diamond-like Carbon (DLC)	2.7-3.0	CVD
Parylene-N	2.7	CVD
SILK ™ [2]	2.7	spin-on
Fluorinated Polyimides	2.5-2.9	spin-on
Methyl silsesquioxane (MSQ)	2.6-2.9	spin-on
Fluorinated DLC	2.4-2.8	CVD
Fluorinated Parylene	2.5	CVD
Polytetrafluoroethylene (PTFE)	1.9	spin-on
Porous PAE	1.8-2.2	spin-on
Porous HSQ	1.7-2.2	spin-on
Porous MSQ	1.8-2.2	spin-on
Porous SILK	1.5-2.0	spin-on

[1] Carbon incorporated silicon oxide; [2] SiLK is a fully dense aromatic hydrocarbon

Nonporous low dielectric materials

Porous ultra low dielectric materials

Table 1.3 b Trademarks of low k materials for ILD

Company	Trademarks	Composition
Dow Chemical	SiLK ™	Organic polymer
	CYCLOTENE	Organic polymer
Honeywell International Inc.	FLARE	Organic polymer
	HOSP	Hybrid organic siloxane
	NANOGLASS	Aerogel
Schumacher	MesoELK	Porous SiO_2
Asachi	ALCAP	Porous Silica
Dow Corning Corporation	FOx	HSQ
	XLK	Porous HSQ
W.L. Gore & Associates, Inc	SPEED FILM	PTFE/siloxane
Applied Materials, Inc	Black Dimand	SiCOH
DuPont	Teflon	PTFE
JSR Corporation	LKD	Porous MSQ
Shipley (Rohm and Haas)	Zirkon LK	Porous MSQ
Novellus	CORAL	fluorosilicate

Table 1.3c Molecular structure of some candidates for low dielectrics

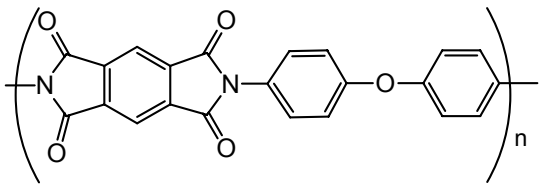

PMDA-ODA [a] Polyimide

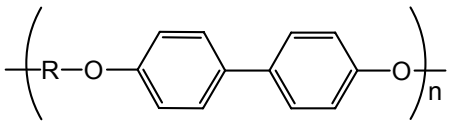

Poly (aryl ether), PAE

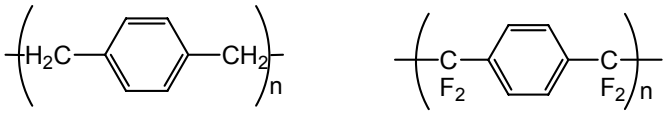

Parylen-N Parylen-F

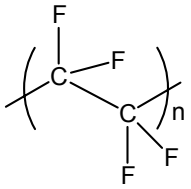

Polytetrafluoroethylene (PTFE)

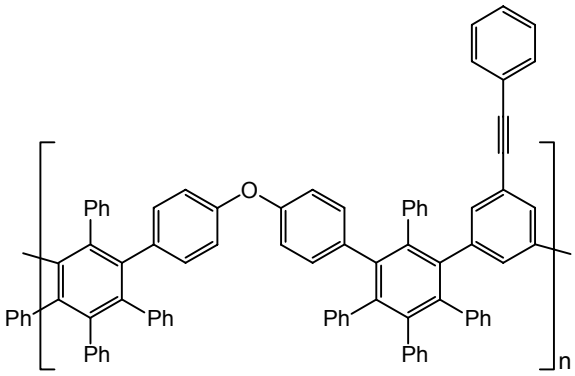

SiLK ™, Dow Chemical

[a]: PMDA-ODA : Pyromellitic dianhydride-4, 4' oxydianiline

Polytetrafluoroethylene (PTFE)

Proposals to use PTFE are aimed toward minimizing the dielectric constant by incorporation of bonds of low polarizability (Table 1.2). Consequently, PTFE has one of the lowest κ values (about 1.9) of any nonporous material, and is normally deposited by spin coating. [18] One drawback of this polymer is that the flexible and not cross-linked chain structure limits the thermal and mechanical stability during integration. A second disadvantage of PTFE, which is a common concern for all fluorine containing materials, is the potential release of fluorine atoms that can cause corrosion of metals in the interconnect structure.

Polyimides (PIs)

Thermal and mechanical properties, better than those of PTFE, can be obtained by incorporating a stiffer polymer chain or by cross-linking the chains. One of the typical examples of PIs is shown in Table 1.3c. The materials have a rigid backbone due to the aryl and imide rings along the chain. However, the rigid chain structure causes the PI chains to align preferentially parallel to the substrate, especially when deposited as thin films, which leads to anisotropic material properties. [19-21] For example, while the out-of-plane κ of PMDA-ODA is 3.1, the more important in-plane value is 3.5. [22] Another drawback of PIs is that they absorb H_2O ($\kappa = 80$) effectively owing to the carbonyl groups, which can raise the dielectric constant further. The release of this water during processing can create blistering of overlying layers. [23]

Poly(aryl ethers) (PAE)

In poly(aryl ethers), the contained aryl rings provide better thermal and mechanical properties than those of PTFE, but the flexible aryl linkages allow bending of the chain, which results in a more isotropic material than for PIs. Additionally, the lack of polar groups leads to a lower κ value and reduced water uptake compared to PIs. Fluorinated PAE have a κ value of 2.4 while typical values of the non fluorinated PAE are in range of 2.8-2.9. [24] A disadvantage for not cross-linked PAEs is that they have a relative low glass transition temperature (T_g) of 275°C. To increase the T_g reactive functional groups can be incorporated along the backbone, which allows for cross-linking of the film during cure. Unfortunately, cross-linking can also lead to an increase in the dielectric constant.

Parylenes

Another class of organic polymers that have been considered for ILD application are parylene-N and the fluorinated derivative, parylene-F. [25-28] The material are semicrystalline polymers formed by CVD at low temperature (ca. 13°C). Both materials show excellent thermal stability and high transition temperature. But, as with the PIs, the parylenes have a large degree of in-plane versus out-of-plane anisotropy owing to the preferential alignment of the polymer chains parallel to the substrate in the thin film. [27] The crystallinity and anisotropy of the thin films typically increase with annealing. The out-of-plane κ values are in the range of 2.2 and 2.6 for the fluorinated and normal parylene, respectively, whereas the in-plane values are relatively high.

Silsesquioxanes

Mechanical and thermal stability is difficult to obtain with purely organic materials; thus there has been much interest in inorganic hybrid materials. The idea behind the silica based material is to use the much stronger and more rigid SiO_2 network as a starting point and lower the dielectric constant by lowering the density through the incorporation of chemical substituents or voids. Organosilicate resins are materials in which one or two of the orthosilicate $(SiO_2)_n$ oxygen bridging atoms have been replaced with alkyl, hydrido or aromatic organic residues. Removal of one bridging oxygen leads to silsesquioxanes, $(RSiO_{1.5})_n$ which can be vitrified by heating to produce a three-dimensional network. [29] In the silsesquioxanes, each Si atom is bound to one terminating group, such as –H, $–CH_3$. In the ladder-structure HSQ, each silicon is attached to three oxygen atoms and one hydrogen atom. The terminal silicon atoms at either end are attached to one hydrogen atom, two oxygen atoms and one hydroxyl group. The polymer cross-links by condensation of two Si-OH groups to give Si-O-Si bonds (see Table 1.3c). This results in a less dense network than for silica, and one that is intrinsically hydrophobic rather than hydrophilic. The reduction in κ relative to SiO_2 ($\kappa = 4.0$) is thought to be mainly due to the reduction in density. For example, the density of polymerized hydrogen silsesquioxane (HSQ) ($\kappa = 2.8$-3.0) is about one third less (1.4 g/cm^3) [30,31] than that of SiO_2 (2.4 g/cm^3). Most fully cured silsesquioxane derivatives are thermally stable even beyond of 400°C. The mechanical properties of HSQ and methyl silsesquioxane (MSQ) are generally superior to most organic polymers. Additionally the silsesquioxanes have an advantage over many other spin-on materials in that they have good crack resistance. Many other materials experience a large amount of shrinkage during curing. That leads to high tensile stresses that can crack the films. This often limits the maximum

thickness of such films to only a few thousand Å. The silsesquioxanes undergo much less shrinkage, are less prone to cracking, and therefore can be prepared in thick layers of μm scale. [32] The observation is in good agreement with our measurements of film thickness *f* on new type of silsesquioxane polymers in Chapter 2. In Chapter 5 we focused on the discussion of results with silsesquioxane polymers as the matrix for nanoparticles. Additional properties for common organosilicate films are listed in Table 1.4.

Table 1.4 Properties for silicate-based materials

Property	MSQ	HSQ	SiO_2
Diel. Constant κ	2.8	3.0	4.0
E Modulus (G Pa)	3-5	6	59
Density (g/cm^3)	1.2-1.3	1.4-1.5	2.4
Tensile Strength σ (M Pa)	50	80	-

Nanoporous materials

As very few dense materials have a κ value less than 2.5, there has been much interest in investigating porous materials in order to get to ultra low-κ values (< 2.0). Most of these materials are not as well developed as the fully dense materials. Nevertheless, a wide variety of porous materials have been prepared and some initial integration studies have been done. [33] There are two alternative methods to prepare the porous materials: one is through direct construction of a porous network and the second is indirectly by depositing a composite material, containing a component which is afterwards removed by thermal treatment. The first type of material, including aerogels and xerogels, is often prepared by a gel process in solution. [34-36] Solvent-impregnated gel films can be dried either supercritically or by evaporation. [37-38] Using this technique, highly porous films (> 80%) can be generated with dielectric constants in the range of 1.1-1.8. Unfortunately, the high porosity and the extremely low material densities result in poor mechanical properties unsuitable for the integration.

Other nanoporous materials can be formed using a templating scheme with matrix resin and surfactant additive (pore generator). Porosity is constructed by thermal removal of sacrificial components. The most useful templates are triblock, diblock and random copolymers of poly(ethylene oxide) and poly(propylene oxide) because of the relatively low decomposition temperature. [39-42] There are several available resin matrices for this approach and they can be divided into non-Si polymers (amorphous carbon) and silsesquioxane based polymers. Typical examples for the non-Si containing polymers are polyarylether (PAE),

polyimides and SiLK™. The porous structures of these materials lead to a lower dielectric constant between 1.5 and 2.2 (see Table 1.3a). Another potential candidate for this approach are silsesquioxanes with three-dimensional network like hydrogen silsesquioxane (HSQ) and methyl silsesquioxane (MSQ), where porosity can be created in the matrix using triblock copolymers. Porous HSQ and MSQ have κ values in the range of 1.7-2.2, which are lower than for dense HSQ (κ = 2.8-3.0) and MSQ (κ = 2.6-2.9).

There are a number of reliability concerns that are particularly prominent for porous ILDs. The pore structure of these low-κ dielectric materials strongly affects important material properties other than the dielectric constant such as mechanical strength, moisture uptake, coefficient of thermal expansion, and adhesion to different substrates. Another potential problem involves the size and distribution of the pores in the material. For instance, if the pores are too large, feature sizes and shapes will not be well defined during integration. Additionally, the porous films have a low breakdown voltage and mechanical strength. The characterization of the pore structure is needed by material engineers to help optimise and develop future low-κ materials and processes. With the large number of possible materials and processes, there is a strong need for high quality structural data to help understand correlations between processing conditions and the resulting physical properties.

1.4 Outlook

In order to reduce the κ value of insulating material, it is necessary either to incorporate atoms and bonds that have a low polarizability, or else to lower the density of the atoms and bonds in the material, or both. While porous thin films of ULK is a young field and knowledge only begins to emerge for Cu/ low–κ interconnect circuits, there remains much work to be done to understand structure-property relationships in the porous materials. Although lowering the density can lower the dielectric constant, it will also decrease the mechanical strength of the film. This has serious implications for integration of porous materials. The porosity, pore structure and pore diffusion on the interface all influence the dielectric constant, mechanical strength, thermal stability, adhesion of the substrate, breakdown voltage, hardness and uptake of moisture. A better understanding of the relationship between these properties is necessary in order to lower the dielectric constant while holding the good adhesion and high mechanical strength. A great deal of work will be required on the development of new evaluation techniques for porous materials, material characterization and optimisation of the pore systems.

The progress in silicon technology, the decreasing feature size connected with a simultaneously increasing integration density has raised a fundamental interest in low dielectric constant materials. Thin porous films with $\kappa < 2.5$ as isolator in the interconnect circuits can be prepared either by CVD or spin-on techniques. Nonetheless, the vastly different properties of spin-on porous ultra low–κ (ULK) materials compared to silicon dioxide lead to unique challenges during the semiconductor manufacturing process. Generally, every single process step has to be optimised to ensure that the ULK materials are not damaged. Because of the mechanical weakness of the porous dielectric materials, CMP becomes a very critical process, and alternatives to conventional CMP would be very advantageous for the integration of ULK materials. Due to the high porosity, every production step that exposes the low–κ material to plasma, or a wet chemical treatment, has to be critically examined. The best integration in this case is the one avoiding exposure of the ULK material to such processes. More work is needed for reliability studies of porous low–κ material to ensure successful integration of future interconnect circuits. Clearly, these challenges make ULK material development a very exciting area for future research.

1.5 References

[1] G.E. Moore, *Electronics*, **1965**, *38(8)*, 114.

[2] M. Bohr*, Tech. Digest IEEE Int. Electronic Device Meeting*, **1995**, 241.

[3] D. Edelstein, J. Heidenreich, R. Goldblatt, R. Schulz, L. Su, and J. Slattery, *IEEE Int. Electronic Device Meeting*, **1997**, 773.

[4] S. Verkatesan, V. Misra, J. Cope, D. Tuttel, R. Cardwell, I. Yang, N. Bhat, G. Hamliton and Y. Yu, *IEEE Int. Electronic Device Meeting*, **1997**, 769.

[5] D. Edelstein, G. Sai-Halasz and Y. Mii, *IBM J. Res. Dev.*, **1995**, *39*, 383.

[6] W. Lee and P. Ho, *MRS Bull.*, **1997**, *22*, 19.

[7] a) *The international Technology Roadmap for Semiconductor*, Semiconductor Industry Association, San Jose, C.A. 1997

b) *The international Technology Roadmap for Semiconductor*, Semiconductor Industry Association, San Jose, C.A. 1999

c) S. Martin, J. Godschalx, M. Miller, E. Schaffer and P. Townsend, *Adv. Mater.*, **2000**, *12*, 1769.

[8] P.H. Townsend, S.J. Martin, J. Godschalx, D.R. Romer, R. DeVries, G. Buske, N. Rondan, S. Froelicher, J. Marshall, and E.O. Shaffer, *MRS Symp Proc.,* **1997**, *476*, 9.

[9] K. Miller, H. Hollinger, J. Grebowicz and B. Wunderlich, *Macromolecules*, **1990**, *23*, 3855.

[10] S. Pine, *Organic Chemistry*, *5th edn*, McGraw-Hill, New York, **1987**.

[11] C. Nguyen, R. Beyers, C. Hawker, J. Hendrick and R. Jaffe, *Polymer*, **1999**, *40*, 398.

[12] J. Bremmer, Y. Liu, K. Gruszynski and F. Dall, *Mater. Res. Soc. Symp. Proc*., **1997**, *476*, 37.

[13] S. Kim, D. Yoon, C. Nguyen, J. Jan and R. Jaffe, *Mater. Res. Soc. Symp. Proc*., **1998**, *511*, 37.

[14] D.W. Krevelen, *Properties of Polymers, 3rd edn*., Elsevier, New York, **1990**.

[15] R. Seymour and C. Carraher, *Structure-Property Relationships in Polymers*, Plenum Press, New York, **1984**.

[16] D. Baeriswyl, G. Harbeke, H. Kiess and W. Meyer, in *Electronic Properties of Polymers*, ed. by J. Mort and G. Pfister, John Wiley & Sons, New York, **1982**.

[17] *The international Technology Roadmap for Semiconductor*, Semiconductor Industry Association, San Jose, C.A. 2001

[18] C. Rosenmayer, J. Bartz, and J. Hammes, *Mater. Res. Soc. Symp. Proc*., **1997**, *476*, 231.

[19] S. Chen and H. Wagner, *J. Electron. Mater*., **1993**, *22*, 797.

[20] L. Lin and S. Bastrup, *J. App. Polymer Sci. E*, **1994**, *54*, 533.

[21] S. Hardaker, S. Moghazy , C. Cha and R. Samuels, *J. Polymer Phy. Polymer Phy.*, **1993**, *31*, 1951.

[22] M. Ree, K. Chen and D. Kirby, *J. App. Phy*., **1992**, *72*, 2014.

[23] T. Wetzel, Y. Li, S. Filipiak, B. Nguyen and E. Travis, *Mater. Res. Soc. Symp. Proc*., **1995**, *381*, 217.

[24] N. Hendricks, K. Lau, S. Smith and W. Wan, , *Mater. Res. Soc. Symp. Proc*., **1995**, *381*, 59.

[25] D. Kirkpatrick and B. Wundlich, *J. Polymer Sci. Polymer Phy*., **1986**, *24*, 931.

[26] E. Ryan, M. Miller and P. Ho, *Mater. Res. Soc. Symp. Proc*., **1997**, *476*, 225.

[27] J. Blackwell, Y. Park, S. Chvalun, K. Mailyan and I. Kardash, *Polymer Preprint*, **1998**, *39*, 892.

[28] M. Morgen, J Zhao, S. Rhee. E. Ryan and H. Ho, *Mater. Res. Soc. Symp. Proc*., **1999**, *565*, 69.

[29] R. Baney, M. Itoh, A. Sakakibara and T. Suzuki, *Chem. Rev*., **1995**, *95*, 1409.

[30] J. Bremmer, Y. Liu, K. Gruszynski and F. Dall, *Mater. Res. Soc. Symp. Proc*., **1997**, *476*, 37.

[31] Y. Liu, J. Bremmer, K. Gruszynski and F. Dall, *VLSI Multilevel Interconnection Conf.*, **1997**, 655, Santa Clara, CA.

[32] N. Hacker, G Davis, L. Figge T. Krajewski and S. Leffert, *Mater. Res. Soc. Symp. Proc*., **1997**, *476*, 25.

[33] E. Ryan, H. Ho, W. Wu, P. Ho, D. Gidley and J. Drage, *Proc. IEEE Int. Interconnect Technol. Conf.*, **1999**, 187.

[34] N. Hüsing and U. Schubert, *Angew. Chem. Int. Ed.*, **1998**, *37*, 22.

[35] M. Jo, H. Park, D. Kim, S. Hyun, S. Choi and J. Park, *J. Appl. Phys.*, **1997**, *82(3)*, 1299.

[36] L. Hrubesh and S. Buckley, *Proc. Mater. Res. Soc.*, **1997**, *476*, 99.

[37] J. Fricke, *Sci. Am*., **1988**, *258*, 92.

[38] S. Prakash, C. Brinker, A. Hurd and S. Rao, *Nature*, **1995**, *374*, 439.

[39] N. Hüsing and U. Schubert, *Angew. Chem. Int. Ed.*, **1998**, *37*, 22.

[40] L. Hrubesh and S. Buckley, *Proc. Mater. Res. Soc*. **1997**, *476*, 99.

[41] D. Zhao, Q. Huo, J. Feng, B. Chmelka and D. Stucky, *Science*, **1998**, *279*, 548.

[42] A. Hozumi, Y. Yokogywa, T. Kameyama, H. Sugimura and N. Okido, *Adv. Mater*., **1998**, *10(16)*, 1380.

[43] S. Li, *Proc. IEEE Int. Interconnect Technol. Conf.*, **2001**, 146.

[44] T. Scherban, *Proc. IEEE Int. Interconnect Technol. Conf.*, **2001**, 275.

[45] S. Maitrejean, *Proc. IEEE Int. Interconnect Technol. Conf.*, **2002**, 206.

[46] G. Kloster, *Proc. IEEE Int. Interconnect Technol. Conf.*, **2002**, 242.

Chapter 2

A new type of low-κ dielectric thin film based on functional silsesquioxane polymers

Abstract

A new type of organic/inorganic hybrid copolymer with a low dielectric constant (κ = 2.1 - 2.7) was prepared by platinum catalysed hydrosilylation or hydrolytic condensation of functionalised silsesquioxanes. These copolymers were deposited as thin films by spin coating. By controlling the parameters for spin coating (spin-speed, -acceleration, -time, gel composition, etc.) coherent films with a thickness ranging from 22 - 28 μm were prepared. The preparation and characterization of the copolymers and the films including film thickness, dielectric constant κ, adhesion, hardness, breakdown voltage, morphology and thermal stability are described.

2.1 Introduction

Improving the performance of increasingly miniaturized ultra-large scale integrated circuits requires reduction in the dielectric constant of the insulators used in circuit interconnected structures. [1,2] Such structures consist of a three-dimensional network of conducting lines and are constructed above the semiconductor substrate interconnecting the active gates and cells fabricated on the semiconductor surface. Figure 2.1 shows the cross section of a typical multi-layer interconnect element. The insulator, or dielectric, separating the conducting elements, must have a low dielectric constant in order to minimize the capacitance between lines and, thereby, minimize both the "*RC*"- time, characterizing the delay of signals travelling along lines, and the capacitive "cross-talk" between lines.

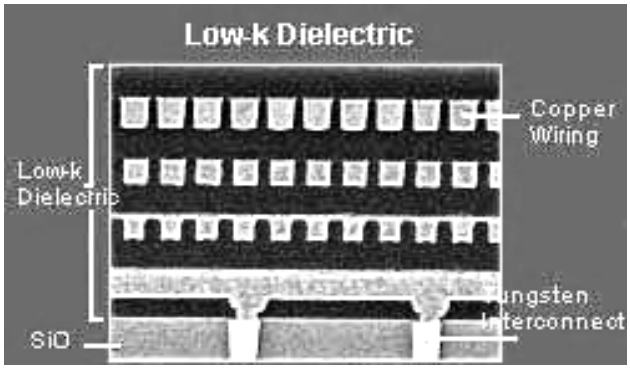

Fig. 2.1 Construction of a multi-layer interconnect element

Promising candidates for low dielectric constant interconnection materials are polymers based on silsesquioxanes. Latter have the empirical formula $(RSiO_{1.5})_x$, where R is alkyl, alkylene, aryl, arylene, or corresponding organo - functional derivates. They have been widely utilized in electronics industry [3-6] since the first commercialization of silicon polymers as electrical insulation materials for use at high temperatures. Well-defined layers of polysilsesquioxanes have been suggested as substitute for insulating SiO_2 - layers (κ = 4.0) incorporated in microchips, because of their outstanding properties. Requirements include low dielectric constant κ, high breakdown voltage, good mechanical strength, high thermal stability during processing, etch selectivity, etc. [7,8] Especially, a low dielectric constant is one of the most important properties for applications in microelectronic industry. So far, the best low dielectric materials employed in industry have dielectric constants κ in the range 2.5 - 3.3. [18-25] In this paper, we present the synthesis of silsesquioxane polymers with dielectric constant κ between 2.1 - 2.7, which were formed from sol-gel copolymerisation and

condensation using cubic $R_8Si_8O_{12}$ octamers with 4, 4' cage structure. Important synthetic goals are the controlled catalytic hydrosilylation of $H_8Si_8O_{12}$, T_8^H (**5**), $(HSiMe_2O)_8Si_8O_{12}$, $Q_8M_8^H$ (**6**) with 1,5-hexadiene and hydrolytic condensation of monomers such as $[(EtO)_3Si(CH_2)_2]_8Si_8O_{12}$, T_8^R (**7**) and $[(EtO)_3Si(CH_2)_2SiMe_2O]_8Si_8O_{12}$, $Q_8M_8^R$ (**8**) in a clean chemical reaction, which gives few side products and occurs under mild reaction conditions, i.e., at room temperature. Fabrication of a spin coating film usually involves preparation of a polysilsesquioxane gel, followed by spinning the solution onto a substrate. The electronic and mechanical properties of the coating films based on these silsesquioxane polymers were determined. These include thickness, dielectric constant κ, adhesion, hardness, breakdown voltage, composition, morphology and thermal stability.

2.2 Results and discussion

There are different strategies for the synthesis of silsesquioxane polymers from the corresponding monomers. [9-13] We have chosen: (i) platinum-catalysed hydrosilylation [10,11] and (ii) hydrolytic polycondensation of alkoxysiloxanes. [12-14] The main advantage of these reactions is that they constitute a general and versatile approach to silsesquioxane polymers.

The first option, catalytic hydrosilylation is a well – studied method of forming Si-C linkages by adding Si-H moieties to CC double bonds. Hydrosilylation can be realized under mild conditions in a non-aqueous environment. Thus, hydrosilative copolymerisation of dienes and hydrido-functionalized silsesquioxanes, e.g., $H_8Si_8O_{12}$, T_8^H (**5**) and $(HSiMe_2O)_8Si_8O_{12}$, $Q_8M_8^H$ (**6**) (see Table 2.1), should provide access to copolymers with well-defined structures (three-dimensional network). We investigated the reaction of monomers (**5**) and (**6**) with hexadiene using platinum sponge as heterogeneous catalyst. After the reaction, the catalyst was quantitatively removed by filtration. The reactions are shown in Equation 1.

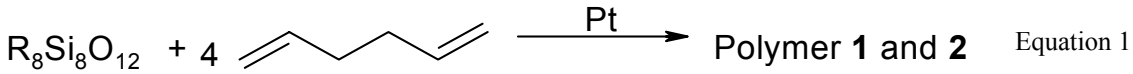

Equation 1

R_1: -H and R_2: -$OSiMe_2H$

Another common process to obtain polysilsesquioxanes [14-16] with silicon - oxygen skeletons is the hydrolytic condensation of trifunctional monomers $(Y_3SiX)_8Si_8O_{12}$, where X is a chemically stable organic bridging group, and Y a highly reactive substituent, such as

alkoxy. We have employed the polycondensation of $[(EtO)_3Si(CH_2)_2]_8Si_8O_{12}$, T_8^R (**7**) and $[(EtO)_3Si(CH_2)_2SiMe_2O]_8Si_8O_{12}$, $Q_8M_8^R$ (**8**) (Table 2.1) with water. The polycondensation reaction is shown in Equation 2. The molecular precursors **7** and **8** were synthesised by platinum-catalysed hydrosilylation of $R_8Si_8O_{12}$ (R: H for **7** and R: $OSiMe_2H$ for **8**) and $(CH_2=CH)Si(OEt)_3$. The precursors react fast with water and, therefore, were handled under inert atmosphere (nitrogen).

$$R_8Si_8O_{12} + H_2O \longrightarrow \text{Polymer } \mathbf{3} \text{ and } \mathbf{4} \qquad \text{Equation 2}$$

R_3: $-(CH_2)_2Si(OEt)_3$ and R_4:$-OSiMe_2(CH_2)_2Si(OEt)_3$

Table 2.1: Chemical structure of silsesquioxanes **5** – **8**

Structure of $R_8Si_8O_{12}$	Derivative
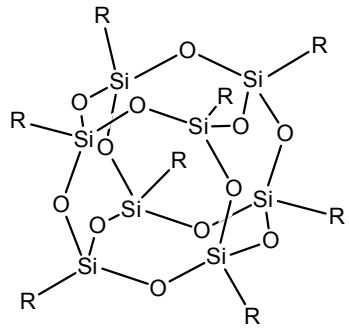	R_5: -H
	R_6: $-OSiMe_2H$
	R_7: $-(CH_2)_2Si(OEt)_3$
	R_8: $-OSiMe_2Si(OEt)_3$

The copolymerisation of monomers **5** - **8** provided a clear solution, from which the solvent (toluene) was partially removed to obtain a gel based on the copolymers of silsesquioxanes **1** - **4** as highly viscous liquid. The chemical structure of the copolymers is shown in Figure 2.2. In the three dimensional network, each edge of a silsesquioxane cube is linked via an organic bridge X to another silsesquioxane cube. However, because of steric reasons, some of the corners are not connected, but instead, are terminated by an end - group R. The chemical characterisation of the copolymers was fully consistent with this three-dimensional structure of the copolymers.

Thin films were prepared using spin on coating techniques. Steel plates were used as electrically conducting substrates. The gels of copolymers **1** - **4** were used for spin coating and the films obtained, dried in vacuum. The electrical properties were determined after vapour

deposition of small aluminium circles with 2.5 mm diameter on top of the film. This allowed measuring the capacity and the breakdown voltage of the films. The dielectric constant κ can be calculated from the capacity using the formula $\kappa = c\ d / A\ \varepsilon_0$, where c is the observed capacity, d the film thickness, A the aluminium area and ε_0 the free permittivity. After the electrical measurements, the film hardness was measured first, then the plate cut into two halves and the film thickness determined by light microscopy. The adhesion of the coating films was tested on a different steel plate with cross cutting according to reference. [17]

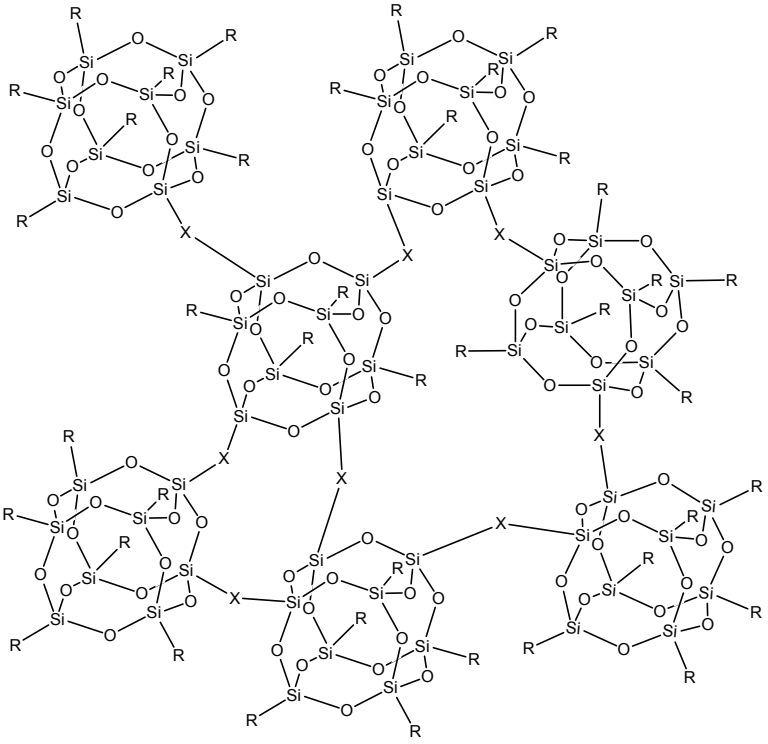

R_1: -H or $-(CH_2)_4CH=CH_2$	X_1: $-(CH_2)_6-$
R_2: $-OSiMe_2H$ or $-OSiMe_2-(CH_2)_4CH=CH_2$	X_2: $-OSiMe_2-(CH_2)_6-SiMe_2O-$
R_3: $-(CH_2)_2-Si(OH)_3$	X_3: $-(CH_2)_2-Si(O)_3-Si-(CH_2)_2-$
R_4: $-OSiMe_2(CH_2)_2Si(OH)_3$	X_4: $-OSiMe_2-(CH_2)_2-Si(O)_3-Si-(CH_2)_2-SiMe_2O-$

Figure 2.2: Three-dimensional network of copolymers **1 - 4**

Table 2.2 shows the results on the characterization of coating films, which include film thickness, dielectric constant κ (at 1 MHz), breakdown voltage, mechanical adhesion and film hardness. The film thickness of copolymers **1 - 4** was uniform and varied in a narrow range between 22 - 28 μm. The dielectric constant κ of the coating films was low compared to

literature data, which are typically in the range 2.7 – 4.0. [18-23] The lowest dielectric constant was observed for **2** (κ = 2.1), the highest for **4** (κ = 2.7), whereas **1** and **3** had an intermediate dielectric constant (κ = 2.5 and 2.4, respectively). The breakdown voltage correlated with the length of organic bridge X. A long chain led to an increase in the breakdown voltage. The breakdown voltage was high for copolymers **2** and **4**, which have a chain with 10 atoms, compared to a relatively low breakdown voltage of copolymers **1** and **3**, which have short chains (6 and 7 atoms). Thus, a long linker led to an increase in the breakdown voltage. Similarly, the hardness increased with the number of atoms in the chain, with higher hardness of **2** compared with **1** and of **4** relative to **3**. Overall, the results suggest that the physical properties of copolymers such as adhesion and hardness of films are closely associated with the length of the chain between the silsesquioxane cubes. The result of adhesion measurements showed for all thin films good quality in the cross cutting test (damage category 1).

Table 2.2: Characterization of coating films

Copolymer	Film thickness (μm)	Dielectric constant κ	Breakdown voltage (MV/cm)	Adhesion Cross cutting*	Hardness HU** (N/mm^2)
1	25	2.5	0.22	1	139
2	22	2.1	0.53	1	200
3	28	2.4	0.32	1	70
4	23	2.7	0.40	1	120

*: Damage category of cross cutting according to EN ISO 2409

**: HU: universal hardness

The morphology was studied using a scanning electron microscope (SEM). The SEM images of copolymers **1** - **4** showed featureless flat surfaces of all copolymers (for an image of copolymer **2** see Figure 2.3). However, after the films had been pealed from the surface, there were also holes with 0.5 - 1.5 μm diameter. Probably, these mechanically weak points led to electrical shortcuts, when applying a high voltage and are the reason for the relatively low breakdown voltage (0.2 - 0.5 MV/cm) compared to typical values (1 - 5 MV/cm) reported previously. [26,27] Light microscopy was used to measure the film thickness und characterize the film quality. Fig. 2.4 shows a cross-section of a copolymer film (copolymer **1**) after spin

on coating. The uniform film thickness (25 μm) and sharp interface with resin demonstrate that the film quality is good. Pores were not observed at this magnification.

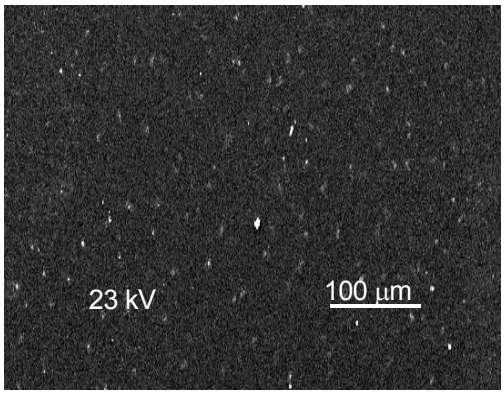

Figure 2.3: SEM image of the surface of the film obtained for copolymer **2**

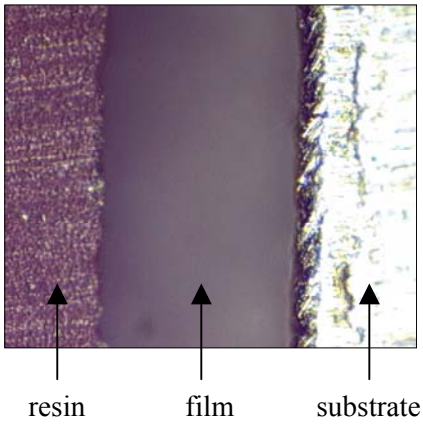

Figure 2.4: Light microscopy image of a cross – section of the film obtained for copolymer **1**

All copolymers showed good-to-excellent thermal stability in nitrogen. With heating until 400 °C no mass loss by copolymers **2** - **4** was observed. For copolymer **1** the onset temperature for the mass loss (3 % wt) was around 230 °C in the first heating - cooling cycle. In contrast, no mass loss was observed in the subsequent cycle. The mass loss is tentatively attributed to the evaporation of solvent entrapped inside the copolymer.

2.3 Conclusions

We have shown that a new type of organic/inorganic hybrid copolymer with low dielectric constant κ can be synthesized by (i) platinum catalysed hydrosilylation of $H_8Si_8O_{12}$ (T_8^H) and $(HSiMe_2O)_8Si_8O_{12}$ ($Q_8M_8^H$) with hexadiene or ii) hydrolytic condensation of

$[(EtO)_3Si(CH_2)_2]_8Si_8O_{12}$ (T_8^R) and $[(EtO)_3Si(CH_2)_2SiMe_2O]_8Si_8O_{12}$ ($Q_8M_8^R$) with water. To fabricate copolymer films spin on coating techniques were found suitable. The film thickness of copolymer **1** - **4** was in a small range 22 - 28 μm and the film surface showed excellent quality in the cross cutting test. The result of dielectric constant measurements showed, that the new copolymers have a relatively low κ (2.1 - 2.7) compared to the reference data. The properties like film adhesion and hardness were found to be closely correlated with the length of cross linker. With scanning electron microscopy (SEM) the morphology of the film surface was studied. All copolymer films were planar and flat. Thermal analysis indicated that the copolymer **1** - **4** were thermally stable to 400 °C.

2.4 Experimental

Materials and Methods:

Preparation of polymeric materials was carried out in an atmosphere of dry nitrogen using standard Schlenk techniques. Toluene was distilled from sodium under nitrogen. All other reagents were obtained from Aldrich and were used as received. Monomers **5** ($H_8Si_8O_{12}$) and **6** ($(HSiMe_2O)_8Si_8O_{12}$) were purchased from ABCR and Aldrich, respectively.

^1H, $^{13}C\{^1H\}$, and ^{29}Si - NMR spectra were performed on a JEOL GX 400 instrument and referenced in ppm relative to the solvent shift [28] or tetramethylsilane. Infrared spectra were obtained on a Perkin-Elmer FT - IR 2000 spectrometer as KBr disks taking 30 scans per spectrum. Elemental analyses were performed by the micro-analytical laboratory of the Technische Universität München.

Preparation of monomers **7** and **8**:

Monomers **7** and **8** were prepared by reacting equal amounts of triethoxyvinylsilane and hydrido silsesquioxanes **5** and **6**, respectively, in toluene using platinum sponge catalyst (10 mol %). For monomer **7,** octahydridosilsesquioxane $H_8Si_8O_{12}$, T_8^H (**5**) (300 mg , 0.71 mmol) and platinum sponge (14 mg, 0.071 mmol) were added to 20 ml dry toluene in a 50 ml Schlenk flask. The solution was cooled to 0 °C, degassed and purged with nitrogen three times. Then, triethoxyvinylsilane (1.19 ml, 5.65 mmol) was added. The mixture was allowed to warm slowly to room temperature and stirred overnight. After removal of the platinum catalyst by filtration over a glass microfibre filter, a colourless gel was obtained. The product **1** was obtained as colourless solid by solvent evaporation. Monomer **2** was prepared in the same way from **6** (300 mg, 0.29 mmol) and triethoxyvinylsilane (488 μl, 2.32 mmol).

For monomer **7:** EA (%): Found: Si, 23.5; C, 39.1; H, 8.1. Calcd($C_{64}H_{152}Si_{16}O_{24}$): Si, 23.1; C, 39.5; H, 7.9. FTIR (KBR, cm^{-1}): ν C-H: 2981, 2936, 2898; δ CH_3: 1390; ν Si-H: 2258.4; ν Si-C: 1149; ν Si-O: 1071. ^{1}H-NMR (400 MHz, C_6D_6): δ 3.83 (q, -OCH_2, *J* = 7 Hz), 1.15 (t, CH_3, *J* = 7 Hz), 0.97 (m, -CH_2Si), 1.35 (m, -CH_2Si). ^{29}Si-NMR (71.5 MHz, C_6D_6 dept_nondecoup): -45.2 (-CH_2-Si$(OEt)_3$), -66.2 (-CH_2Si$(OSi)_3$).

For monomer **8:** EA(%): Found: Si, 25.6; C, 38.2; H, 8.1. Calcd: Si, 26.5; C, 37.8; H, 7.9. FTIR (KBR, cm^{-1}): ν C-H: 2981, 2936, 2898; δ CH_3: 1390; ν Si-H: 2258.4; ν Si-C: 1149; ν Si-O: 1071.

Preparation of copolymers **1** and **2**:

Copolymers **1** and **2** were prepared by reacting equal amounts of hydrido silsesquioxane **5** or **6** and hexadiene in toluene using platinum sponge catalyst (10 mol %). For copolymer **1,** octahydridosilsesquioxane $H_8Si_8O_{12}$, T_8^H (**5**) (300 mg , 0.71 mmol) and platinum sponge (14 mg, 0.071 mmol) were added to 40 ml dry toluene in a 100 ml Schlenk flask. The solution was cooled to 0 °C, degassed and purged with nitrogen three times. Then, hexadiene (335 µl, 2.82 mmol) was added. The mixture was allowed to warm slowly to room temperature and stirred overnight. After removal of the platinum catalyst by filtration over a platinum glass microfibre filter, a colourless solution was obtained. Part of the toluene was removed in a partial vacuum to obtain the gel for film coating as highly viscous liquid. Copolymer **2** was prepared in the same way from monomer **6** (300 mg, 0.29 mmol) and hexadiene (140 µl, 1.18 mmol).

For copolymer **1**: EA(%): Found: Si, 41.9; C, 15.3; H, 4.3. Calcd: Si, 44.5; C, 14.3; H, 3.2. FTIR (KBR, cm^{-1}): ν C-H: 2950, 2924, 2853; ν Si-H: 2261; ν Si-C: 1123; ν Si-O: 1070. ^{13}C{^{1}H} (100 MHz, toluene-d_8): 16.3 (-CH_2), 17.8 (-CH_2), 18.6 (-CH_2). ^{29}Si-NMR (71.5 MHz, toluene-d_8 dept_nondecoup): -68 (-$(CH_2)_6$-Si), -82.8 ($HSiO_3$).

For copolymer **2:** EA(%): Found: Si, 42.8; C, 18.1; H, 3.7. Calcd: Si, 41.8; C, 24.0; H, 5.2. FTIR (KBR, cm^{-1}): ν C-H: 2960, 2924, 2858; δ CH_2: 1458, δ CH_3: 1411; ν Si-H: 2147; ν Si-CH_3: 1256; ν Si-O-Si: 1086; ν Si-CH_2: 778. ^{29}Si-NMR (71.5 MHz, C_6D_6 dept_nondecoup): 11.9 (-CH_2-SiMe_2-O); -2.7 (H-SiMe_2-)O.

Preparation of copolymers **3** and **4**:

For copolymers **3** and **4**, the monomers $[(EtO)_3Si(CH_2)_2]_8Si_8O_{12}$, T_8^R (**7**) and $[(EtO)_3Si(CH_2)_2SiMe_2O]_8Si_8O_{12}$, $Q_8M_8^R$ (**8**) were synthesized. 8 equivalents of $(CH_2=CH)Si(OEt)_3$ (5.68 mmol for **5** and 2.32 mmol for **6**) were added to a mixture

containing 300 mg (0.71 mmol) $H_8Si_8O_{12}$, T_8^H (**5**) or 300 mg (0.29 mmol) $(HSiMe_2O)_8Si_8O_{12}$, $Q_8M_8^H$ (**6**) in toluene (30 ml) and 10 mol% platinum sponge. After the mixture had been stirred overnight, the toluene was removed and the product dried under vacuum at room temperature. For polycondensation a solution of **7** or **8** was stirred at room temperature in an open flask, which led, after a certain period of time (ca. 5 hours), to a transparent colourless gel. Latter was used for the preparation of the coating film.

For copolymer **3:** EA(%): Found: Si, 28.7; C, 30.4; H, 5.7. Calcd.: Si, 23.1; C, 39.5; H, 7.9. FTIR (KBR, cm^{-1}): ν C-H: 2971, 2924, 2878; δ CH_3: 1385; ν Si-H: 2249; ν Si-CH_2: 1133; ν Si-O-Si: 1058, ν Si-H: 862. ^{29}Si-NMR (71.5 MHz, C_6D_6 dept_nondecoup): -45.2 (-CH_2-Si$(OEt)_3$), -66.2 (-CH_2Si$(OSi)_3$), -85.8 ($HSiO_3$).

For copolymer **4:** EA(%): Found: Si, 27.2; C, 33.5; H, 4.6. Calcd: Si, 28.5; C, 37.5; H, 5.3. FTIR (KBR, cm^{-1}): ν C-H: 2965, 2918, 2877; δ CH_2: 1438 δ CH_3: 1385; ν Si-H: 2133; ν Si-CH_3: 1248; ν Si-O-Si: 1116.

Preparation of thin films:

The thin films based on polysilsesquioxanes were prepared by spin on coating techniques. The steel plates were first placed in a toluene solution for 10 minutes, then rinsed with distilled water and dried. A coating film was prepared by spin coating a toluene solution of polysilsesquioxanes **1** - **4** on steel plates using RC Spin Coater CT 62C101 (Karl Suss France S. A.). The thin films of copolymer **1** - **4** were spin coated at a speed of 2500 - 3500 rpm for 15 seconds. Spin coating was combined with argon purging at a reduced pressure (1 mbar) in order to evaporate the solvent.

Properties of thin films:

Aluminium vapour was deposited on the coating film in circles with 2.5 mm diameter (Table 2). The capacity was measured with a HP 4284 A Precision LCR Meter at 1 MHz frequency. On the same steel plate the breakdown voltage was measured with a Brandburg PS 1008 for high Voltage Unit. The thickness of polysilsesquioxane coating films was measured with a Zeiss Axiokop 50. The adhesion of the coating films on the steel plate was tested on a different steel plate with cross cutting. [17] The hardness of the coating films on steel plate was determined with a Fischerscope H - 100 interfaced with a PC using Win - HCU software to collect data. The morphology was studied using a scanning electron microscope (SEM) JSM - 5900. DSC was measured on a Perkin-Elmer DSC - 7 differential scanning calorimeter under nitrogen. Samples (5 - 10 mg) were typically equilibrated at 28 °C for 1 minute, ramped to the desired temperature (400 °C) at 10 °C/min, held at that temperature for 1 minute, and allowed

to cool back to room temperature naturally. At least two heating - cooling cycles were collected for each analysis. All data on film thickness, dielectric constant κ, breakdown voltage, film adhesion and film hardness are summarised in Table 2.

2.5 References:

[1] N.P. Hacker, *MRS Bulletin* , **1997**, *22*, 61.

[2] D.C. Edelstein, G.A. Sai-Halasz Y.J. Mii, *IBM J. Res. Develop.*, **1995**, *39*, 383.

[3] M.H. Tsai, W.T. Whang, *Copolymer*, **2001**, *42*, 4197.

[4] Y. Abe, K. Kagayama, N. Takamura, N. Takahashi, *J. Non-Cryst. Solids*, **2000**, *261*, 39.

[5] B. Zhu, D.E. Kattttsoulis, F.J. McGarry, *Copolymer*, **2000**, *41*, 7559.

[6] Q. Pan, G.B. Gonzalez, R.J. Composto, D.H. Berry, *Thin Solid Films*, **1999**, *345*, 244.

[7] W.W. Lee, P.S. Ho, *MRS Bulletin* **1997**, *22***(10)**, 19.

[8] Handbook of multilevel Metallization for integrated Circuits, in: S.R. Wilson, C.J. Tracy, J. L. Freeman Jr (Eds). Materials, Technology, and Applications, Noyes Publications, Park Ridge, NJ 1993.

[9] P.G. Harison, *J. Organomet. Chem.*, **1997**, *542*,141.

[10] Ch.X. Zhang, F. Babonneau, C. Bonhomme, A.F. Yee, *J. Am. Chem. Soc*. **1998**, *120*, 8380.

[11] R.M. Laine, A. Sellinger, V. Chu, C. Viney, *J. Polym. Sci.: Part A, Polym. Chem.*, **1994**, *32*, 3069.

[12] P.A. Agaskar, *Inorg. Chem*. **1991**, *30*, 2707.

[13] T.E. Gentle, A.R. Bassindale, *J. Inorg. Organomet. Polym.*, **1995**, *5* (3), 281.

[14] G. Cerveau, R.J.P. Corriu B. Dabiens, *J. Mat. Chem.*, **2000**, *10*, 1113.

[15] G. Cerveau, R.J.P. Corriu, *Coord. Chem. Rev*., **1998**, *178 – 180*, 1051 and references therein.

[16] D.A. Loy, J.P. Carpenter, T.M. Alam, J.H. Small, K.J. Shea, *J. Am. Chem. Soc.*, **1999**, *121*, 5413.

[17] Damage category of cross cutting based on EN ISO 2409.
For check of film adhesion a grid system surface must be scratched on the film: With a sharp knife six parallel and six vertical lines are scratched in a distance of 1 mm into the surface. Then a tape is stuck over the grid system and taken off evenly. The surface can be evaluated to place the material in the appropriate damage category.

[18] R.H. Baney, M. Itoh, A. Sakakibara, T. Suzuki, *Chem. Rev*., **1995**, *95*,1409.

[19] H.S. Yang, S.Y. Choi, S.H. Hyun, H.H. Park, J.K. Hong, *J. Non-Cryst. Solids*, **1997**, *221*, 151.

[20] Y. Abe, K. Kagayama, N. Takamura, T. Gunji, *M. R. S. Symp. Proc.*, **1999**, *565*, 247.

[21] C. Maddalon, K. Barla, E. Denis, C. Lair, E. Dehan, *Microelectron. Eng.*, **2000**, *50*, 33.

[22 J.K. Lan, Y.L. Wang, Y.L. Wu, H.C. Liou, Y.L. Cheng, *Thin solid films*, **2000**, *377-378*, 776.

[23] J.K. Lee, K. Char, H.W. Rhee, D.Y. Yoon, *Copolymer*, **2001**, *42*, 9085.

[24] R.F. Cook, E.G. Liniger, D.P. Klaus, S.A. Cohen, *M. R. S. Symp. Proc.*, **1998**, *511*, 31.

[25] J.F. Remenar, C.J. Hawker, J.L. Hedrick, D.Y. Yoon, *M. R. S. Symp. Proc.*, **1998**, *511*, 69.

[26] S.J. Ding, P.F. Wang, D. W. Zhang. W.W. Lee, *Materials Letters*, **2001**, *49*, 154.

[27] S.M. Kim, D.Y. Yoon, *Mat. Res. Soc. Symp. Proc.* **1998**, *511*, 39.

[28] H.E. Gottlieb, V. Kotlyar, A. Nudelman, *J. Org. Chem.* **1997**, *62*, 7512.

Chapter 3

Using of microporous nanocrystalline particles silicaite-1 to increase the film porosity for ultra low-κ dielectric application

Abstract

The synthesis and the characterization of a novel composite material containing zeolite nano-crystals (silicalite-1) and silsesquioxane polymers are reported for the first time. The new group of materials has low density and values for the dielectric constant as low as 1.7. The material can be spin coated as is compatible with typical handling procedures in the semiconductor industry.

3.1 Introduction

As on-chip device densities increase and active device dimensions shrink, propagation delay, cross-talk, and power dissipation become significant factors due to increased resistance-capacitance (RC) coupling. Integration of low dielectric materials will partially mitigate these problems. Intense research has been directed towards materials with low dielectric constants (κ) for inter-metal-dielectric integrated-circuit (IMD-IC) applications. [1] Currently, the industrial standard for dielectric materials is SiO_2 with κ = 4.0. In order to reduce the κ value relative to that of SiO_2, it is necessary to incorporate atoms and bonds that have a lower polarizability and/or to lower the density of the material. [2] The synthesis strategy for the silica-based materials described here is to use a strong and rigid SiO_2 network as a starting point and to lower the κ value by reducing the material density through incorporation of organic substituents and voids into the film.

The most promising potential candidates for low κ interconnection materials are inorganic/organic hybrid materials. [3] Especially silsesquioxanes, which generally adopt a polyhedral geometry with O-Si-O backbones, are suitable precursors. [8-11] In the silsesquioxanes, each silicon atom is bound to one chemical substituent group such as hydrogen, alkyl, or phenyl, which results in a nominal stoichiometry $R_8Si_8O_{12}$. The cross-linking density and the material density strongly depend upon these terminating groups. The low dielectric constant of materials based on silsesquioxanes is mainly attributed to the generally low density. For example, the density of crystalline hydrogen silsesquioxane $H_8Si_8O_{12}$ (κ = 2.9, ρ = 1.4 g/cm^3) [4] is about one third lower than that of SiO_2 (ρ = 2.5 g/cm^3).

Recently, we have reported on silsesquioxane based polymers with dielectric constants κ in the range of 2.1 - 2.7 [5] having good mechanical strength, and high thermal stability. The polymers are formed in a sol-gel process where cubic $R_8Si_8O_{12}$ octamers with 4,4' cage structure are connected to form a well-defined three-dimensional network. In the polymer each silicon atom of one cage is connected through organic linkers (containing alkyl-chains) to another silsesquioxane cage. It is well known, that the C-C single bonds in alkyl-chains have one of a very low electronic polarizability. Concurrently, the material density is reduced by a relatively open structure of the polymers.

Incorporated gases have κ values close to one, although the low breakdown voltage, low mechanical strength (induced by voids) and low thermal conductivity are

disadvantageous. Therefore, further reduction in dielectric constant will be achieved by introducing porosity into the materials. Here, we report on introducing silicalite-1 nano-particles into the polymer matrix to increase its effective porosity. Silicalite-1 is a hydrophobic zeolite of the MFI type. [7, 15-17] The pore system of zeolite nano-particles will be closed by incorporation in the polymer matrix potentially providing a low diffusivity for ions, such as Cu cations. The main function of the polymer is to provide mechanic stability and flexibility.

Here we report our first results on a new series of composite films based on silicalite-1, and a silsesquioxane polymer, which is formed by hydrolytic condensation of the monomer $[(EtO)_3Si(CH_2)_2]_8Si_8O_{12}$. Film composition, atomic density and porosity of the composite films were determined by elastic recoil detection analysis (ERDA). [12-14]

3.2 Results and Discussion

The polymer matrix for the composite films was synthesized by hydrolytic condensation of monomers $[(EtO)_3Si(CH_2)_2]_8Si_8O_{12}$ with water. [5] The reaction is very selective, gives few side products and occurs at room temperature. To chemically connect the nano-particles of silicalite-1 with the polymer (see Equation 3.1), the precursor $[(EtO)_3Si(CH_2)_2]_8Si_8O_{12}$ (referred to as A) was first reacted with the terminal OH-groups of the silicalite-1 nanoparticles (referred to as B). Subsequently, the remaining ethoxy groups were reacted with water to form the polymer matrix. The reaction was performed with volume ratios of A/B = 9:1, 8:2, 7:3, i.e., the concentrations of the reactants were chosen in such a way that the ratio between the volume of polymer matrix and the volume of the nanoparticles in the final material was A/B. The calculations were based on the known densities of silicalite-1 (ρ=1.81 g/cm^3) and polymer (ρ = 1.20 g/cm^3).

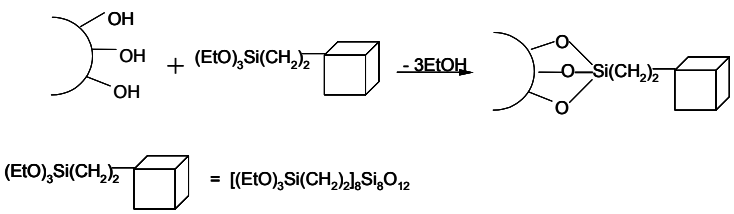

Equation 3.1 Hydrolytic polycondensation between silsesquioxane and terminal Si-OH groups of silicalite-1.

A colourless highly viscous gel was obtained after partial removal of the solvent and was spin coated as thin film on a support (steel plate, Si-wafer). Table 3.1 summarizes the

physical data of the prepared composite films including film thickness, density, porosity, dielectric constant, breakdown voltage and film hardness. Composite films were typically prepared with a thickness between 400 and 640 nm, although thinner and thicker films can be obtained. Fig. 3.1a shows an AFM image of the composite film (A/B = 9:1). Embedded nanoparticles of silicalite-1, which are close to the surface and give rise to "hills" with less than 5 nm height, are clearly observed (Fig. 3.1a). SEM of the film cross section shows that the composite film has a uniform thickness of 400 nm (Fig. 3.1b).

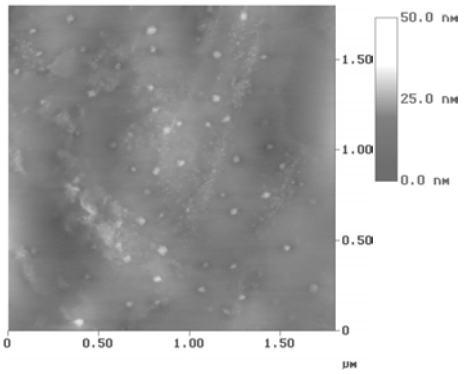

Fig. 3.1 a. AFM image of film surface (A/B = 9:1)

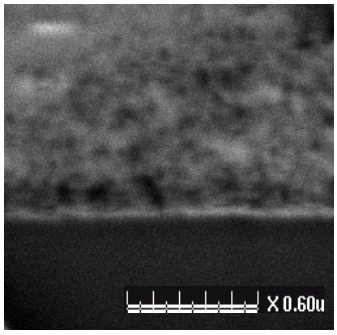

Fig. 3.1 b. SEM image of cross section (A/B = 8:2)

Unlike traditional homogenous dielectric materials, the two phase structure of the porous network significantly alters the electric and mechanical properties. The dielectric constant κ of the nano-porous composite films decreased from 2.4 for the pure silsesquioxane polymer [5] linearly with the fraction of zeolite added to 1.7 for a composite material with 10 vol% zeolite embedded (Fig. 3.2). This is highly surprising as the expected dielectric constant of the zeolite should be around κ = 2.5 based on the density of the Si-O tetrahedra in the zeolite structure [21] and the dielectric constant of SiO_2.

For a given chemical composition, the κ value of a material is determined by its intrinsic density and porosity. In the present case the heterogeneous material consists of a zeolite component and the silsesquioxane polymer each having an intrinsic material density, which leads to dielectric constants, which are significantly lower than that of pure SiO_2. By incorporating nanoparticles in the polymer matrix, voids are created adding to the porosity of the resulting material and reducing the overall density in the material.

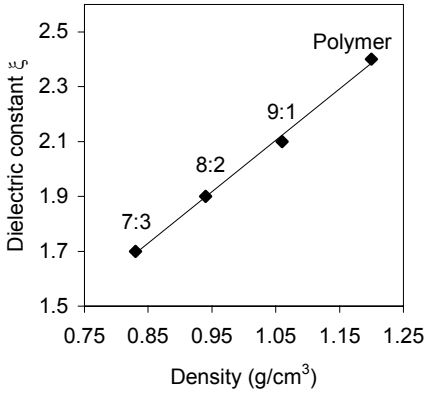

Fig. 3.2 Dependence between the density and the dielectric constant of the composite films. The ratios indicate the volume ratios between matrix and silicalite-1 in the composite.

To explore the porosity of the composite films the overall film density was determined from the elemental composition using elastic recoil detection analysis (ERDA). The method is based upon directing a beam of high-energy ions (^{127}I, 170 MeV) towards the sample surface and measuring number direction and energy distribution of the scattered particles. Both depend upon the mass of each element (H, C, O, Si) in the sample and the composition of the film. ERDA was used to determine the density of the composite films, as the closed pore system is not accessible to more conventional techniques, such as physisorption of unreactive gases at low temperatures. The porosity P was calculated from the density ρ of the composite film according to $P = 1- \rho /\rho_0$, and is given relative to the porosity P_0 for the parent polymer film (ρ_0 =1.20 g/cm^3). Clearly the porosity of the composite films increased linearly with increasing amount of silicalite-1 in the composite.

Table 3.1 Characteristic data of the composite films.

Volume ratio of A/B	Film thickness (nm)	Film density (g/cm^3)	Porosity (%)	Dielectric constant κ	Breakdown voltage (MV/cm)	Hardness HU** (GPa)
10:0	480	1.20	≡ 0	2.4	0.38	0.51
9:1	400	1.06	11.7	2.1	0.35	0.37
8:2	640	0.94	21.7	1.9	0.30	0.29
7:3	530	0.83	30.8	1.7	0.28	0.18

*: $[(EtO)_3Si(CH_2)_2]_8Si_8O_{12}$ referred to as A and silicalite-1 referred to as B

**: HU: universal hardness

When following the rule-of-mixture [6] the dielectric constant of a composite should be the weighted sum of the dielectric constants of the single components. With a density ρ = 1.20 g/cm^3 and κ = 2.4 for the parent polymer film and ρ = 1.81 g/cm^3 [21] and κ = 2.8 for crystalline silicalite-1, an increase in the dielectric constant of the film is to be expected. It is important to note, however, that pressed silicalite-1 discs and silicalite-1 films show values for κ between 2.1 [22] and 2.2 [23]. This indicates that additional voids in these films are being created in the process of forming the disc or the pure silicalite-1 film. For a powderous sample of the silicalite-1 nanoparticles used in this study we have determined ρ = 0.26 g/cm^3 and κ = 1.02 ± 0.08 (calculated with 100 mg silicalite-1 in volume of 0.385 cm^3 (radius: 15 mm, depth: 0.5 mm). The extremely low density notifies that the particles could not be packed more densely because of their small diameter (30 - 50 nm). Additionally, defects on the surface of the particles might also lead to the apparently much lower density than measured for larger crystals of silicalite-1. This is also supported by a high BET surface area of the nanoparticles which was 568 m^2/g. Closer inspection of the adsorption isotherm showed that the micropore and mesopore surface areas were 100 and 468 m^2/g, respectively. Latter corresponds to the outer surface area of the particles and is much higher than for more conventional materials. In this respect it is known that the surface area of particles increases relative to the volume when the particle size decreases. Assuming perfect spheres, [24] a density of 0.26 g/cm^3 is calculated for particles with 50 nm diameter and 468 m^2/g outer surface area.

Parallel to the decreasing density the dielectric constant κ of the composite films decreased almost linearly with increasing zeolite concentration in the film (see Fig. 1). This suggests that the introduction of zeolite crystals into the polymer leads to the formation of additional pores and/or to the formation of a less dense silsesquioxane polymer. The relative contributions of the two potential effects are unclear at present. The constant impact per weight fraction of zeolite in the polymer film suggests that the generation of a more open structure is a generic property of the zeolites, or at least of silicalite-1. As the apparent density and porosity of the sample is directly related to the dielectric constant, the direct proportionality between the dielectric constant and the film porosity is a logical consequence.

Both proposed causes for the reduced density of the material seem equally plausible. In the initial phase for the synthesis of silsesquioxane monomers react with the hydroxy groups of the mildly activated zeolite, forming ethanol. As only Si-OH groups are present on the outside of the zeolite the linking to the hydroxy groups occurs directly to the outer surface of the zeolite. These hydroxy groups are well separated and may - with a spherical particle -

cause a dendrimer-like growth of the silsesquioxane polymer. Such a situation should lead to an area of reduced material density around zeolite particles. On the other hand patches free of hydroxy groups on the particle surface may inhibit binding of silsesquioxane monomer and hence lead to voids once the polymer densifies around the zeolite particle. A lower density of the polymer in the proximity of nanoparticles could clearly be confirmed by TEM of a composite film, which had been detached from the support (Fig. 3.3).

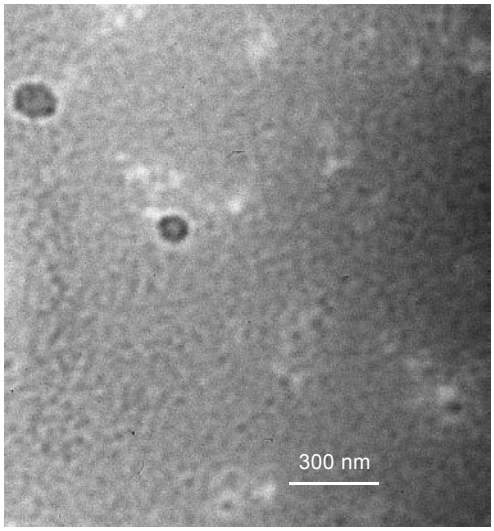

Fig. 3.3 TEM image of a composite film (A/B =9/1)

The diameter of the silicalite-1 pores (5.5-6.5 Å) is too small to allow silsesquioxane cubes (d = 1.8 nm) to penetrate into the micropore system (Fig. 3.4). Because the particles are completely surrounded by the polymer matrix, the micropores are micro- and macroscopically closed in the composite film. The closed pores and their inaccessibility to substrate or gas molecules in turn suggest drastic reduction of the migration of metal-ions through the dielectric layer. Metal-ion migration occurs with high selectivity through the zeolite channels. Note that a reduction in ion migration has significant advantages in the integration technology as the composite material can be used as passivation layer or as diffusion barrier. Especially, Cu diffusion in the low κ interconnection layer needs to be minimized.

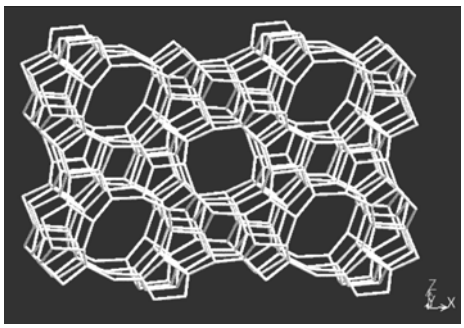

Fig. 3.4 Pore system of MFI zeolites

The low scatter between measurements at different points in the film suggests that, if pores are present in the material they must be small and well-spaced. Similarly, the electric breakdown should be limited by the absence of any randomly occurring large pores. [2] The results show that the breakdown voltage of the composite films is in the range of 0.28-0.35 MV/cm. Although decreasing slightly with the amount of embedded silicalite-1 the breakdown voltage is of the same magnitude as for the polymer film (0.38 MV/cm). The lower breakdown voltage relative to typical values (1-5 MV/cm) reported for industrial dielectrica [18,19] appears to be intrinsically linked to the low density of the composite.

The embedded silicalite-1 particles currently have a particle size between 30 and 50 nm (Fig. 3.5). This allows a homogeneous packing of the nanoparticles in the dielectric layers used in current microprocessors with design features of 180 nm. It has been predicted that by 2005 the design features will be smaller than 65 nm and dielectric materials with κ lower than 2.2 are required. [1] The size of particles included in the film must then be lower than 10 nm and synthesis conditions to obtain such zeolite particles are described in Chapter 4. The question arises at this point, however, whether or not microporous materials are necessary to induce the lowering of the dielectric constant.

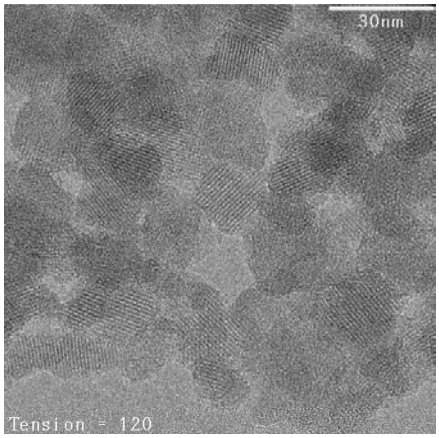

Fig. 3.5 TEM image of silicalite-1 nanoparticles

3.3 Conclusions

A novel composite consisting of zeolite nanoparticles and a silsesquioxane polymer matrix with ultra low dielectric constant has been synthesized. Thin composite films were prepared with the monomer $[(EtO)_3Si(CH_2)_2]_8Si_8O_{12}$ and silicalite-1 nanoparticles (30 - 50 nm diameter). The films display very interesting electronic properties, in particular, a much lower dielectric constant in the range 1.7 - 2.1 compared to the polymer film (κ = 2.4). This decrease is concluded to result from the zeolite directed reduction of the intermolecular packing of the silsesquioxane cubes in the polymer or the generation of well distributed small voids around the particles. The new preparation procedure leads in the first step to a coating of the zeolite nanoparticles with the silsesquioxane monomer by chemical reaction of the zeolite hydroxy groups with the silsesquioxane monomer. Given the solvent polarity it can be safely assumed that in such a situation the polymer will have a maximum spread distance around the zeolite particle. The initial coating appears to induce controlled hydrolysis in the second stage in such a way that the distances between silsesquioxane units are maximized and hence the physical density of the resulting film is minimized.

3.4 Experimental

Materials and Methods

Polymeric materials were prepared in an atmosphere of dry nitrogen using standard Schlenk techniques. Toluene (Aldrich, dry, ≤ 0.2% H_2O) was distilled from sodium under nitrogen. All other reagents were obtained from Aldrich and were used as received. Octahydridosilsesquioxane $H_8Si_8O_{12}$ was synthesised according to the procedure described by *Agaskar*. [20] TEOS and TPAOH were purchased from Merck and Chempur, respectively.

Preparation of monomer $[(EtO)_3Si(CH_2)_2]_8Si_8O_{12}$

Octahydridosilsesquioxane $H_8Si_8O_{12}$, T_8^H (300 mg, 0.71 mmol) and platinum sponge (14 mg, 0.071 mmol) were added to 20 ml dry toluene in a 50 ml Schlenk flask. The solution was cooled to 0°C, degassed and purged with nitrogen three times. Then, triethoxyvinylsilane (1.19 ml, 5.65 mmol) was added. The mixture was allowed to warm slowly to room temperature and stirred overnight. The platinum catalyst was completely removed by filtration over a glass microfibre filter (GF/D, Whatman®). The compound $[(EtO)_3Si(CH_2)_2]_8Si_8O_{12}$ was obtained as colorless solid after evaporation of the solvent.

EA(%): Found: Si, 23.5; C, 39.1; H, 8.1. Calcd($C_{64}H_{152}Si_{16}O_{24}$): Si, 23.1; C, 39.5; H, 7.9. FTIR (KBr, cm^{-1}): ν C-H: 2981, 2936, 2898; δ CH_3: 1390; ν Si-H: 2258.4; ν Si-C: 1149; ν Si-O: 1071. ^{1}H-NMR (400 MHz, C_6D_6): δ 3.83 (q, -OCH_2, *J* = 7 Hz), 1.15 (t, CH_3, *J* = 7 Hz), 0.97 (m, -CH_2Si), 1.35 (m, -CH_2Si). ^{29}Si-NMR (71.5 MHz, DETP-Experiment, C_6D_6): -45.2 (-CH_2-Si$(OEt)_3$), -66.2 (-CH_2Si$(OSi)_3$).

Synthesis of Silicalite-1 [15]

A precursor sol was prepared by hydrolyzing tetraethyl orthosilicate (TEOS) with a dilute solution of tetrapropylammonium hydroxide (TPAOH) in water/ethanol at room temperature to give a clear homogeneous solution with the following molar composition: 9 TPAOH : 25 SiO_2: 480 H_2O : 100 ethanol. The sol was hydrolyzed at room temperature for at least 24 hours by shaking on a gyratory shaker. The transparent solution was then refluxed for 12 hours in a preheated oil bath maintained at 98°C. The solids were separated from the mother liquor by centrifugation and repeatedly washed with distilled water until the wash water had a pH lower than 8. The sample was re-dispersed in distilled water and freeze-dried. The yield on silicon basis was > 75%. The sample was then calcined in a stream of nitrogen at 550°C for 2 hours and, subsequently, in a flow of air for 10-12 hours at the same temperature. The mean particle size was determined to 30-50 nm by dynamic light scattering.

Nanoporous composite material

A solution of $[(EtO)_3Si(CH_2)_2]_8Si_8O_{12}$ in toluene (30 cm^3) was mixed with a suspension of silicalite-1 in ethanol (10 cm^3) and heated to reflux (111°C) for 24 hours under nitrogen (quantities see Table 2). The flask was then opened to ambient air and stirred for another 2 h allowing the monomer to react with moisture at the room temperature. Partial removal of the solvent provided a viscous gel. Prior to their use steel plates and Si-wavers were first placed in a toluene solution for 10 minutes, rinsed with distilled water and dried. Coating films were prepared by spin coating the viscous gel on the steel plates using a RC Spin Coater CT 62C101 (Karl Suss France S. A.). All thin films were spin coated at a speed of 2500 - 3500 rpm for 10-15 seconds. Subsequently, the film was heated at 130°C for 120 min in air to remove any residual solvent.

Table 2 Quantities of silsesquioxane and silicalite-1 used in the synthesis of composite material

Volume ratio of A/B*	Amount of $[(EtO)_3Si(CH_2)_2]_8Si_8O_{12}$ (mg)	Amount of silicalite-1 (mg)
10:0	100	—
9:1	82	18
8:2	66	32
7:3	55	45

*: $[(EtO)_3Si(CH_2)_2]_8Si_8O_{12}$ referred to as A and silicalite-1 referred to as B

Properties of thin films

Aluminum vapor was deposited on the coating film in circles with 2.5 mm diameter and the capacity was measured with a HP 4284 A Precision LCR Meter at 1 MHz frequency. The breakdown voltage was measured on the same sample with a Brandburg PS 1008 for high Voltage Unit. The thickness of the composite films was subsequently measured with electron microscopy (SEM, JSM – 5900) after cutting the plate. To investigate the porosity of the composite films the film density was determined from the elemental composition using elastic recoil detection analysis (ERDA) with high energy ions (^{127}I, 170 MeV). The hardness of the coating films was determined with a Fischerscope H - 100 interfaced with a PC using Win - HCU software to collect the data. The morphology of the nano-particles and the film surface was studied by TEM (JEOL 2010) and atomic force microscopy AMF (Multi Mode^{TM} Digital Instruments, Incorporated), respectively. For TEM images of the composite films, films were prepared on NaCl plates, the NaCl dissolved in water and films floating at the surface transferred to TEM grids. The measurement of nitrogen sorption was determined using a ASAP 2010 (Micrometrics). Pore size distributions were obtained from the N_2 desorption branch, using the BJH method, and surface areas where calculated by the BET method.

3.5 References

[1] *The International Technology Roadmap for Semiconductor*, Semiconductor Industry Association, San Jose, C.A. 2001.

[2] Morgen, M.; Ryan, E. T.; Zhao J. H.; Hu, C.; Cho, T. & Ho, P. S. Low dielectric constant materials for ulsi interconnects. *Annu. Rev. Mater. Sci*., **2000**, *30(1)*, 645.

[3] Shea, K. J. & Loy, D.A. Bridged polysilsesquioxanes. Molecular-engineered hybrid organic-inorganic materials. *Chem. Mater.*, **2001**, *13***,** 3306.

[4] Bremmer, J. N.; Liu, Y.; Gruszynski, K. G. & Dall, F. C. Cure of hydrogen silsesquioxane for intermetal dielectric applications*. Mat. Res. Soc. Symp. Proc.,* **1997**, *476*, 37.

[5] Su, R. Q.; Müller, T. E.; Procházka J. & Lercher, J. A. A new type of low-κ dielectric films based on polysilsesquioxanes. *Adv. Mat.,* **2002**, *14(19)*, 1369-1373.

[6] Kirschhock, C. E. A.; Ravishankar, R.; Verspeurt, F.; Grobet, P. J.; Jacobs, P. A. & Martens J. A. Identification of precursor species in the formation of MFI zeolite in the TPAOH-TEOS-H_2O System. *J. Phys. Chem. B*,, **1999**, *103*, 4965.

[7] Xu, J.; Moxom, J.; Yang, S.; Suzuki R. & Ohdaira, T. Dependence of porosity in methyl-silsesquioxane thin films on molecular weight of sacrificial triblock copolymer. *Chem. Phys. Letters*, **2002**, *364(3)*, 309.

[8] Chang, T. C.; Mor, Y. S.; Liu, P. T.; Tsai, T. M.; Chen, C. W.; Sze S. M. & Mei, Y. J. Improvement of low dielectric constant methylsilsesquioxane by boron implantation treatment. *Thin Solid Films*, **2001**, *398-399*, 637.

[9] Maddalon, C.; Barla, K.; Denis, E.; Lous, E.; Perrin, E.; Lis, S.; Lair C. & Dehan E. Planarization properties of hydrogen silsesquioxane (HSQ) influence on CMP, *Microelectron. Eng.*, **2000**, *50(1-4)*, 33.

[10] Lee, J.-K.; Char, K.; Rhee, H.-W.; Ro, H. W.; Yoo D. Y;. & Yoon D. Y. Synthetic control of molecular weight and microstructure of processible poly(methylsilsesquioxane)s for low-dielectric thin film applications. *Polymer,* **2001**, **42(21)**, 9085.

[11] Gracin, D.; Jaksic, M.; Bogdanovic-Radovic, I.; Medunic, Z.; Car T. & Pracek B. Characterization of amorphous silicon carbon alloys by IBA technique and optical spectroscopy. *Vacuum,* **2002**, *67(3-4)*, 519.

[12] Mayer, M. Ion beam analysis of rough thin films. *Nucl. Instr. Meth. B.*, **2002**, *194(2)***,** 177.

[13] Lieb, K. P. Thin film analysis via accelerator-based nuclear methods. *Thin Solid Films,* **2000**, *380/1-2*, 269.

[14] Dollinger, G.; Frey, C.M.; Bergmaier, A. & Faestermann, T. Elastic Recoil Detection with single atomic layer depth resolution. *Nucl. Instr. Meth. B.,* **2002**, *138*, 603.

[15] Larlus, O.; Valtchev, V.; Patarin, J.; Faust A.-C. & Maquin B. Preparation of silicalite-1/glass fiber composites by one- and two-step hydrothermal syntheses. *Micropor. Mesopor. Mater.*, **2002**, *56(2)*, 175.

[16] Tosheva, L.; Valtchev V. & Sterte J. Silicalite-1 containing microspheres prepared using shape-directing macro-templates. *Micropor. Mesopor. Mater.*, **2000**, *35-36*, 621.

[17] Tsay C. S. & Chiang A. S. T. The synthesis of colloidal zeolite TPA–silicalite-1. *Micropor. Mesopor. Mater.*, **1998**, *26(1-3)*, 89.

[18] Ding S.-J.; Wang P.-F.; Zhang D.W.; Wang J.-T.; Lee W.W. A novel structural amorphous fluoropolymer film with an ultra-low dielectric constant. *Materials Letters,* **2001**, *49(3-4)*, 154.

[19] Kim S. M. & Yoon, D. Y. *Mat. Res. Soc. Symp. Proc.,* **1998**, *511*, 39.

[20] Agaskar, P. A. New synthetic route to the hydridospherosiloxanes O^h-$H_8Si_8O_{12}$ and D^{5h}-$H_{10}Si_{10}O_{15}$. *Inorg. Chem.*, **1991**, *30(13)*, 2707.

[21] Density of single crystals, Database of Zeolite Structures, IZA Structure commision, 2000, http://www.crystal.mat.ethz.ch/IZA-SC/Atlas_pdf/MFI.pdf

[22] EIS (Electrochemical Impedance Spectroscopy) measurements on a silicalite-1 wafer showed that silicalite-1 is a pure capacitive resistor with $\kappa = 2.1(2)$.

[23] Dielectric constant of silicalite-1 films, Wang, Z. B.; Mitra, A.; Wang, H. T.; Huang, L. M.; Yan Y. Pure silica zeolite films as low-k dielectrics by spin-on of nanoparticle suspensions. *Adv. Mater.*, **2001**, *13(19)*, 1463.

[24] The equation $\delta_{bulk} = 3 / (r \times S_{BET})$ was used based on the formuli for the volume and surface area of spheres; δ_{bulk} density of a single particle, r radius of the particles, S_{BET} BET surface area.

Chapter 4

Synthesis and characterization of mesostructured SBA-15 nanoparticles and silicalite nanocrystalline particles

Abstract

Mesoporous material SBA-15 is an interesting class of materials for technological applications as it provides well-ordered mesoporous structures with uniform pore size combining high porosity. The material is generally synthesized under weakly acidic conditions using triblock copolymers ($EO_xPO_yEO_x$) as template. However, during traditional hydrothermal calcination to remove the surfactant template, particles with nanoscopic size tend to sinter together to larger agglomerates. In this work we present new alternative routes for removing the surfactant templates using room temperature photochemical methods (UV/O_3 or UV/H_2O_2). The effectiveness of these methods for removing the template in comparison to classic calcination is studied using BET, temperature programmed oxidation, XRD and TEM measurements.

Silicalite-1 and silicalite-2 microporous materials with particle size in the nano-scale range were synthesized from clear aqueous solutions of TEOS and tetra alkylammonium hydroxide as the organic structure-directing agent. The template was removed by hydrothermal treatment at > 500°C. The nanocrystalline particles were characterized using X-ray diffraction, scanning electron microscopy (SEM), nitrogen adsorption, and electron transmission microscopy (TEM). In Chapter 5 it will be shown that these materials are good candidates for embedding in silisesquioxane polymers for low-κ dielectric applications.

4.1.1 Introduction

As integrated circuit (IC) dimensions continue to decrease, RC delay, crosstalk noise, and power dissipation of the interconnect structure become limiting factors in ultra large scale integration (ULSI) microelectronic devices. Therefore low κ materials have been introduced as inter-level dielectrics (ILD) with reduced dielectric constant (Fig. 4.1.1). As very few dense materials have a κ below 2.5, there has been much interest in developing porous materials to achieve ultra low κ values (< 2.0). [1-5] However, there are a number of reliability concerns that are prominent for porous ILDs. One of these is mechanical strength as films with a certain distribution of voids will undoubtedly be weaker than similar fully dense materials. Another problem involves the size and shape of the pores, which can often not be controlled. This porosity makes integration very difficult, especially due to gas diffusion between interlayer materials and interaction of mobile metal cations with the processors. Composite material with a closed pore system in a homogenous matrix would therefore be especially suitable as solution to these problems. However, as the minimum device dimension reduce beyond 100 nm, the particles for this special application should be smaller than 1/10 of the device dimension, thus below 10 nm diameter.

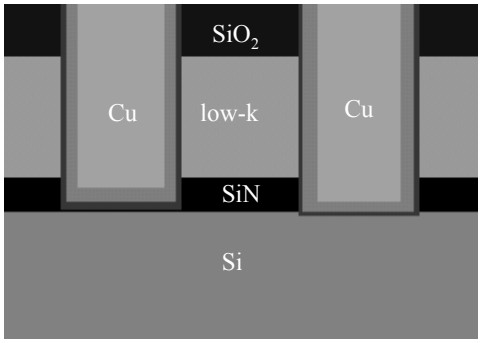

Fig. 4.1.1 Schematic diagram of the Cu/low-κ integration structure.

To construct a network of pores in the nanoparticles the main method involves the use of a surfactant template. Generally a template is described as a central structure around which a network is formed. The templating process typically comprises the use of a synthesis solution containing the template molecules or assembly of molecules. When the material which makes up the walls has reached a sufficient degree of condensation, the template molecules are no longer needed and can be removed to leave a porous structure behind. Latter is an essential step in the preparation of the nanoparticles, which can be used for low κ dielectric applications. Incorporation in a polymer matrix is described in Chapters 2 and 5.

The most common method to remove the template is calcination. In this method, the as-synthesized material is heated (usually to 450°C) in flowing oxygen or air, to burn away the organic chains. [15-18] For low κ applications the diameter of the embedded nanoporous particles needs to be below 10 nm. However such small particles tend to sinter together upon such strong heating. Consequently it is difficult to obtain well-separated nanoparticles with an ordered pore system. Alternative methods such as plasma edging and supercritical fluid extraction [14] were investigated to remove the organic surfactant, while other studies have used extended washing or ion exchange of the surfactant. [20,21] These alternative methods either also involve heating to high temperatures or great amounts of organic solvent are required. With large amounts of organic solvent the separation of nanoparticles (< 50 nm) becomes problematical.

Ordered mesoporous silica can be synthesized using poly(alkylene oxide) triblock copolymers as surfactant. The triblock copolymers exhibit outstanding interfacial stabilization properties and their ordering properties can be tuned nearly continuously by adjusting solvent composition, molecular weight, or copolymer architecture. This type of template has the particular advantage that poly (alkylene oxide) can be decomposed below 200°C under mild conditions. [12] This can be used in the synthesis of nanoparticles for low κ applications. Typically, the mesoporous silica structure of SBA-15 is prepared using triblock poly(ethylene oxide)-poly(propylene oxide)-poly(ethylene oxide) ($EO_xPO_yEO_x$). Most of the applications of SBA-15 with well-defined mesoscopic morphology are in the fields of catalysis and sorption. [11-15] In recent years, interest in the preparation and characterization of mesoporous silica has grown continuously because of their remarkable electronic, magnetic and optical properties, which differ from the bulk materials. [6,7] In this chapter we present the investigation of new methods to remove $EO_xPO_yEO_x$ from the as-synthesized SBA-15 via room temperature UV/ozone and UV/H_2O_2 treatment.

4.1.2 Results and Discussion

Well-ordered mesoporous silica structures of SBA-15 with tunable large uniform pore sizes (up to ~300 Å) are obtained by use of amphiphilic block copolymers as organic structure-directing agents. [9,10] In particular, poly (alkylene oxide) triblock copolymers with a hydrophobic polypropylene oxide (-$OCHCH_3CH_2$-) (PO) and two hydrophilic polyethylene oxide (-OCH_2CH_2-) (EO) components are good candidates, as such surfactants result in a stable textile structure and even pore diameter. The major route for synthesizing highly

ordered SBA-15 is a templating scheme where an aqueous acidic solution (HCl) containing the amphiphilic triblock copolymer is reacted with a silicate source such as tetraethoxysilicate (TEOS). The pH of the $EO_xPO_yEO_x$ solution determinates the association of H_2O molecules with the EO moieties through hydrogen-bridges. The interaction is enhanced in acid conditions, where hydronium ions, instead of H_2O molecules associate with the oxygen atoms of EO. Long range Coulomb interactions enable the co-assembly process. Stucky and his coworkers proposed that under strongly acidic conditions (pH < 1) the formation of the mesoporous structure from silica species occurres via an H-bonding based $(S^0H^+)(X^-I^+)$ pathway,[7] where S^0 is the surfactant, X^- is Cl^-, and I^+ is a protonated Si-OH moiety, such as $[SiOH_2]^+$ (Fig. 4.1.2).

It is known that the EO/PO ratio and the length of the EO blocks of the copolymer are influential factors in controlling the formation of the silica mesophase. [26-28] A low EO/PO ratio (< 0.2) of the copolymer moieties supports the formation of lamellar structured silica. Oppositely, a high ratio (>2.0) favors cubic structured silica whereas a EO/PO ratio in the range of 0.2 and 2.0 favors the formation of hexagonal mesoporous silica. Additionally, the EO chain length influences the wall thickness largely, while highly ordered domains and well-defined particles are rather dependent on the length of the PO chain. The PO chain is strongly hydrophobic, whereas the EO chain is hydrophilic, although the EO chain becomes more hydrophobic at elevated temperature. In other word, the PO chain is not appreciably hydrated, whereas the degree of hydration of the EO chain dramatically decreases at higher temperatures. [35]

$(S^0H^+)(X^-I^+)$

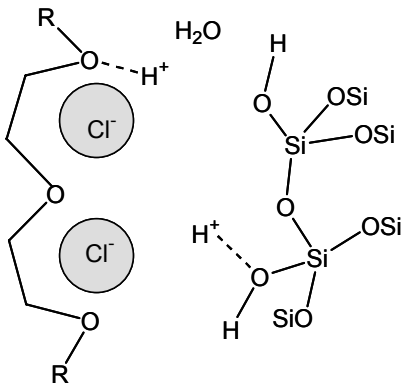

Fig 4.1.2. $(S^0H^+)(X^-I^+)$ pathway for the formation of SBA-15

In the present work, SBA-15 was synthesized with triblock copolymers (denoted as TCP) with a selection of different molecular weights and in the EO/PO ratio. The molecular

weight and EO/PO ratios are listed in Table 4.1.1. The synthesis was carried out in a similar manner as reported elsewhere. [7,8] In our preparation of SBA-15, tetraethyl orthosilicate (TEOS) as silicate source was added under stirring to a homogenous mixture of TCP, hydrochloric acid and distilled water. The resulting clear solution was kept at room temperature for 24 hours after which it was heated to 100 °C for three days.

Table 4.1.1. Triblock copolymers EO_x-PO_y-EO_x used in this study

Triblock copolymer	Molecular weight (g/mol)	(EO)x	(PO)y	EO/PO
TCP 1	8400	80	30	5.3
TCP 2	5800	20	70	0.6
TCP 3	1900	11	16	1.4

In Table 4.1.2 the synthesis conditions and characterization data of as-synthesized SBA-15 nanoparticles are summarized. Samples of 702/3 and 902/1, which were prepared using TCP 1 at pH= 0.6 and 0.9 have a similar particle size in the range. A sample synthesized using TCP3 at these two pH values had much larger particles in the range of 100-400 nm. Apparently, the shorter TCP 3 has a high tendency to form large assemblies during the templating process consisting of roughly $0.1 – 8\times10^6$ polymer molecules. Each assembly is then responsible for the formation of one SBA-15 particle. The pH value shows no influence on the synthesis with TCP 1 und TCP 3. In contrast, the pH-value showed a more pronounced influence in the synthesis with TCP 2. At pH = 0.9 the particles of 702/4 had a particle size of 45 ± 17 nm and were larger than the particles of 702/2 synthesized at pH = 0.9 (particle size 136 ± 21 nm). At low pH the hydrophilic EO chains are associated with protonated silica species through weak electrostatic interactions mediated by the negatively charged chloride ions. [29-31] TCP 2 has a relatively small EO/PO ratio of 0.6, which contains a long PO chain with 70 units. Thus, a small change in the pH will dramatically modify the strength of the overall electrostatic interaction.

Table 4.1. 2 Characteristic data of as-synthesized SBA-15 nanoparticles

Sample	Template	pH value during synthesis	Average particle size (nm)[+]	Elemental analysis C [%]	H [%]	TCP wt %
702/3	TCP 1	0.9	64 (19) *	15.2	3.4	26.0
902/1	TCP 1	0.6	56 (5) *	15.1	3.4	25.8
702/2	TCP 2	0.9	136 (21) *	16.4	3.6	27.3
702/4	TCP 2	0.6	45 (17) *	16.3	3.6	27.2
1002/1 (a)	TCP 3	0.6	100-400 **	15.7	3.5	27.0
1002/1 (b)	TCP 3	0.9	100-400 **	15.6	3.5	27.0

[+]: the standard deviation (of typically ten measurements) is given in brackets
*: particle size determined in suspension by dynamic light scattering (DLS) measurement
**: estimated from TEM images

The bulk structure of calcined SBA-15 samples was analyzed by X-ray diffraction. For the sample 702/4 a weak peak at $2\theta = 1.03°$ (d spacing of 86 Å) was observed which is in perfect agreement with the lattice spacing of 84 Å observed in TEM (Fig. 4.1.4d). For all other samples no XRD reflections of SBA-15 can be distinguished (Fig. 4.1.3). This is in agreement with a small particle size, which leads to broadening of the XRD signals. Because of the weakness of the patterns it was not possible to determine the structural phases from XRD.

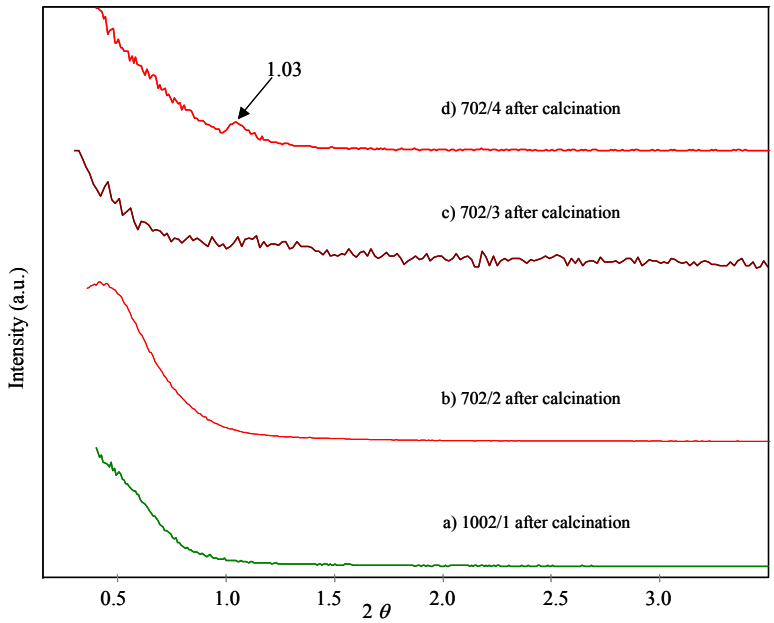

Fig. 4.1.3 XRD patterns of calcined SBA-15 synthesized with different TCPs

TEM images of SBA-15 materials are shown in Fig. 4. With TCP 1 – consisting of a central core of 30 PO units surrounded by two long chains of EO (80 units) – the synthesized SBA-15 samples 702/3 and 902/1 construct as less ordered aggregates of cubic symmetry (see Fig. 4a, 4f). Generally, the formation of hexagonal mesostructured silica was observed in syntheses with TCP 2 containing two short EO chains of 20 units and a PO chain with 70 units (Fig. 4b-d). Especially, TEM images of sample 702/4 show well-organized hexagonal features (Fig. 4c-d). At higher magnification hexagonally packed cylinders with relatively uniform ordering with spacing of ca. 84 Å can be distinguished. In comparison to TCP 2, TCP 3 contains not only short EO chains (11 units) but also a short PO chain (16 units). The TEM images of 1002/1 samples, which were prepared using TCP 3, show also hexagonal features in less ordered aggregates. It is noteworthy that particles prepared with TCP 3 were spherical whereas the particles were of irregular shape with TCP 1 and TCP 2. This strongly suggests that, in deed, large assemblies of TCP 3 molecules are reproduced by the templating scheme.

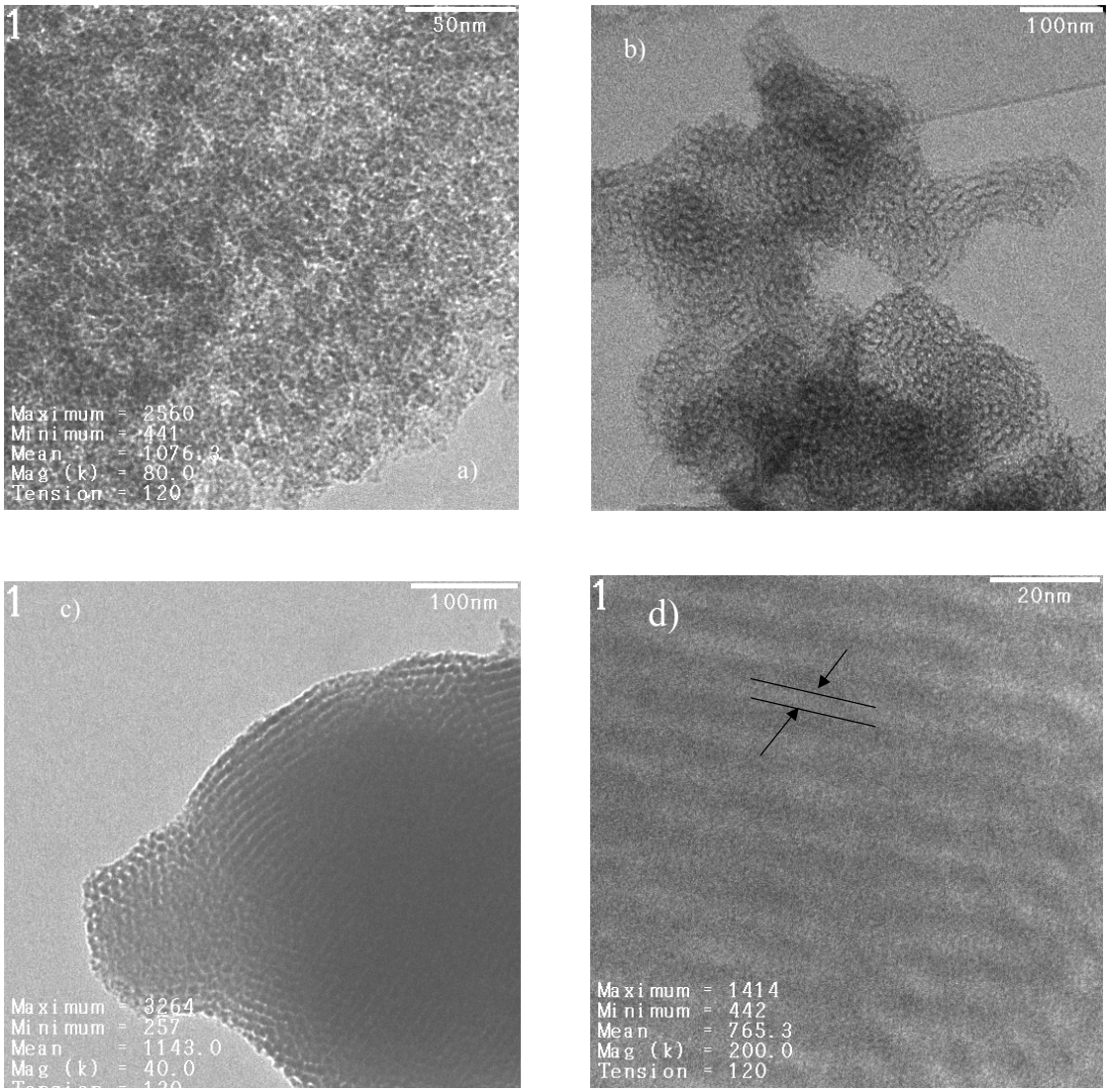

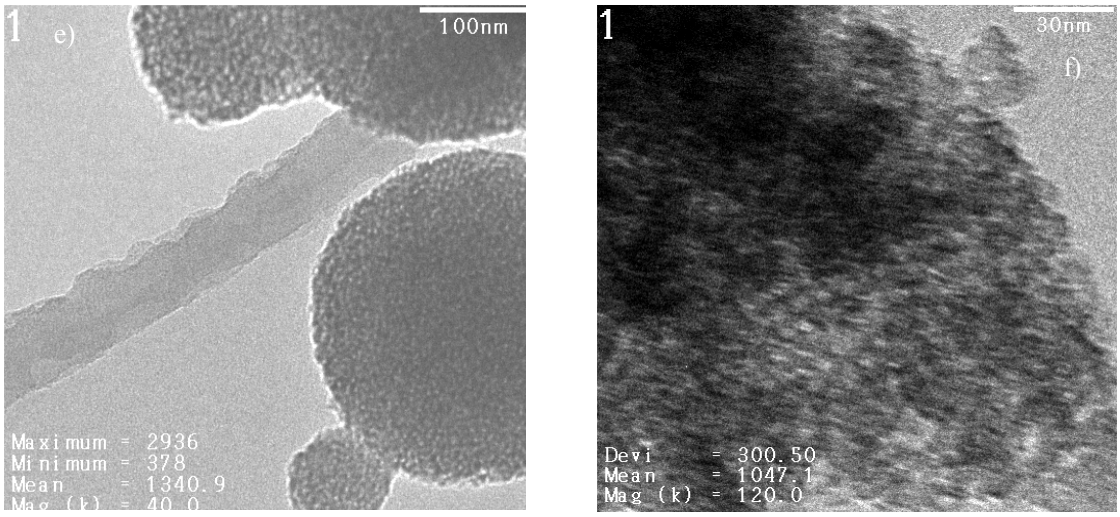

Fig. 4.1.4. Transmission electron micrographs of SBA-15 samples recorded for (a) 702/3, (b) 702/2, (c)-(d) 702/4, (e) 1002/1 and (f) 902/1

Fig. 4.1.5 shows the FT-IR spectra of SBA-15 after synthesis with different TCP as surfactant templates. The sharp band at 3735 cm^{-1} assigned to isolated SiO-H stretch vibrations, is accompanied by a broad band around 3400 cm^{-1} assigned to stretch vibrations of hydrogen bound silanol groups. Infrared vibrations at around 2800 - 3000 cm^{-1} and 1350 - 1450 cm^{-1} are assigned to C-H vibrations of the TCP templates.

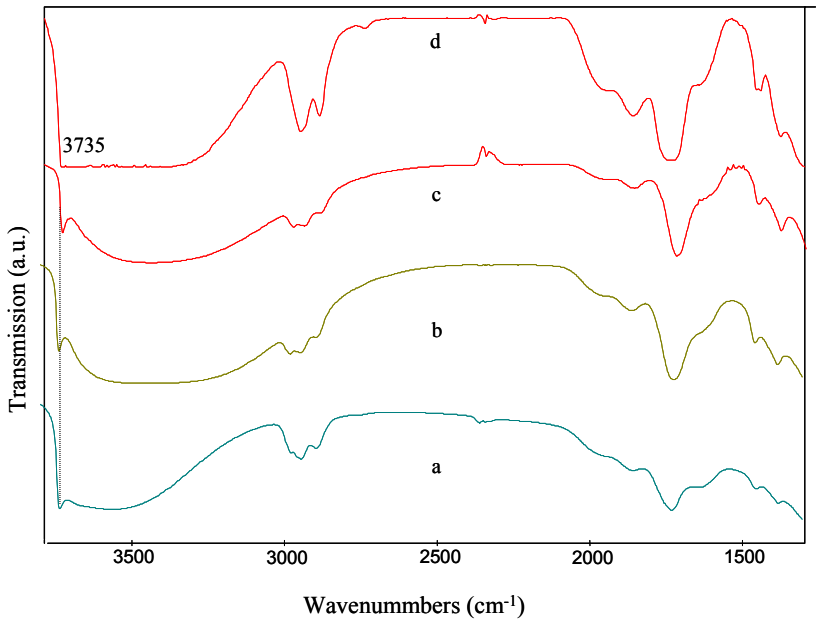

Figure 4.1.5. FT-IR spectra of as-synthesized SBA-15 nanoparticles: a) 702/2, b) 702/3, c) 702/4, d) 902/1

Removal of template

Nanoparticles with a pore system were required for the application as building block for low-κ dielectric materials. However, very small particles have much higher tendency to agglomerate compared to macroscopic particles. At the high temperatures usually used for calcination condensation reactions and thus agglomeration become faster. Therefore, a mild method for removing the template from SBA-15 nanoparticles was required. We have compared the effectiveness of three methods for removing the TCP templates including classic calcination, treatment with UV irradiation and ozone at room temperature and treatment with *in situ* generated OH radicals at room temperature. After removal of the template the samples were fully characterised with elemental analysis, powder X-ray diffraction, TEM measurements and FT-IR spectroscopy in order to confirm the final morphology and mesoscopic ordering.

Firstly the minimum temperature required for removal of TCP species from as-synthesized SBA-15 by calcination was investigated with temperature programmed oxidation. The rate of oxidation was followed by on line mass spectroscopy (Fig. 4.1.6). The oxidation reaction started at 120°C. The desorption of water, CO and CO_2 commenced in parallel reaching a first maximum at 133°C (H_2O) and 139°C (CO and CO_2) and a second maximum at 150°C. The rate of water and carbon oxide formation became very low at temperature above 190°C. Thus, the TPC template can be considered as oxidized after heating to 190°C. After calcination for three hours at 190°C in a flow of air, the samples contained between 3.3 and 3.8 wt%. This calcination temperature is substantially lower than reported for classic calcination procedures where temperatures between 450 and 550°C are used for removing TPAOH [32,33] or cationic CTA^+ surfactants. [14,15]

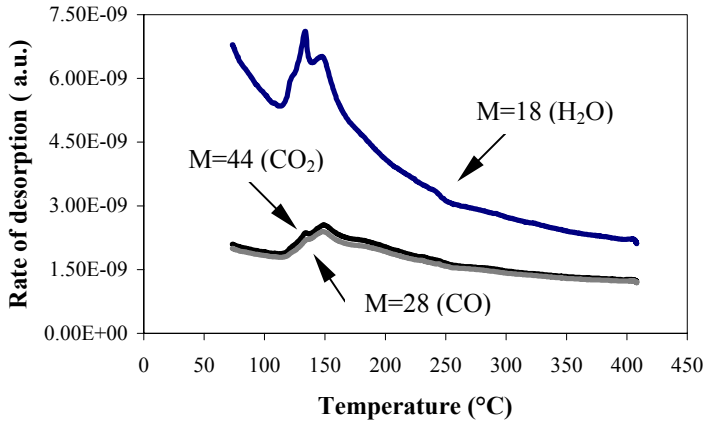

Fig 4.1.6. Temperature programmed oxidation of SBA-15 sample 702/2

The first studies of room temperature UV/O_3 treatment to remove surfactant template from as-synthesized MCM-41 was reported by Keene *et. al.* [22] and Brinker *et. al.* [23] In Keene's group mesoporous MCM-41 was prepared using cetyltrimethylammonium bromide (CTABr). It was observed that the pore size of the UV/O_3-treated sample was larger, the pore size distribution narrower and the hexagonal long-range ordering of the pores improved compared with common calcined samples. However, questions remain in which form nitrogen and bromine are removed from the pores. Brinker and coworkers investigated the UV/O_3-treatment for MCM-41 films using Brij56 ($C_{16}H_{33}(OCH_2CH_2)_{10}OH$) as template. The results established that the UV/O_3 treatment leads to complete removal of the template, strengthens the inorganic skeleton and renders the thin film surface highly hydrophilic.

Ozone is a high-energy form of oxygen with a high specific oxidation potential (2.07 V). The room temperature UV/O_3 treatment could be an efficient alternative for the removal of organic surfactants as the majority of products are thought to be water and carbon oxide. The expected advantage of ozone treatment over conventional thermal treatment is that elimination of organic molecules can be applied at much lower temperatures, which is essential for thermally unstable nanoparticles. However, ozone has a very short life span ("half-life") of 20-30 minutes. [25] If an ozone molecule cannot react on time with target species (surfactant template) it simply reverts back to oxygen. Therefore the ozone was generated in situ.

Typical experiments involved the exposure of as-synthesized SBA-15 powder to UV light (λ=257 nm), which was produced by a low pressure Hg grid-lamp in a quartz envelope at room temperature. In this way O_3 was formed in the oxygen atmosphere in vicinity to the nanoparticles. The required exposure time for removal of the template significantly depended on the distance of the sample from the lamp and amount of the sample. After treatment the sample was washed with H_2O and then freeze dried. The UV/O_3 treated samples were characterized with elemental analysis (EA), BET surface analysis and XRD. All characterization data of SBA-15 nanoparticles after removal of surfactant TCP are listed in Table 4.1.3.

Table 4.13. Data of SBA-15 nanoparticles after removal of the template

Sample	Treatment	Elemental analysis C [%]	H [%]	TCP weight %	BET surface area (m^2/g)	Micropor. Surface (m^2/g)	Pore size d (nm)
702/3 (a)	190 °C, in air	2.1	1.8	3.6	680	120	3.0
702/3 (b)	UV/O_3	1.3	1.7	2.2	765	70	3.1
902/1	UV/ H_2O_2	< 0.5	1.9	< 0.9	730	83	3.5
702/2 (a)	190 °C, in air	2.3	2.1	3.8	426	238	3.6
702/2 (b)	UV/O_3	1.5	1.7	2.5	513	177	3.8
702/4	UV/ H_2O_2	0.8	1.9	1.3	518	122	4.1
1002/1 (a)	190 °C, in air	1.9	1.7	3.3	950	210	3.8
1002/1 (b)	190 °C, in air	2.0	1.8	3.4	1024	240	3.5

The results of elemental analysis showed that SBA-15 sample 702/2 contained still 3.8 wt% of TCP 2 after calcination at 190°C. In contrast, the sample contained only 2.5 wt% TCP 2 after UV/O_3 treatment. Similar results were obtained for the sample 702/3 where the TCP 1 contents was 3.6 wt% for the calcined sample and 2.2 wt% for the UV/O_3 treated sample. From the N_2-adsorption/desorption isotherm it was concluded that the pore size of the UV/O_3 treated sample 702/2 was 3.8 Å whereas calcined 702/2 had a pore size of 3.6 Å. Also, calcined 702/2 had a BET surface area of 426 m^2/g (238 m^2/g micropore surface) while the UV/O_3 treated sample had a BET surface area of 513 m^2/g (177 m^2/g micropore surface). The results of sample 702/3 show a similar trend: the UV/O_3 treated sample has a larger BET surface area (765 m^2/g) with smaller micropore surface (70 m^2/g) than the calcined sample, while the pore size of the calcined sample and UV/O_3 treated sample are almost the same. Fig. 4.1.7c shows a typical TEM image of sample 702/3 after treatment, in which the particle size can be estimated to 20 nm.

In Fig. 4.1.7(a-b) the XRD patterns of calcined and UV/O_3 treated samples 702/2 and 702/3 are compared. Because of the small particle size it is difficult to distinguish the XRD patterns for SBA-15. However, the maximum at $2\theta = 0.5°$ for the UV/O_3 treated sample 702/2 clearly demonstrates that this sample has a higher degree of ordering than the corresponding calcined sample.

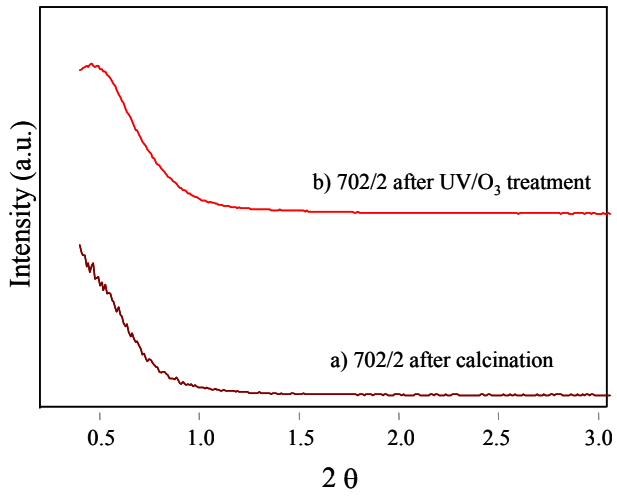

Fig. 4.1.7a XRD pattern of sample 702/2 after different treatments to remove the template

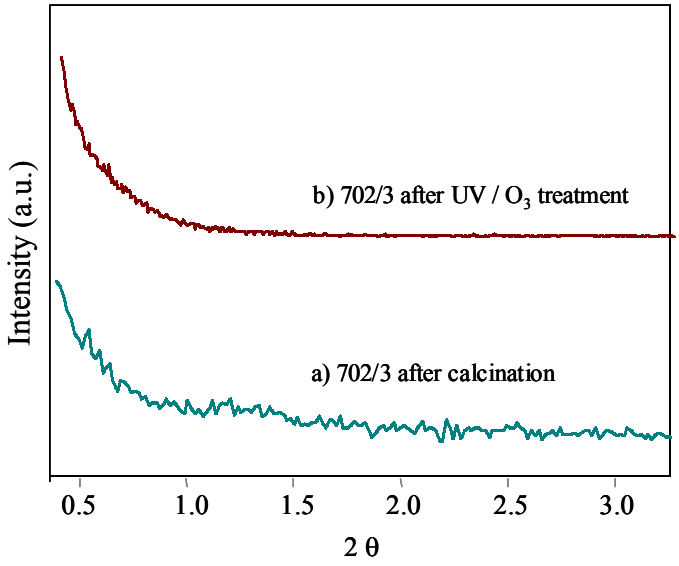

Fig. 4.1.7b XRD patterns of sample 702/3 after different treatments

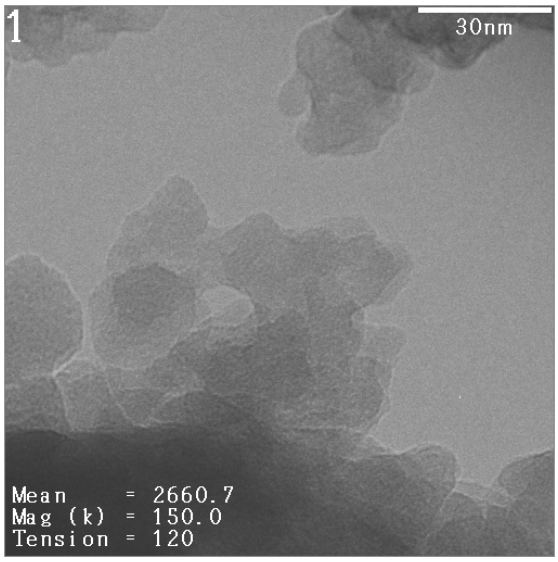

Fig. 4.1.7c TEM image of sample 702/3 after UV/O_3 treatment

Both methods, calcination at 190°C and UV/O_3 treatment, require a dry sample of the nanoparticles. However, even mild drying procedures, such a freeze-drying, can lead to formation of agglomerates. We have therefore tested the oxidation of the template in suspension using OH radicals. This treatment is used to remove organic substances from waste water. [34] OH Radicals can be generated readily by ultraviolet radiation (UV) of hydrogen peroxide. Hydroxyl radicals $[OH]^{\bullet}$ are highly powerful oxidizing species (specific oxidation potential 1.78 V) and are able to oxidize organic compounds as, e.g. ethylene oxide *EO* and propylene oxide *PO*. Organic radicals $[R]^{\bullet}$ are formed which are also highly reactive and can be further oxidized. The main reactions that occur during UV/H_2O_2 treatment are as follows:

$$H_2O_2 \xrightarrow{h\nu} 2OH^{\bullet} \quad (1)$$

$$nOH^{\bullet} + EO_xPO_yEO_x \longrightarrow CO_2 + H_2O \quad (2)$$

All experiments of UV/H_2O_2 treatment were carried out in an aqueous suspension of SBA-15 nanoparticles. After addition of H_2O_2 solution the mixture was exposed to UV irradiation with 254 nm wavelength. Subsequently, the suspension was concentrated and the particles were washed with water and ethanol. The freeze-dried samples were characterised by elemental analysis, XRD, nitrogen adsorption and FT-IR.

The elemental analysis showed that the samples contained very little TCP after UV/H_2O_2 treatment, < 0.9 wt% TCP 1 for sample 902/1 and 1.3 wt% TCP 2 for sample 702/4. Thus, UV/H_2O_2 treatment is much more effective to remove template than UV/O_3 treatment

and calcination. UV/H_2O_2 treated sample 902/1 had a BET surface area of 730 m^2/g (83 m^2/g microporous surface) which is in the same range as that of UV/ O_3 treated samples. For the sample 702/4 a BET surface with 518 m^2/g (122 m^2/g microporous surface) was observed. X-ray diffraction patterns of calcined 702/4 showed a weak *(100)* reflection at 1.04° which corresponds to a d-spacing of 86 Å, which is consistent with a unit cell parameter a = 99 Å ($a = d_{100} \times 2/\sqrt{3}$ for a hexagonal mesostructure). [7] The UV/H_2O_2 treated 702/4 sample had a d-spacing of 72 Å (2θ = 1.22°), which corresponds to a cell parameter a = 83 Å (Fig. 4.1.8). It is particularly noteworthy that the pore sizes of the UV/H_2O_2 treated sample, as determined from N_2 adsorption, were larger than those of calcined and UV/O_3 treated samples (3.5 Å of 902/1 and 4.1 Å of 702/4, respectively).

The IR spectrum of as-synthesized SBA-15 sample 902/1 (Fig. 4.1.9) showed the peaks resulting from C-H stretching vibration (2950-2850 cm^{-1}) as well as a broad peak at 3700-3300 cm^{-1} assigned to hydrogen bonded Si-OH groups. In the UV/H_2O_2 treated sample the peaks characteristic for C-H can no longer be observed, whereas a sharp peak at 3742 cm^{-1} assigned to Si-OH was found. This confirms complete removal of the TCP template by UV/H_2O_2 treatment.

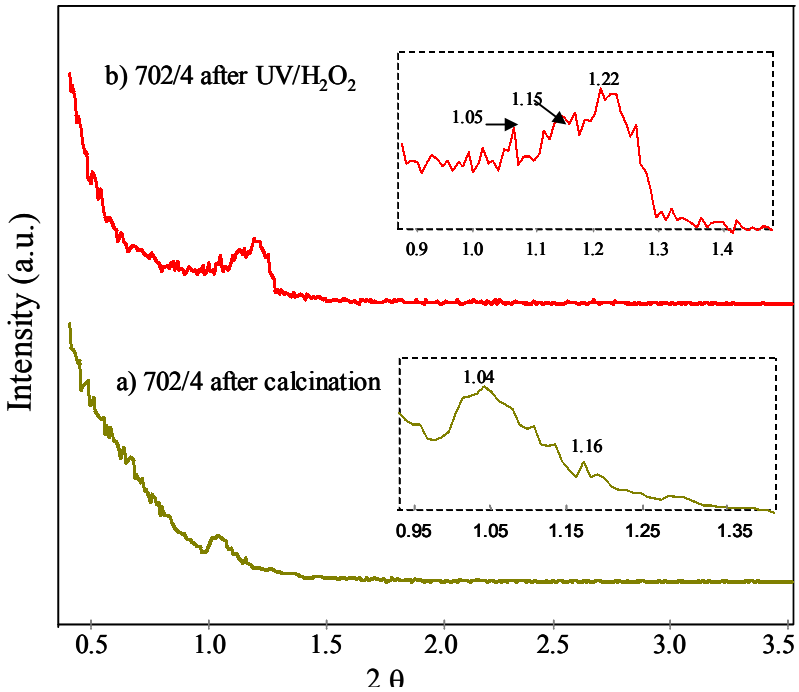

Fig. 4.1.8 XRD pattern of 702/4 after different treatments to remove the template

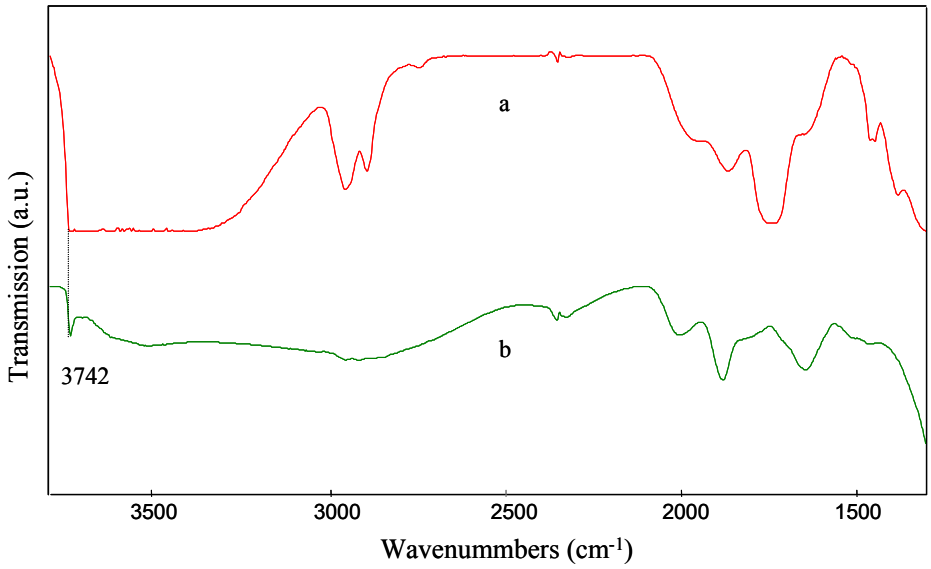

Figure 4.1.9: FT-IR spectra of a) as-synthesized SBA 902/1, b) UV/H_2O_2 treated sample 902/1

4.1.3 Experimental

Triblock copolymers $EO_xPO_yEO_x$ were obtained from Aldrich. TEOS, hydrochloric acid, H_2O_2, and EtOH were purchased from Merck.

Synthesis of SBA-15

SBA-15 was prepared using triblock copolymers $EO_xPO_yEO_x$ (denoted as TCP) as the surfactant and tetraethylorthosilicate (TEOS, 98%, Merck) as the silica source, following the synthesis procedure reported by Zhao et al. [7] In a typical process, 8.5 g TEOS was added to a homogeneous mixture comprising 4.0 g TCP (Table 4.1.1), 120 g hydrochloric acid (2M) and 30 g water. The mixture was magnetically stirred until TEOS was completely dissolved. The mixture was then kept at room temperature for 24 hours without stirring. Subsequently the resulting gel was placed in an oven at 100°C for three days. The product was filtered, washed and freeze-dried.

Removal of surfactant TCP by calcination

Temperature programmed oxidation (TPO) was performed in a flow system consisting of a tubular quartz reactor heated uniformly by a furnace (2°C/min, 70-400°C, 3 hours at 400°C). A fraction of gases from the reactor outlet was directed via a heated stainless steel

capillary into a mass spectrometer (Balzers QMG 200), where the partial pressure of the reactants was continuously monitored.

As-synthesized SBA-15 samples (100 mg) were placed in an air stream with 5ml/min flow and heated with a rate of 1 °C/min up to 190 °C and held at 190 °C for 3 hours.

Removal of surfactant TCP using UV/O_3 treatment

Ozone was produced from oxygen by UV irradiation with a low-pressure mercury lamp in a quartz envelope, λ = 257 nm. The UV/O_3 treatment in the solid phase was performed in a closed sample chamber (Fig. 4.1.10). The required photolysis time for 100 mg SBA-15 samples containing 26 % $EO_{80}PO_{30}EO_{80}$ as template was approximately 3 hours. After exposure the samples were washed with ethanol three times and twice with water. The samples were then freeze-dried.

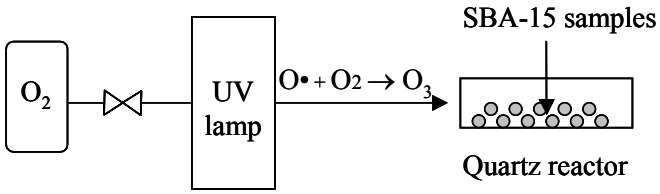

Fig. 4.1.10 Schematic diagram of the setup for UV/O_3 treatment.

Removal of surfactant TCP using UV/H_2O_2 treatment

All experiments were performed in a well-stirred cylindrical photo-reactor with a total volume of 100 ml. The reactor is made of quartz. At the top, the reactor has inlets for feeding reactants, and ports for measuring temperature and withdrawing samples. The reactor was open to air with a magnetic stirring bar placed in the bottom to provide proper mixing. The UV irradiation source was a 16 W low-pressure mercury vapour lamp with a monochromatic wavelength emission at 254 nm encased in a quartz tube. Because the light source produces heat, the photo-reactor was placed in a cooling bath. The lamp was axially centred and was immersed in the suspension (Fig. 4.1.11). An aqueous suspension of SBA-15 was mixed with an equal volume of hydrogen peroxide (30 wt% aqueous solution). The UV-treatment was stopped after 5 hours. The solutions were concentrated by partial evaporation. The solid residue was washed with ethanol three times and twice with water and freeze-dried.

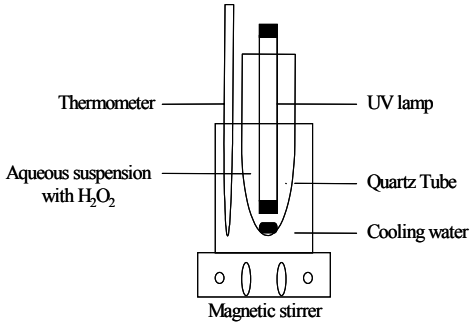

Fig. 4.1.11 Schematic diagram of the setup for UV/ H_2O_2 treatment

Characterization of SBA-15

XRD patterns were recorded on a Philips X'Pert 3040 X-ray diffractometer with Cu K_α radiation (λ: 1.54 Å). The nitrogen adsorption and desorption isotherms were recorded at 77 K using a ASAP 2010 system (Micrometrics). The samples were pretreated at 200 °C overnight under vacuum. The pore size distribution was calculated from the adsorption branch of the isotherms using the BJH method. The pore volume was determined at the $P/P_0 = 0.98$ single point. The surface area was calculated by the BET method. Transmission electron microscopy images (TEM) of samples deposited on carbon copper grids were taken with a TEM JEOL 2010 operating at 200 kV. The samples were prepared by dispersing the powder as slurry of ethanol, which was then deposited and dried on copper grids covered with a holey carbon thin film. Infrared spectra were taken on a Bruker IFS 40 FTIR spectrometer.

4.1.4 Conclusions

The general route for producing silica-based SBA-15 materials is a templating scheme where an aqueous acidic solution containing a triblock copolymer $EO_xPO_yEO_x$ (TCP) is reacted with a silicate source such as tetraethoxysilicate (TEOS). TCP with EO/PO ratios of 0.6 and 1.4 result in the formation of hexagonal mesoporous structures whereas a larger EO/PO ratio (5.3) tends to favor the formation of a cubic mesoporous structure. It is observed that at two different pH values the particles size formed using TCP 1 and TCP 3 as templates were in the same range, while with TCP 2 as template the particle size was relatively larger at pH = 0.6 than at pH = 0.9.

As the $EO_xPO_yEO_x$ are oxidized easily, as-synthesized SBA-15 samples can be calcined at only 190°C to remove the template. The relatively low temperature reduces the degree of particle agglomeration. Furthermore, methods employing UV-light to generate O_3 or $OH^\bullet$ radicals are shown to provide efficient alternatives for removing the surfactant

template. The main advantage of the UV-treatment with H_2O_2 and O_3 is the non-thermal processing by oxidation of the organic species into the main products water and carbon dioxide. While solid samples are required for calcinations and the UV/O_3 treatment, the UV/H_2O_2 treatment is carried out in aqueous suspension. The solvent layer between the particles completely prevents that the particles stick together. UV treated samples have larger BET surface area than calcined samples. In particular, the pore size of the UV/H_2O_2 treated samples is considerably larger than that of the calcined and UV/O_3 treated samples.

4.1.5 References

[1] M. Fayolle, G. Passemard, O. Louveau, F. Fusalba and J. Cluzel, *Microelectr. Engineering,* **2003**, *70(2-4)*, 255.

[2] K. Ibrahim, *Thin Solid Films,* **2003***, 434(1-2),* 178.

[3] K. Mosig, T. Jacobs, K. Brennan, M. Rasco, J. Wolf and R. Augur, *Microelectr. Engineering*, **2002**, *64(1-4)*, 11.

[4] The International Technology Roadmap for Semiconductors, Semiconductor Industry Association, San Jose, CA, 2001.

[5] P.T. Liu, T.C. Chang, K.C. Hsu, T.Y. Tseng, L.M. Chen, C.J. Wang and S.M. Sze, *Thin Solid Films,* **2002**, *414(1)*, 1.

[6] C.T. Kresge, M.E. Leonoewitz, W.J. Roth and J.S. Beck, *Nature* **1992**, *359*, 710.

[7] a) D. Zhao, Q. Huo, J. Feng, B.F. Chmelka and G.D. Stucky, *J. Am. Chem. Soc.* **1998**, *120*, 6024.

b) D. Zhao, J. Feng, N. Fredirckson, B.F. Chmelka and G.D. Stucky, *Science* **1998**, *279*, 548.

[8] M. Kruk , M. Jaroniec, H. Chang and R. Ryoo, *Chem. Mater*., **2000**, *12*, 1961.

[9] C. G. Göltner and M. Antonietti, *Adv. Mater.*, **1997**, *9*, 431; M. Antonietti and C. Göltner, *Angew. Chem. Int. Ed. Engl*., **1997**, *36*, 910 .

[10] G. Wanka, H. Hoffmann and W. Ulbricht, *Macromolecules* **1994**, *27*, 4145; B. Chu and Z. Zhou, in Nonionic Surfactants: Polyoxyalkylene Block Copolymers, vol. 60 of Surfactant Science Series V, M. Nace, Ed. (Dekker, New York, 1996), p. 67.

[11] A. Corma, *Chem. Rev.*, **1997**, *97*, 2373.

[12] J.Y. Ying, C.P. Mehnert and M.S. Wong, *Angew. Chem. Int. Ed. Engl.*, **1999**, *38*, 56.

[13] F. Schüth, A. Wingen and J, Sauer, *Micropor. Mesopor. Mater.*, **2001**, *44-45*, 465.

[14] K.K. Unger, D. Kumar, S. Lüdtke, K. Schumacher and R. Renker, *J. Chromatogr. A.*, **2000**, *892*, 47.

[15] M. Vallet-Regi, A. Ramila and J. Perez-Pariente, *Chem. Mater.*, **2001**, *13*, 308.

[16] J. Beck, J. Vartuli, W. Roth, M. Leonowwicz, J. Higgins and J. Schlenker, *J. Am. Chem. Soc.*, **1992**, *114*, 10843.

[17] C. Chen, H. Li, M. Davis, *Micropor. Mater*., **1993**, *2*, 17.

[18] J. Blanchard, P. Trens, M. Hudson, F. Schüth, *Micropor. Mesopor*. Mater., **2000**, *39*, 163.

[19] S. Kawi and M. Lai, *Chem. Commun*., **1998**, *13*, 1407.

[20] P. Tannev and P. Pinnavaia, *Chem. Mater*., **1996**, *8*, 2068.

[21] S. Hitz and R. Prins, *J. Catal*., **1997**, *168*, 194.

[22] M. Keene, R. Denoyel and P. Llewellyn, *Chem. Commun*., **1998**, *20*, 2203.

[23] T. Clark, J. Ruiz, H. Fan, J. Brinker and A. Parikh, *Chem Mater*., **2000**, *12*, 3879.

[24] F. Kleitz, W. Schmidt and F. Schüth, *Micropor. Mesopor. Mater.*, **2003**, *1*, 65.

[25] S. Baba, S. Satoh and C. Yamabe, *Vacuum,* **2002**, *65/3-4*, 489.

[26] G. Soler-Illia, E.L. Crepaldi, D. Grosso and C. Sanchez, *Curr. Opinion Colloid Interf. Sci.*, **2003**, *8*, 109.

[27] T. Yamada, H. Zhou, K. Asai and I. Honma, *Mater. Letters*, **2002**, *5*, 93.

[28] K. Flodström and V. Alfredsson, *Micropor. Mesopor. Mater.*, **2003**, *2-3*, 167.

[29] N.A. Melosh, P. Lipic, F. Wudl, G.D. Stucky, G. H. Fredrickson and B.F. Chmelka, *Macromolecules*, **1999**, *32*, 4332.

[30] P. Kipkemboi, A. Fogden, V. Alfredsson and K. Flodström, *Langmuir*, **2001**, *17*, 5398.

[31] B. Smarsly, S. Polarz and M. Antonietti, *J. Phys. Chem. B*, **2001**, *105*, 10473.

[32] C. Kirschhock, R. Ravishankar, F. Verspeurt, P. J. Grobet, P. A. Jacobs, and J. A. Martens, *J. Phys. Chem. B*, **1999**, *103*, 4965.

[33] L. Tosheva, V. Valtchev and J. Sterte, *Micropor. Mesopor. Mater.*, **2000**, *35-36*, 621.

[34] R. Andreozzi, V. Caprio, A. Insola and R. Marotta, *Water Res.*, **1999**, *34(2)*, 463.

[35] S. Hoon, R. Ryoo, M. Kruk and M. Jaroniec, *J. Phys. Chem. B*, **2002**, *106*, 4640.

4.2.1 Introduction

Zeolites are microporous molecular sieves with a framework made of silicon and aluminium tetrahedra. Depending on the structure, these materials can be prepared within a large composition range. Some of these microporous solids can be synthesized in the absence of aluminium. This is important when the material shall be employed in low-κ dielectric applications as aluminium leads to an increased polarity of the lattice and, thus, an increased dielectric constant. Well-known examples for aluminium-free zeolites are silicalite-1 [1] and silicalite-2,[2] which have MFI and MEL framework topologies, respectively (see Fig. 4.2.1). The framework structures MFI and MEL represent the two end members of the same family with pentasil structure. They can be considered as silicon analogues of zeolites ZSM-5 and ZSM-11. The synthesis of these materials with nanoscale particle size has been investigated intensively and was optimised in the last years. [3-12]

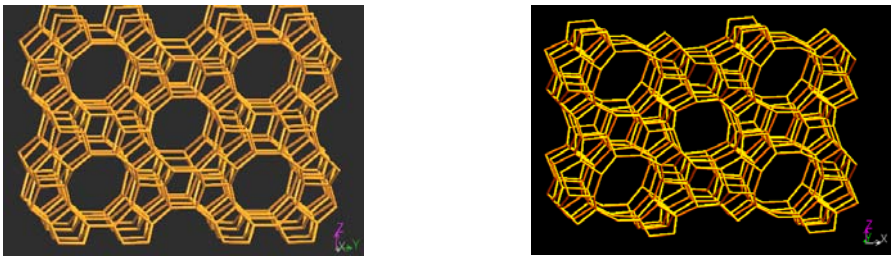

Fig. 4.2.1: Structure framework of a) silicalite-2 (MEL), b) silicalite-1 (MFI)

One of the most commonly used templating agents in the synthesis of silicalite-1 is tetrapropyl ammonium hydroxide (TPAOH) in combination with tetraethylorthosilicate (TEOS) as silica source. Alternatively, silicalite-1 can be synthesized by using tetraethylammonium hydroxide (TEAOH) as templating agent. [1] Nanocrystalline (colloidal) silicalite-1 is typically prepared under mild hydrothermal conditions (ca. 100°C) from a clear TPAOH–H_2O–TEOS precursor sol. Synthesis of zeolite crystals with uniform particle size requires homogeneous distribution of the nuclei present in the reaction mixture. Therefore, the homogeneity of the starting system and simultaneity of the events leading to the formation of precursor gel particles and their transformation into crystalline zeolitic material are of primary importance. In order to obtain such homogeneous starting systems abundant amounts of TPAOH and water were employed. Generally, the synthesis of zeolites and related silica-based molecular sieves requires a long crystallization time. Many efforts have been done to decrease the synthesis time by systematically optimising the synthesis parameters, mainly the

chemical composition of the initial reaction gel mixture. Kumar and co-workers reported that the addition of small amounts of certain oxyanions (ClO_4^-, PO_4^{3-}, AsO_4^{3-}, etc.) as promoters significantly enhances the nucleation and the crystallization processes of a variety of zeolite structures (ZSM-5, TS-1, silicalite-1). Promoters reduce the synthesis time to a varying degree. In the present work phosphate PO_4^{3-} was added as promoter to the TEOS–TEAOH–H_2O system. It was also reported, that the crystallite size of ZSM-5 samples prepared in the presence of phosphate was smaller than that of corresponding samples prepared without promoter. [18,19]

Similarly, colloidal silicalite-2 (MEL type) was prepared in the presence of tetrabutylammonium hydroxide (TBAOH) from the reactant system TBAOH–TEOS–H_2O. However, TBA^+ cations promote silicalite growth not as effectively as TPA^+ since the large TBA^+ cations do not conform to the silicalite lattice, whereas the TPA^+ cations occupy all channel intersections of the silicalite formed. Alternatively, TEA^+ with short alkyl chains can be used as template, but often leads to intergrowth of silicalite-1 and silicalite-2. [20,21] Therefore, the synthesis gel was preformed using a binary mixture of templates containing TBAOH and TEAOH.

Most of the applications of these microporous materials are in the fields of catalysis, sorption and sensors. Nanosized crystallites have attracted a lot of attention due to the fact that they can be used as precursors to prepare zeolite films. [25-27] Recently several studies were focused on the application in optics and electronics. [13-15] In particular, scattered activities are observed in novel applications for low-κ material. [16-17] It has been predicated that dielectric materials with κ lower than 2.0 will be needed for microprocessors with design features smaller than 100 nm. Thus, silicalite with uniform pore size below 2 nm, which is significantly smaller than integrated circuit (IC) features, is a potential component of porous dielectrics with ultra low dielectric constant.

In the present work, silicalite-1 and silicalite-2 were synthesized using TPA^+, TEA^+/ PO_4^{3-} and TBA^+/ TEA^+ as templates and TEOS as silica source. Furthermore, the samples were extensively characterized by XRD, BET, SEM and TEM.

4.2.2 Results and Discussion

Generally during the formation of a zeolite particle the following behaviour is observed: (i) globular entities as small as 5 nm are formed in the precursor sol during hydrolysis; (ii) particles of similar size exist after heating and persist throughout the reaction;

(iii) spherical aggregates with uniform size appear after an induction period. [22,23] Their average size starts from ca. 20 nm and grows with time until the end of reaction. The final crystal size depends on the influence of various variables, such as hydrolysis time, alkalinity of the reaction medium and ratio of SiO_2 to template. Table 4.2.1 shows the different reaction conditions used by us in the synthesis of silicalite nanoparticles, as well as characteristic data of the nanoparticles.

Table 4.2.1. Preparation and characterization of silicalite-1 and silicalite-2 nanoparticles

Silicalite-1	Surfactant templates	Hydrolysis time (h)	Synthesis temperature (°C)	BET surface (m^2/g)	Crystal size$^+$ (nm)
301/6	TPAOH	24	98	495	30-80*
502/1	TPAOH	48	98	597	16 (1) **
601/1	TEAOH / PO_4^{3-}	48	100	468	15-50*
Silicalite-2					
802/1	TBAOH/TEAOH	72	140	540	48 (14) **

* estimated from TEM image; ** results from dynamic light scattering measurement (DLS), + the standard deviation is given in brackets

The synthesis mixture using TPAOH as templating agent with molecular composition 9 TPAOH : 25 SiO_2 : 425 H_2O : 100 EtOH resulted in the formation of silicalite-1 samples 301/6 and 502/1. TPAOH is a strong base, thus, the pH value of the reaction mixture was about 14. As the hydrolysis time was increased from 24 (for 301/6) to 48 hours (for 502/1), the crystal size decreased. Fig. 4.2.1 shows TEM images of sample 301/6 from colloidal suspension after heating to 98°C for 20 h. The particles exhibit a nearly spherical shape with a size in the range of 30 - 80 nm. In comparison with 301/6 the colloidal 502/1 sample shows more homogenous units of smaller particle size of 16 nm (DLS). At the end of the crystallization the solid phase of the 301/6 was separated from the solution. After washing and drying the particles were characterised by XRD and scanning electron microscopy. SEM images of 301/6 (Fig. 4.2.5a) showed agglomerates of nano-sized primary particles in spherical form with up to 200 nm diameters. Moreover, XRD measurements of these relatively large particles show the typical pattern of MFI (Fig. 4.2.6). Most important for the determination of the crystalline phase of silicalite-1 are the (-101)/(011), (200)/(020), (-501)/(051) and (051) reflections. [24]

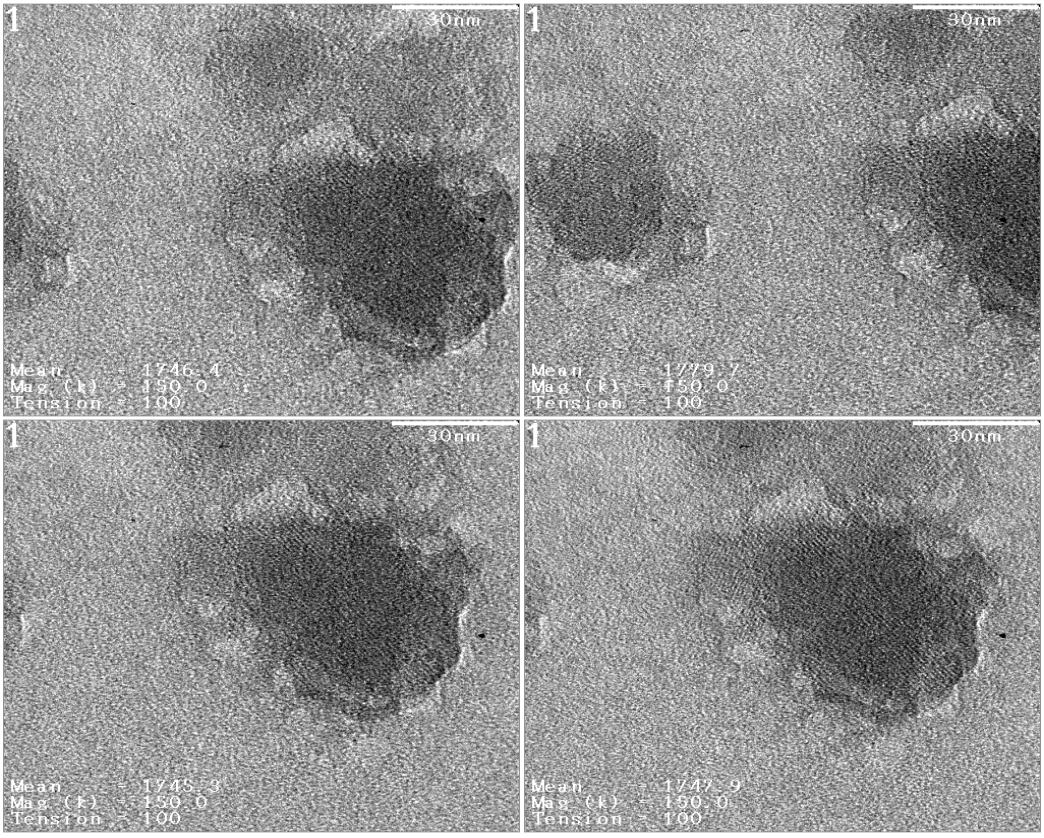

Fig.4.2.1 TEM images of silicalite-1 sample 301/6

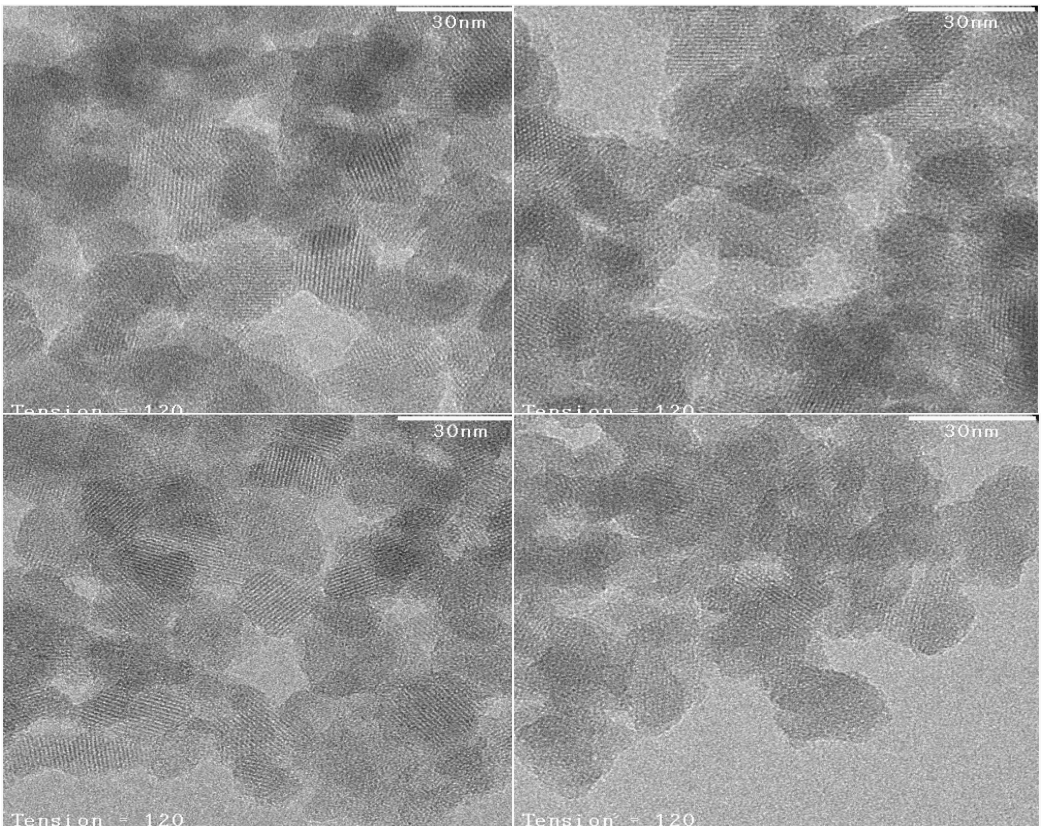

Fig. 4.2.2 TEM images of silicalite-1 sample 502/1

Another possibility to synthesize silicalite-1 is to use TEAOH as templating agent and PO_4^{3-} as promoter for the crystallisation process. The molecular composition of the reaction mixture, which we have used, was 9 TEAOH : 11.5 SiO_2 : 1.3 P_2O_5 : 414 H_2O : 46 EtOH. After addition of H_3PO_4 the pH value of the reaction mixture was about 12. After heating to 100°C for 8 days the particles were isolated (sample 601/1). Transmission electron micrographs are shown in Fig. 4.2.3 including the crystallographic lattice inflexion (Fig. 4.2.3a). The TEM image of the samples shows that the particle size is in the range of 100-150 nm (Fig. 4.2.3b). Smaller particles were obtained, when the heating procedure was extended to 20 hours (sample 802/1). As shown in Fig. 4.2.3c and Fig. 4.2.3d, the particle size of this colloidal silicalite-1 is in the range of 15 – 50 nm. The BET surface area measured for the calcined silicalite-1 samples 301/6, 502/1 and 601/1 was 495, 597 and 468 m^2/g, respectively.

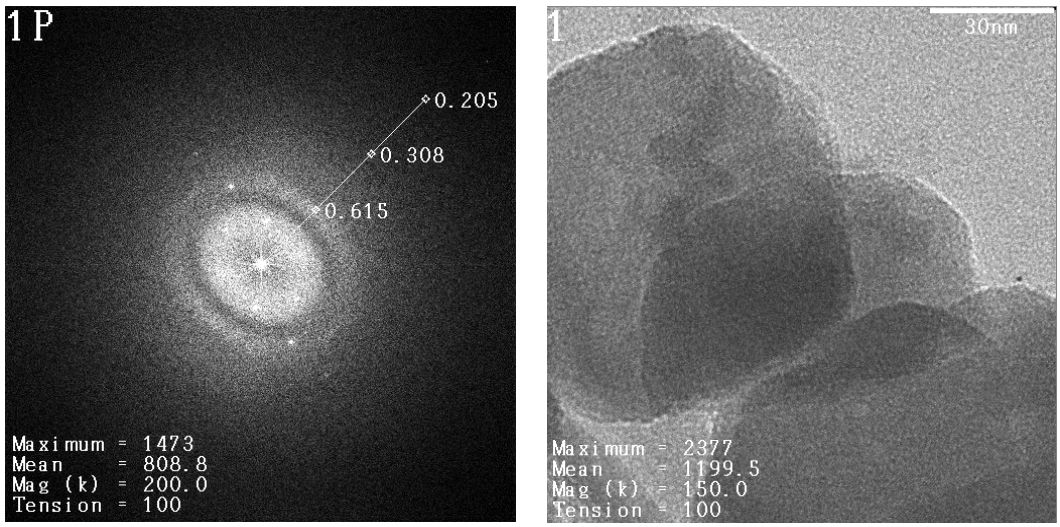

Fig. 4.2.3 a) Crystallography inflexion of 601/1 b) TEM image of 601/1

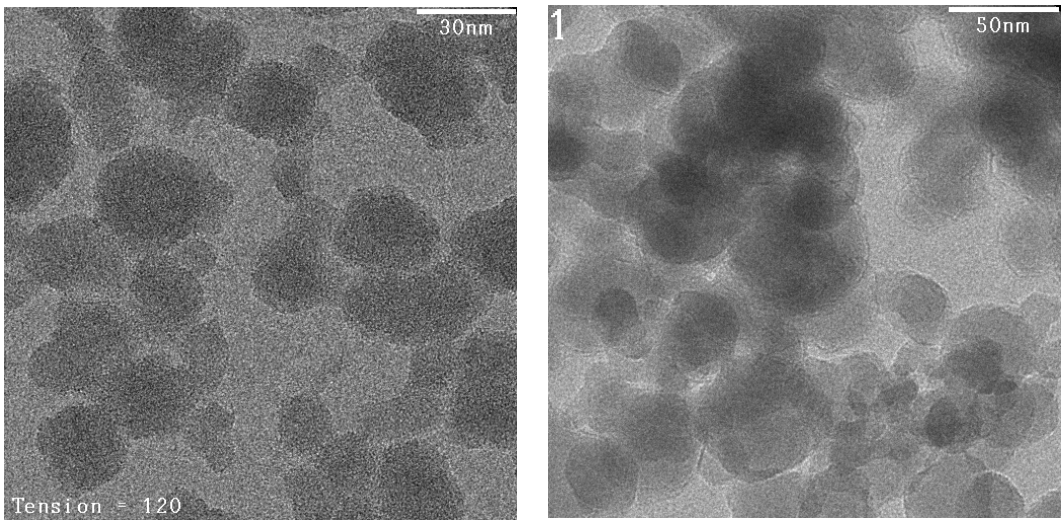

Fig. 4.2.3 c) TEM image of 601/1 d) TEM image of 601/1

For synthesis of silicalite-2 with MEL structure the following molecular composition was used: 9 TBAOH : 76.5 SiO_2 : 22.5 TEAOH : 630 H_2O : 306 EtOH. The pH value of the reaction mixture was about 14. The reaction mixture was heated for 22h to 140°C and separated into several fractions by centrifugation. Fig. 4.2.4 shows TEM images of the colloidal fraction of silicalite-2 (sample 802/1a). The particle size was between 25 and 65 nm. A SEM image of a fraction with large particle size (802/1b) is shown in Fig. 4.2.5b, which represents typical MEL crystals. It is well known that MEL has a very high symmetry, belonging to the space group $\bar{I}4m2$. Consequently the powder X-ray diffraction pattern should have fewer reflections than that of MFI, although silicalite-2 shares many similar structural features with silicalite-1 (Fig. 4.2.6). The BET surface area of the calcined silicalite-2 samples 802/1 was 540 m^2/g.

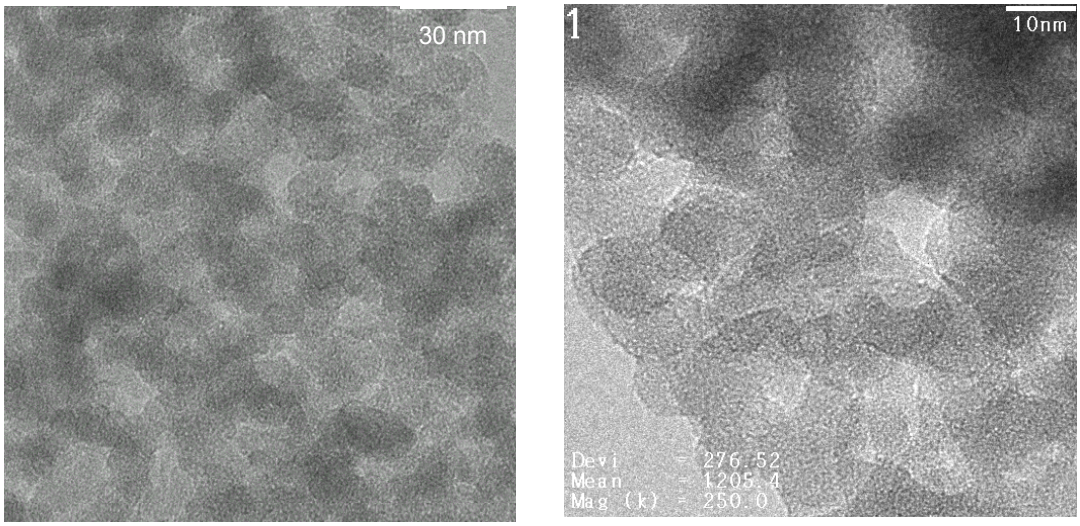

Fig. 4.2.4 TEM image of silicalite-2 802 /1a

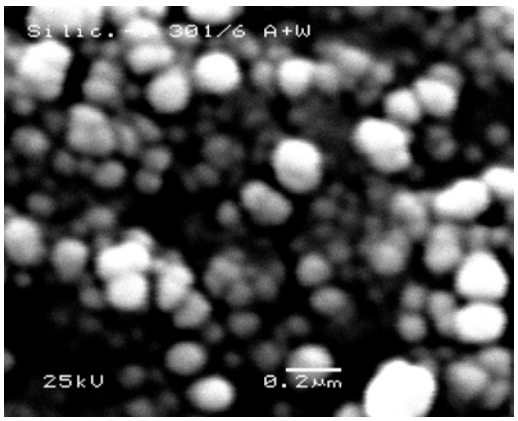

Fig. 4.2.5 a) SEM image of 301/6

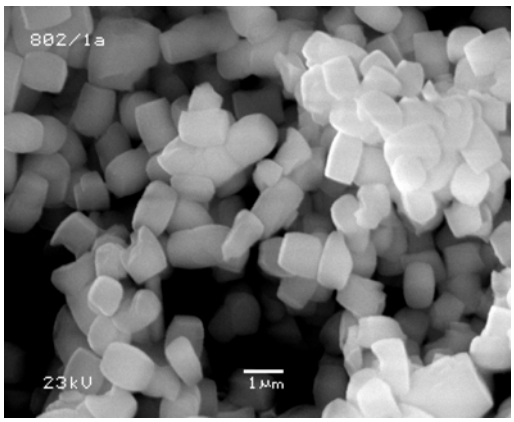

Fig. 4.2.5 b) SEM image of 802/1b

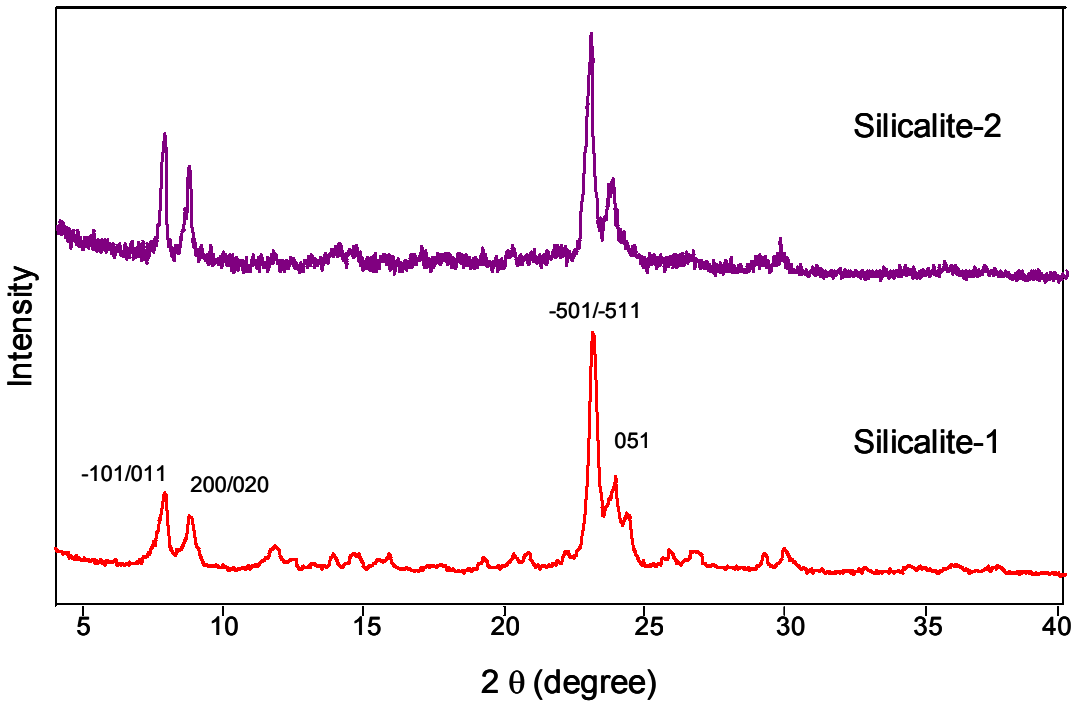

Fig. 4.2.6. XRD spectra of as-synthesized silicalite-1 and silicalite-2

4.2.3 Experimental

Synthesis of Silicalite-1 from TPAOH–H_2O–TEOS

Nanosized silicalite-1 was obtained from a synthesis mixture with the following molar composition: 9 TPAOH : 25 SiO_2 : 425 H_2O : 100 EtOH.

The synthesis mixture was prepared by adding TEOS (Merck, 98 wt%) dropwise to a solution of TPAOH (Chempur, 40 wt%) in double distilled water. A polypropylen reactor and strong stirring were used. After 1 hour the rest of water was added to the mixture. The sol was hydrolyzed at room temperature for 24 to 48 hours by shaking on a gyratory shaker. The transparent solution was then refluxed for 20 hours in an oil bath preheated to 98°C. The solids were separated from the mother liquor by centrifugation and repeatedly washed with distilled water until the wash water had a pH lower than 8. The sample was re-dispersed in distilled water and freeze-dried. The sample was then calcined in a stream of nitrogen at 550°C for 2 hours and, subsequently, in air for 10-12 hours at the same temperature.

Synthesis of Silicalite-1 from TEAOH –H_2O –TEOS with PO_4^{3-} as promoter

Nanosized silicalite-1 was synthesized from a mixture with the following molar composition: 9 TEAOH : 11.5 SiO_2 : 1.3 P_2O_5 : 414 H_2O : 46 EtOH.

The reaction mixture was prepared by adding TEOS (Merck, 98 wt%) dropwise to a solution of TEAOH (Aldrich, 35wt%) in double distilled water. A polypropylene reactor and strong stirring were used. After one hour an aqueous solution of H_3PO_4 (Merck, 85 wt%) was added dropwise to the mixture. After hydrolysis at room temperature the crystallization was carried out in PTFE-lined autoclaves at 100^{o}C. The samples were then centrifuged to separate the solid phase from the mother liquor. After washing with distilled water (pH = 8) and freeze-drying the samples were calcined in air at 550°C for 10 hours.

Synthesis of Silicalite-2 from TBAOH / TEAOH –H_2O –TEOS

Nanosized silicalite-2 was synthesized from a reaction mixture with the following molar composition: 9 TBAOH : 76.5 SiO_2 : 22.5 TEAOH : 630 H_2O : 306 EtOH.

TEOS was added to an aqueous solution of TBAOH (Lancaster, 40 wt%) and TEAOH under vigorous stirring. Subsequently, distilled water was added. The mixture was stirred for 72 h at room temperature until a clear sol was formed. The mixture then heated in a PTFE lined autoclave to 140°C for 22 hours. The as-synthesized product was separated from the mother liquid by centrifugation, washed with distilled water until pH<8, and freeze-dried. The sample was then calcined in air at 550°C for 10 hours.

Characterization

Prior to and after calcination, phase purity and crystallinity were determined by X-ray powder diffraction (XRD) on a Philip X-ray diffractometer (X' Pert 3040) using Ni-filtered Cu K_α radiation. Data were collected in the 2θ range 5–45°. Micrographs of the samples were obtained by scanning electron microscopy (SEM) on a JEOL 5900 LV. Nitrogen adsorption measurements were performed on as-synthesized and calcined samples with a Micromeritics ASAP 2010 surface area analyzer. As-synthesized samples were outgassed at 200°C overnight prior to BET analysis. Particle size and pore structures were investigated using transmission electron microscopy (TEM) on a JEOL 2010 operated at 200 kV.

4.2.4 Conclusions

Crystalline nanoparticles of silicalite-1 with MFI framework and silicalite-2 with MEL framework can be obtained from typical synthesis gels by choosing the appropriate reaction conditions. The use of TPAOH or TEAOH as template results in the crystallization of silicalite-1, whereas silicalite-2 is synthesized using a binary template mixture of TBAOH and TEAOH. When the hydrolysis time was varied in the TEOS-TPAOH-H_2O system, it was observed that increasing hydrolysis time led to decreasing particle size. Also, the addition of PO_4^{3-} to the synthesis mixture resulted in a smaller particle size and enabled the synthesis of nanocrystalline silicalite-1 particles with a particle size below 65 nm.

4.2.5 References

[1] a. E.M. Flanigen, J.M. Bennet, R.W. Grose, J.P. Cohen, R.L. Patton, R.M. Kirchner and J.V. Smith, *Nature*, **1978**, *271*, 512.
b. D.Zhao, S. Qiu and W. Pang, *Zeolite*, **1993**, 478.

[2] D.M. Bibby, N. Milestone and L.P. Aldridge, **1979**, *280*, 664.

[3] A.E. Persson, B.J. Schoeman, J. Sterte and J.-E. Otterstedt, *Zeolites*, **1994**, *14*, 557.

[4] B.J. Schoeman, J. Sterte and J.-E. Otterstedt, *J. Porous Mater.*, **1995**, *1*, 185.

[5] Q. Li, B. Mihailova, D. Creaser and J. Sterte, *Micropor. Mesopor. Mater.*, **2000**, *43*, 51.

[6] J. Weitkamp and L. Puppe, *Catalysis and Zeolites (Fundamentals and Applications)*, **1999**, Springer-Verlag, Berlin, Heidelberg.

[7] R. Ravishankar, C.E.A. Kirschhok, B. Schoeman, P. Vanoppen, W. Maier, J.A. Martens and P.A. Jacobs, *J. Phys. Chem. B*., **1998**, *102*, 2633.

[8] C.E.A. Kirschhock, R. Ravishankar, L.V. Looveren, P.A. Jacobs, and J.A. Martens, *J. Phys. Chem. B*, **1999**, *103*, 4972.

[9] P.M. Piccione, B.F. Woodfield, J. Boerio-Goates, A. Navrotsky and M.E. Davis, *J. Phys. Chem. B*, **2001**, *105*, 6025.

[10] Q. Li, B. Mihailova, D. Creaser and J. Sterte, *Micropor. Mesopor. Mater.*, **2000**, *40*, 53.

[11] O. Terasaki, T. Ohsuna, H. Sakuma, D. Watanabe, Y. Nakagawa and R.C. Medrud, *Chem. Mater.*, **1996**, *8*, 463.

[12] S. Mintova, N. Petkov, K. Karaghiosoff and T. Bein, *Micropor. Mesopor. Mater.*, **2001**, *50*, 121.

[13] J.C. Jensen, G.M. von Rosmalen, *J. Cryst. Growth*, **1993**, *128*, 225.

[14] A. Iwasaki, M. Hirata, I. Kudo and T. Sano, *Zeolites*, **1996**, *16*, 35.

[15] V. Tricoli, J. Sefcik and A.V. McCormick, *Langmuir*, **1997**, *13*, 4193.

[16] Z. Wang, A. Mitra, H. Wang, L. Huang and Y. Yan, *Adv. Mater.*, **2001**, *13*, 746.

[17] Z. Wang, A. Mitra, H. Wang, L. Huang and Y. Yan, *Adv. Mater*., **2001**, *13*, 1463.

[18] R. Kumar, A. Bhaumik, R.K. Ahedi and S. Ganapathy, *Nature*, **1996**, *381*, 298.

[19] R. Kumar, P. Mukherjee, R.K. Pandey, P. Rajmohanan and A. Bhaumik, *Micropor. Mesopor. Mater.*, **1998**, *22*, 23.

[20] A. Tuel and Y. Ben Tarrit, *Micropor. Mater*., **1994**, *2*, 501.

[21] C.S. Gittelman, S.S. Lee, A.T. Bell and C.J. Radke, *Micropor. Mater*., **1995**, *3*, 511.

[22] T.A. Twomey, M. Mackay, H.P. Kuipers, R.W. Thompson, *Zeolites*, **1994**, *14*, 162.

[23] B.J. Schoeman and O. Regev, *Zeolites*, **1996**, *17*, 446.

[24] M.M. Treacy, J.B. Higgins and R. von Ballmoos, *Collection of Simulated XRD Powder Patterns for Zeolites*, **1996**, Elsevier, 524.

[25] T. Masuda, S. Otani, T. Tsuji, M. Kitamura and S.R. Mukai, *Sep. Purif. Tech.*, **2001**, *25*, 251.

[26] Á. Berenguer-Murcia, J. García-Martínez, D. Cazorla-Amorós, Á. Linares-Solano and A. B. Fuertes, *Micropor. Mesopor. Mater.*, **2003**, *59 (2-3),* 147.

[27] K. Weh, M. Noack, K. Hoffmann, K. -P. Schröder and J. Caro, *Micropor. Mesopor. Mater.*, **2002**, *54 (1-2),* 15.

Chapter 5

Composite materials with embedding silcalite and SBA-15 nanoparticles into the silsesquioxane polymers for ultra low-κ dielectric application

Abstract

Nanoporous materials have been identified as an important class of ultra low-κ dielectric materials ($\kappa < 2.0$). Many strategies have been developed to incorporate pores into thin films. Unlike traditional homogenous dielectric material, the structure of the porous network strongly affects properties critical to Cu / low κ integration into current fabrication lines. In this present work a new type of composite material was prepared by incorporating uniform micropore system of nanocrystalline silicalite-1 and silicalite-2 or the mesopore system of SBA-15 nanoparticles in silsesquioxane polymer matrices. The characterizations of spin coated composite films were assessed in detail, including electric properties (κ value, breakdown voltage), mechanical strength (hardness, adhesion), film morphology (using AFM, SEM and TEM) and suitability for CMP.

5.1 Introduction

Performance improvements in microelectronic integrated circuits (ICs) over the past few decades have, for the most part, been achieved by increasing transistor speed, reducing transistor size, and packing more transistors onto a single chip (Fig. 5.1). Smaller transistors work faster, so ICs have become more rapid and more complex. An emerging factor that may disrupt this trend is the relatively slow speed of signal propagation within the chip. Signal delays caused by the interconnection wiring, increase with each generation of scaling and may soon limit the overall performance of the integrated system. New low dielectric interlayer materials ($\kappa < 2.0$) are needed to address the problems associated with power consumption, signal propagation delays, and crosstalk between interconnects in the next generation of integrated circuits. [1-3]

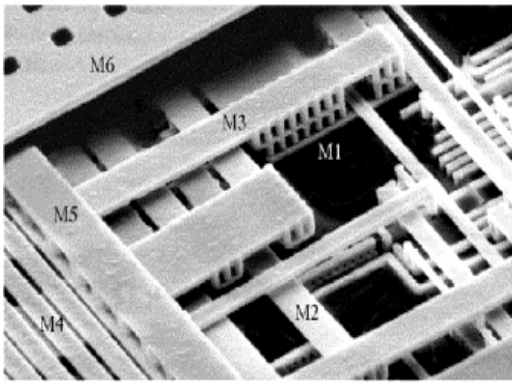

Fig. 5.1 Copper metallization on a microchip with 6metal layers

It is well known that only few fully dense materials have a dielectric constant as low as 2.5. One route to ultra-low-κ dielectric materials is the introduction of nanometre scale pores into a dense material to lower its effective dielectric constant. The earlier materials investigated for ultra-low-κ applications were silica aerogels and xerogels prepared by the sol-gel hydrolytic condensation of tetraethoxysilicate (TEOS) or tetramethoxysilicate (TMOS). [4] Solvent impregnated gel films can be extracted with supercritical fluids or by supercritical evaporation of the solvent, leaving a highly porous film with a dielectric constant in the range of 1.1-1.8. Unfortunately, the high porosity and concomitant low densities result in materials with poor mechanical properties unsuitable for the rigors of integration. As alternative, micro/mesoporous silica films with a well ordered pore structure have been developed by use of a surfactant templating process. For this type of porous films small pores

in the nanometre scale and κ values below 2.0 have been reported. [5-10] For safe integration in the real process the average pore size needs to be substantially smaller (at least ten times) than the minimum feature size in the IC. In other words, for the next generation ICs of the sub 65 nm node the pore size must be smaller than 5 nm. Further drawbacks of the silica films are that the porosity in these materials is open cell and is coupled with a hydrophilic nature of the material leading to moisture uptake and unsuitable mechanical properties.

Another approach to produce porous low κ dielectrics is based on creating voids into organic/inorganic polymers. General method to construct porosity is using the use of molecular templates which are frequently bound coordinatively to the polymer chains. After formation of the thin film the organic template is decomposed by thermal treatment to create porosity. Two classes of materials have been developed involving porous ultra-low-κ polymers. One of them are non-silicon containing polymers with the typical examples polyarylether (PAE), polyimide and SiLK™. [12-17] Secondly, polyhedral oligomeric silsesquioxane (POSS) with a three-dimensional network of non-polar Si-O-Si bonds is a good candidate for the preparation of such porous ultra-low-κ films. Most fully cured silsesquioxane derivates are thermally stable in excess of 400°C and intrinsically hydrophobic although their dielectric constant (κ = 2.5-3.0) [18-24] is not much lower than for SiO_2 (κ = 4.0). However, such porous materials have a dielectric constant κ in the range of 1.5-2.2 depending on pore size and porosity. In this approach, it is critical to completely remove the residual organic compounds and produce a uniform and, at the same time, closed pore system (pore size < 5 nm) in a controlled manner.

At the beginning of this project, we speculated whether a third approach exits, in which nanosized micro/mesoporous silica particles with a well ordered, uniform pore system can be incorporated into silsesquioxane polymers $[R_8Si_8O_{12}]_n$ as matrix to reduce the dielectric constant without adversely affecting the other material properties. As polymer matrix, octameric silsesquioxane $R_8Si_8O_{12}$ which consists of a rigid and cubic silica core with a nanopore of about 0.3 to 0.4 nm in the centre, [18] was chosen, as described in full detail in Chapter 2. The synthesis and characterization of nanoparticles of microcrystalline silicalite and mesoporous SBA-15 was discussed in Chapter 4. Here, we compare the results of characterization of all composite material.

5.2 Results and Discussion

The polymer $[((O)_{3/2}Si(CH_2)_2)_8Si_8O_{12}]_n$ was formed by polycondensation of $[(EtO)_3Si(CH_2)_2]_8Si_8O_{12}$ with water by splitting off ethanol. In the final material, the silsesquioxane cubes are connected with Si-O-Si bonds to construct a three-dimensional network with low density (ρ = 1.2 g/cm^3). It was found that this hydrophobic silsesquioxane polymer has a low dielectric constant of 2.4 and good quality during thermal and mechanical treatment. It is known that microporous silica (zeolites) and mesoporous silica can be prepared as thin films which also show low dielectric constant of 1.5-2.2, depending on their porosity. Due to the open pore system their mechanical strength is often low and, moreover, the films show hydrophilicity because of hydroxyl groups on the pore surface. However, if shaped as nanoparticles, the OH- groups on the surface of silica can be utilized for the condensation reaction with the ethoxysilyl group of the silsesquioxane.

Thus, we adopted a new approach by tethering the surface hydroxyl groups of microporous silicalite-1(2) and mesoporous SBA-15 to the side group of the silsesquioxane. In a second step, the polymer matrix was formed by connecting the remaining to ethoxysilyl groups to a three dimensional network encapsulating the nanoparticles. The composite films are easily processed using spin-coating techniques. The formation of new Si-O-Si bonds by condensation reaction between silsesquioxane and porous silica materials is shown in Scheme 5.1. However, the number of available surface -OH groups is limited, so that the density of silsesquioxane cubes in vicinity of the silica surface is much lower than in the polymer matrix itself. As a consequence, an area of reduced density around the particles can be distinguished in TEM of detached composite films (see Chapter 3).

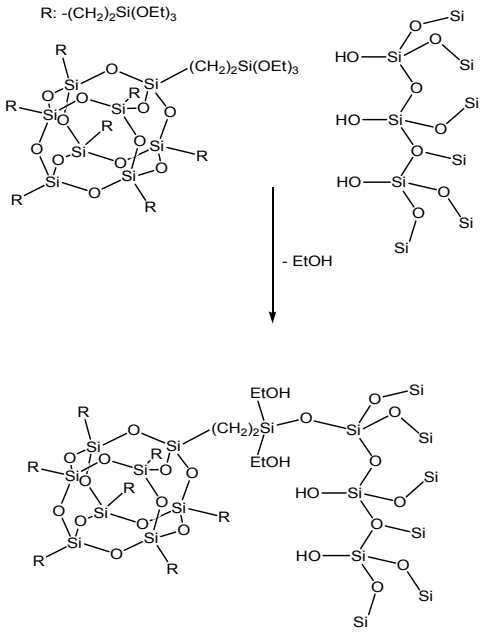

Scheme 5.1 Initial step of the polycondensation of silsesquioxane and silica surface

Table 5.1 summarizes the material properties of composite films containing different amounts (wt%) of silicalite-1, silicalite-2 and SBA-15 particles. The dielectric constant κ was calculated from the observed capacitance *c*, which was determined at a frequency of 1 MHz, according to $\kappa = c \ d / A \ \varepsilon_0$, where *d* the film thickness, *A* the area of the capacitor and ε_0 the free permittivity (see Chapter 2). The dielectric constant of the pure silsesquioxane polymer is related to the contents of micro/mesoporous nanoparticles in the composite films in Figure 5.2.

In general, the dielectric constant κ decreased with increasing concentration of nanoparticles in the film. Remarkably, when 28.8 wt% of silicalite-1 or silicalite-2 were introduced into the polymer the dielectric constant κ was reduced by ca. 12 % from 2.4 to 2.1. Upon further increase of the amount of nanoparticles in the composite film from 28.8 to 46.7 wt% the dielectric constant was reduced by another 9-10 %. For the composite film based on embedding of 501/2 even a reduction of the κ value by 12 % was observed. For all composite films with 60 wt% content of nanoparticles the dielectric constant decreased to 1.7 - 1.74. It should be noted, that for the initial reduction of κ from dense polymer to composite slightly more nanoparticles were needed than for the further decrease in the dielectric constant. The composite films containing 501/2 showed the lowest dielectric constant in comparison to the composite films with embedded silicalite 301/6, 601/1 and 802/1 (particle names and characterisation see Chapter 4b). This phenomenon can be

explained with the smallest particle size (16±1 nm), a narrow size distribution and the largest surface area (597 m^2/g) of the 502/1 sample in comparison to the other nanoparticles. In summary, an approximately linear relationship between the content of nanoparticles and the dielectric constant was found.

Table 5.1a. Characterization of composite films synthesised with the silsesquioxane monomer T_8^R, R = $-(CH_2)_2Si(OEt)_3$, and silicalite-1(2).

Dielectric material	Type of nanoparticles	Amount of nanoparticles (wt %)	Film thickness (nm)	Dielectric constant (κ)	Breakdown Voltage (MV/cm)	Hardness HU (GPa)
Silsesquioxane Polymer	-	0	480	2.4	0.38	0.51
	Silicalite-1					
Composite	301/6	28.8 46.7 59.9	670 750 820	2.12 1.94 1.74	0.36 0.32 0.29	0.36 0.29 0.21
Composite	502/1	29.0 46.9 60.1	285 256 340	2.09 1.85 1.70	0.35 0.32 0.30	0.40 0.31 0.18
Composite	601/1	28.8 46.4 60.1	400 640 530	2.10 1.90 1.70	0.35 0.30 0.28	0.37 0.29 0.18
	Silicalite-2					
Composite	802/1	28.8 46.4 60.1	350 390 460	2.13 1.92 1.72	0.37 0.35 0.30	0.38 0.26 0.23

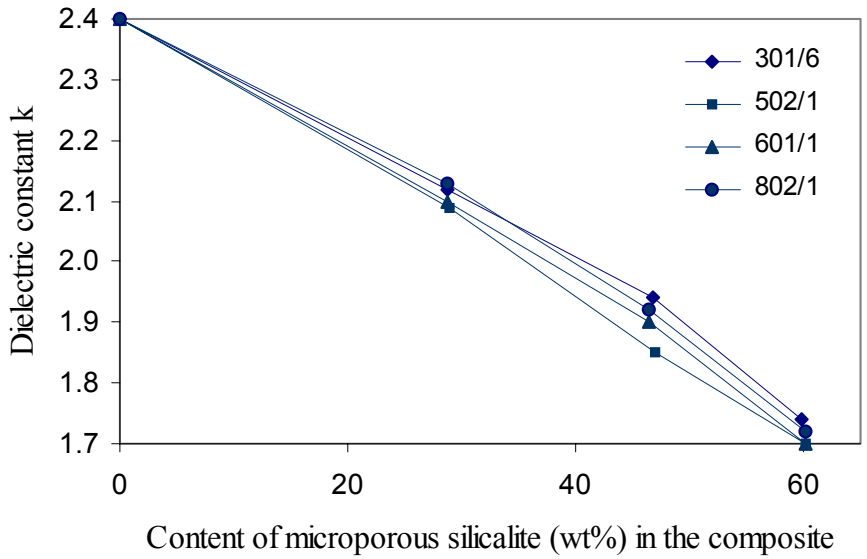

Fig. 5.2 a) Effect of silicalite-1(2) contents on the dielectric constant of composite films

For the composite films with mesoporous SBA-15 the same tendency was observed in electric characterization. With 28.8 wt% SBA-15 synthesized with different tribock copolymers ($EO_xPO_yEO_x$) the composite films showed a dielectric constant in the range of 2.01 - 2.07, which corresponds to a reduction of κ by 13.7 - 16.2% in comparison to the dense polymer with a κ value of 2.4. Increasing content of SBA-15 nanoparticles from 28.8 to 46.4 wt% led to a decrease in κ to 1.83 - 1.89, which corresponds to a reduction of ca. 9 % (Table 5.1 b). All composite films with 60.1 wt% SBA-15 nanoparticles showed dielectric constants between 1.62 - 1.68 which corresponds to a reduction of 11.5 %. The composite films with 902/1 SBA-15 nanoparticles have the lowest dielectric constant in this series of experiments. From the characterization of the SBA-15 nanoparticles (Chapter 4a), it is known that particles of 902/1 are very small and uniform (56±5 nm), and have a narrow particle size distribution and large surface area (730 m^2/g). As with silicalite, a roughly linear relationship between the weight content of nanoparticles and the dielectric constant of the composite was observed (Fig. 5.2 b).

Table 5.1 b. Characterization of composite films prepared with the silsesquioxane monomer (T_8^R, R = $-(CH_2)_2Si(OEt)_3$) and SBA-15

Dielectric material	Type of nanoparticles	Amount of nanoparticles (wt %)	Film thickness (nm)	Dielectric constant (κ)	Breakdown Voltage (MV/cm)	Hardness HU (GPa)
Silsesquioxane Polymer	-	0	480	2.4	0.38	0.51
	SBA-15					
Composite	702/2	28.8 46.2 60.1	480 390 420	2.07 1.89 1.68	0.40 0.34 0.32	0.37 0.34 0.31
Composite	702/3	28.8 46.4 60.1	590 480 520	2.02 1.84 1.64	0.35 0.33 0.29	0.38 0.35 0.32
Composite	902/1	28.8 46.4 60.1	640 550 620	2.01 1.83 1.62	0.34 0.29 0.26	0.33 0.30 0.27

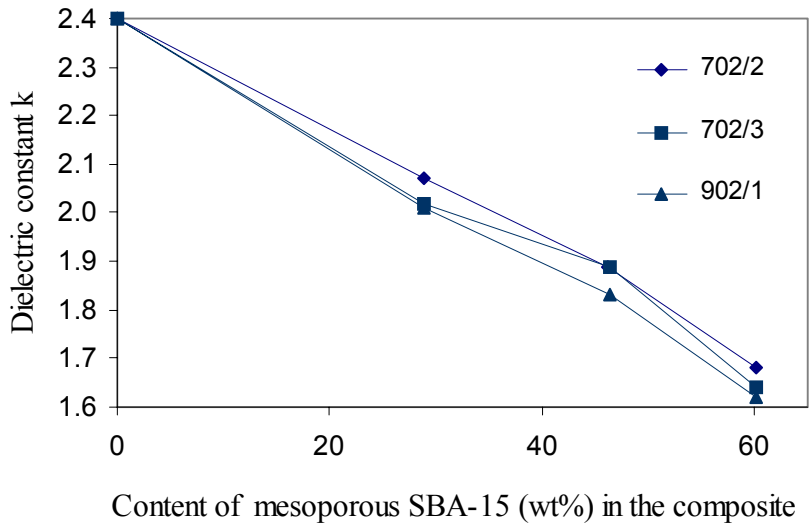

Fig. 5.2 b) Effect of the SBA-15 contents on the dielectric constant of composite films

Atomic force microscopy (AFM) images of the surface topography obtained for representative composite films with different concentration of nanoparticles are shown in Fig. 5.3. For comparison, an AFM image of the silsesquioxane polymer is also shown (Fig. 5.3a). The image of polymer shows a smooth and flat surface, whereas the surface of the composite films is slightly rough due to the agglomeration of the particles. This type of morphological difference may be also influenced by differences in the particle distribution of silicalite-1(2) (Fig. 5.3 b-d) and SBA-15 (Fig. 5.3 e,f) nanoparticles in the polymer matrices. The central position of 2D image (Fig. 5.3 c) was reconstructed as a 3D image (Fig 5.3 d). The 3D image shows that the nanoparticles were really embedded in the polymer surface.

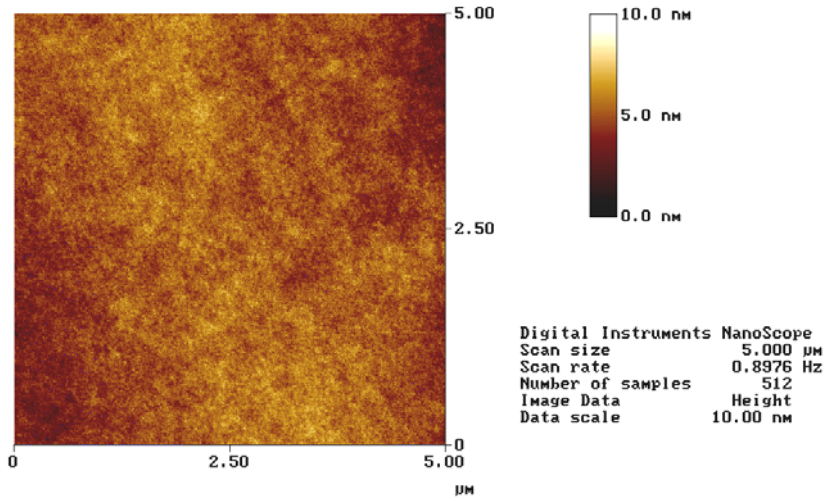

Fig. 5.3 a) AFM image of pure silsesquioxane polymer

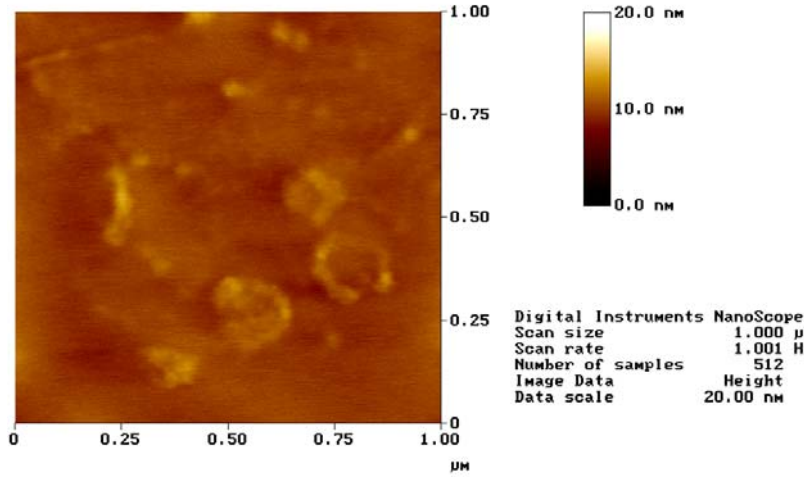

Fig. 5.3 b) AFM image of composite film using silicalite-1 301/6 with 46.7 wt%

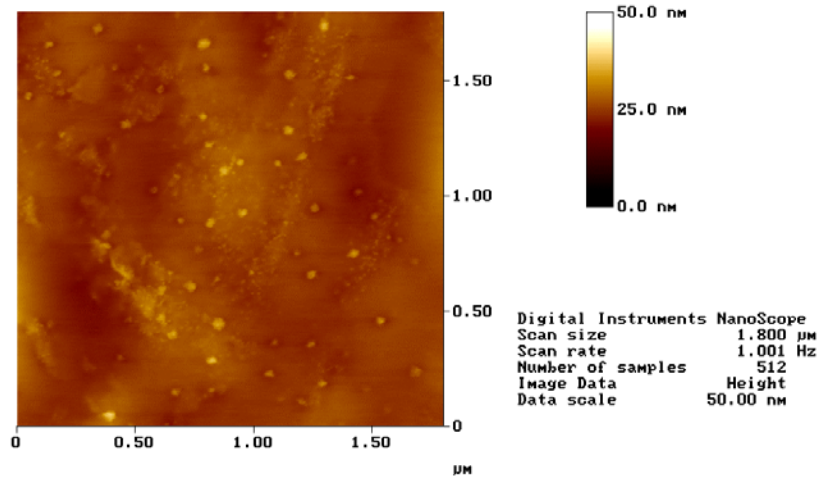

Fig. 5.2 c) AFM image of composite film using silicalite-1 601/1 in 28.8 wt%

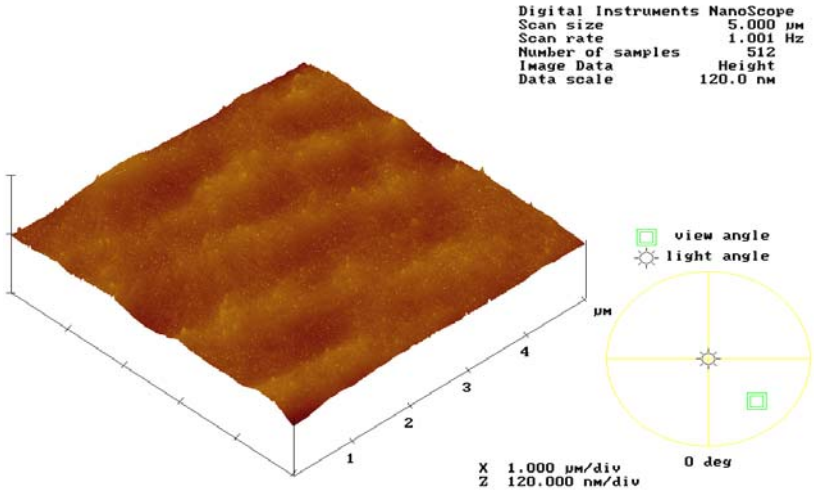

Fig. 5.3 d) 3D-AFM image of composite film with 28.8 wt% silicalite-1 601/1

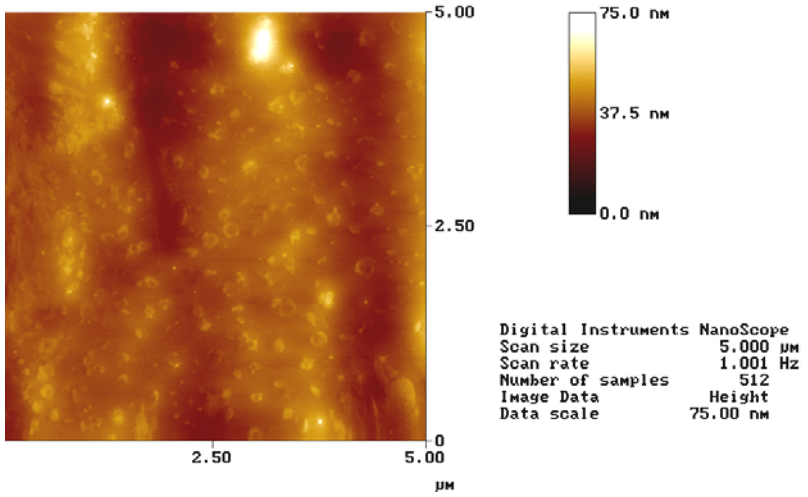

Fig. 5.3 e) AFM image of composite film with 60.1 wt% 702/2

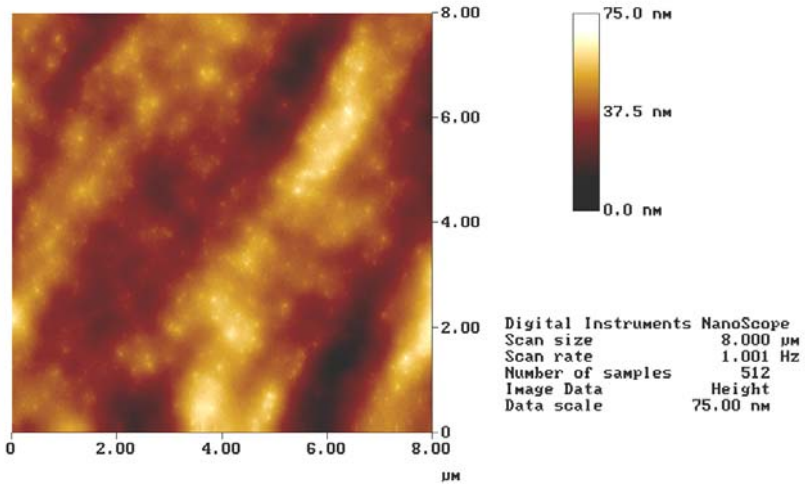

Fig. 5.3 f) AFM image of composite film with 46.4 wt%702/3

SEM micrographs of composite film surfaces are shown in Fig. 5.4. In a) the surface of the parent polymer film is presented; a smooth and homogenous surface with no voids is observed. The surface of a composite film with 60.1 wt% silcalite-1 301/6 shows domains of embedded 301/6 nanoparticles in the continuous polymer phase. The knot points can be accounted for by cross-linking between polymer side chains and porous silica.

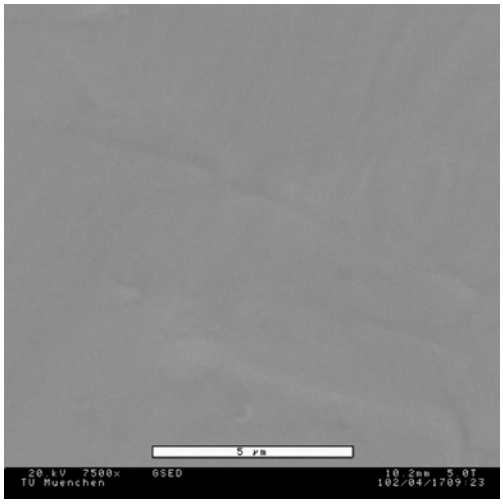

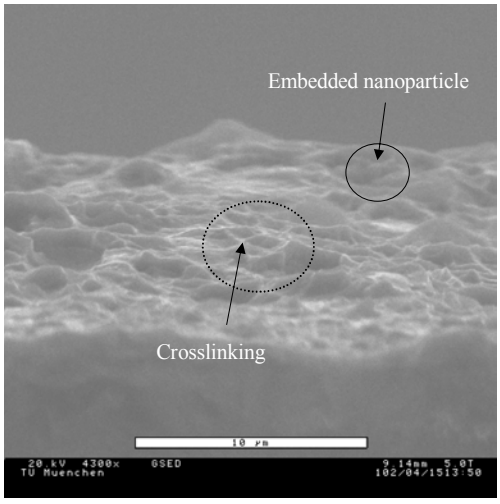

Fig. 5.4 a) SEM micrograph of the parent polymer b) Composite with 60.1 wt% sample 301/6

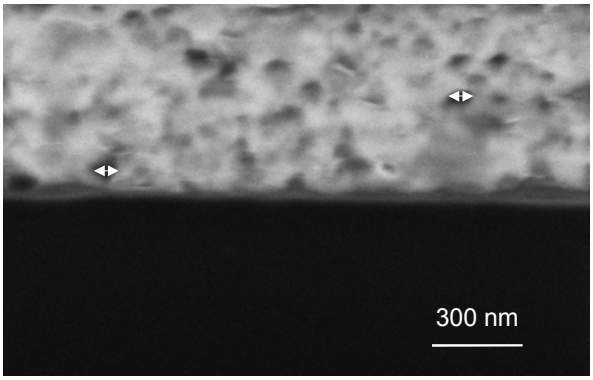

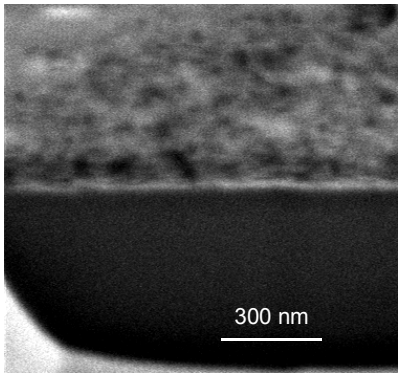

Fig. 5.4 c) Composite with 60.1 wt% 902/1 d) Composite with 60.1 wt% 601/1

The SEM image of a cross section of the composite films with 60.1 wt% 902/1 is shown in Fig. 5.4c. Clearly, apparently dark cluster with 55 nm diameter can be distinguished in conformance with the particle size of SBA-15 employed (see arrows). In the preparation of these samples, the film was cut with a heavy ion beam. The now open pore system makes the particles appear darker, as the electron beam is partially captured, whereas the beam is reflected well by the polymer. The silicalite-1 particles are also featured in the cross section of the composite film with 60.1 wt% 601/1 (Fig. 5.4 d).

A SEM micrograph of a 600 nm thick composite film with silicalite-1 in a low concentration is shown in Fig. 5.5a. Embedded particles which are close to the surface can clearly be distinguished. It is especially noteworthy that a dark circle can be distinguished around each particle. To study this phenomenon more closely, we decided to transfer thin films of the parent polymer and the composite to TEM grids.

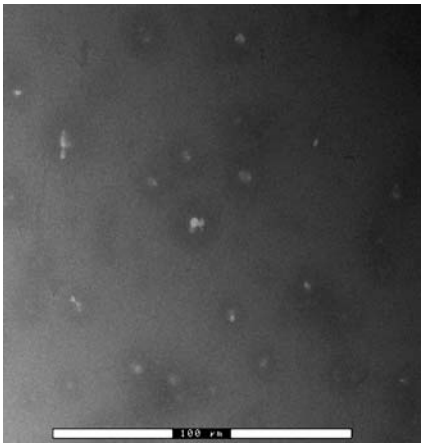

Fig. 5.5a) SEM micrograph of a composite with a low concentration of silicalite-1 particles (scale bar 100 μm).

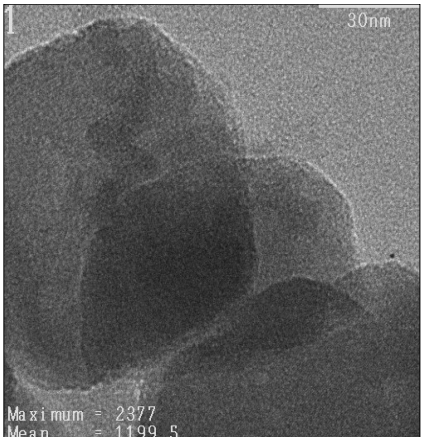

Fig. 5.5b) TEM micrograph of particles 301/6 used in the film shown on the left.

Analysis of the transmission electron microscopy images (Fig. 5.6) showed that the bulk structure of the parent polymer is homogeneous with no visible domains. In comparison, TEM of the composite showed that dark spherical objects with bright contour were distributed in the polymer matrix. The dark domains with 50 nm diameter can clearly be assigned to silicalite-1 nanoparticles. The bright contour with about 5 nm diameter is most likely an area of reduced density. This leads in TEM to a better transmission of electrons (bright contour) whereas fewer electrons are reflected in SEM (dark contour). It is speculated that the voids are generated in the composite because of the coordinative bond between the microporous nanoparticles and the polymer matrix. The locally disturbed structure of the polymer leads to additional porosity which lowers the dielectric constant with increasing content of nanoparticles in the polymer matrix. However, the SEM micrographs shown above indicate that the region of disturbed polymer structure extends far beyond the 5 nm range observed in TEM.

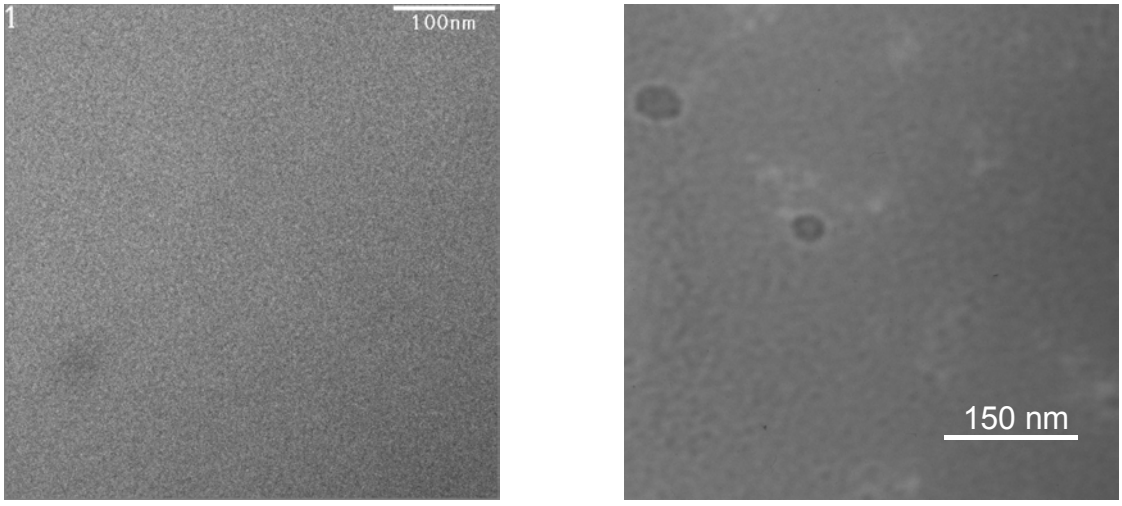

Fig. 5.6 TEM images of
a) the parent polymer film b) a composite film with 28.8 wt% 601/1

Additionally, porous materials provide a number of porosity specific integration challenges including chemical, mechanical, and electrical properties as well as thermal staff. To mitigate these issues, the porosity should be homogenously distributed and the pore size small with respect to the minimum device dimensions. Moreover, the interconnect structure for Cu metallization with porous low-κ materials is a great requirement in the integration process. Because Cu is difficult to mould by dry etching and also to improve the planarization of finished structures, the wiring in advanced multilevel metallization structures is fabricated by damascene technique. The damascene approach is schematically displayed in Figure 5.7. At first, a dielectric material is deposited onto the planarized substrate that is normally a multilevel metallization structure in the process. To from the metal (Cu) wiring in the dielectric, trenches are produced in the dielectric by lithographic patterning and plasma-etching techniques. The trenches are subsequently filled with the metal (Cu) and the wiring inside the dielectric is defined by removing the excess metal using chemical mechanical polishing (CMP). [25,26] Different wiring levels are connected vertically by metal studs (see Figure 5.8) A supplementary set of structural elements and processes are introduced, including the use of barrier layers for isolating Cu to prevent its diffusion into the interlayer dielectric, the capping and etchstop layer (SiN) to cover Cu lines after CMP. These impose stringent requirements on the material properties of the low-κ dielectrics.

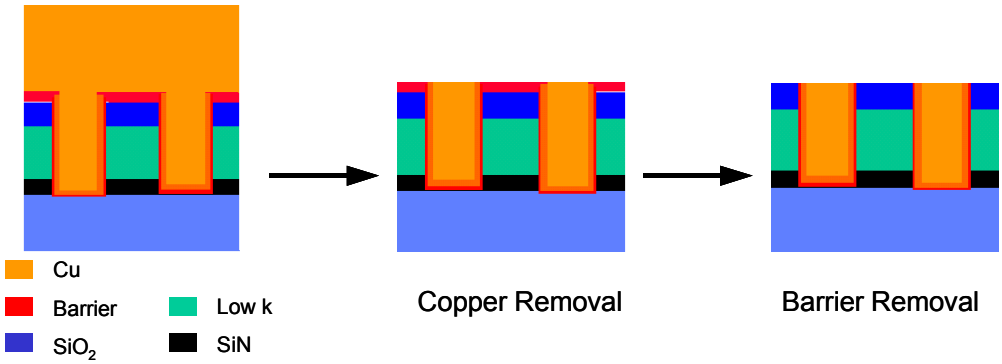

Figure 5.7 Scheme of the CMP process to make a damascene architecture

The dual damascene process combines the fabrication of metal wires and studs. [27] It is based on the repeated pattern transfer into the dielectric to produce the required trench and via structures prior to the metal deposition and CMP step (see Figure 5.9). There are two different approaches to produce aligned trenches and vias (openings) of an intermediate dual damascene structure prior to metal deposition. [28-30] In via-first approach the resist is patterned to produce vias in the trench and via-level dielectrics in one etching step, and stopping on a second Si_3N_4 stop layer on top of the Cu metallization. After stripping the via resist pattern, resist masking is applied for trench etching. Trenches are etched into the dielectric, stopping on the Si_3N_4 layer. The trench and the via layout need to be well aligned in this process. Alternatively, in the trench-first approach the resist is patterned to produce trenches in the trench-level dielectric. Etching is performed down to the Si_3N_4 etchstop layer. After stripping the trench resist pattern, resist masking is applied for via etching. Vias are etched into the via-level dielectric. The constraints in terms of the alignment of the trenches and vias are similar as for the via-first approach.

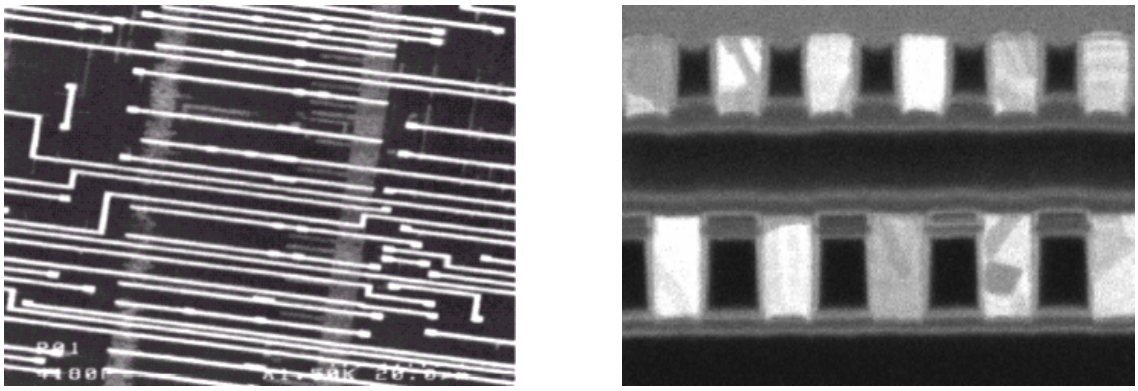

Figure 5.8 SEM (a) top view of a circuit at the second metal level; (b) cross section of M1 and M2

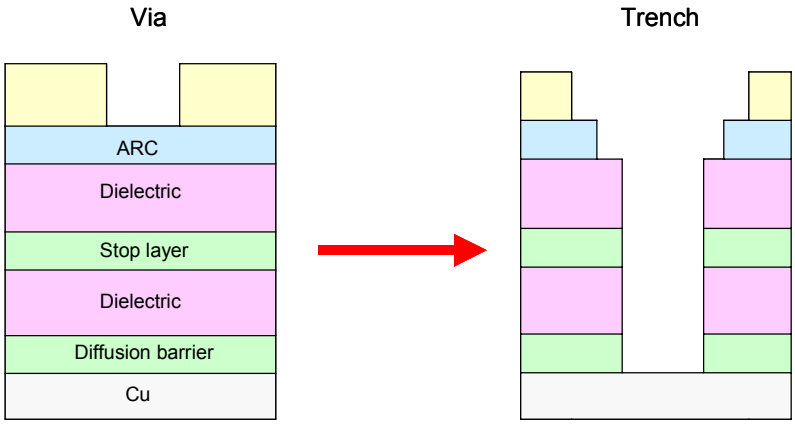

Fig. 5.9 Process for via-first dual damascene structure

Thus, CMP is part of a complex process. In our case, the experiments were not performed with damascene structures. Instead, polishing was carried out directly on flat film surfaces and with films which had been covered with a silver layer (Fig. 5.10).

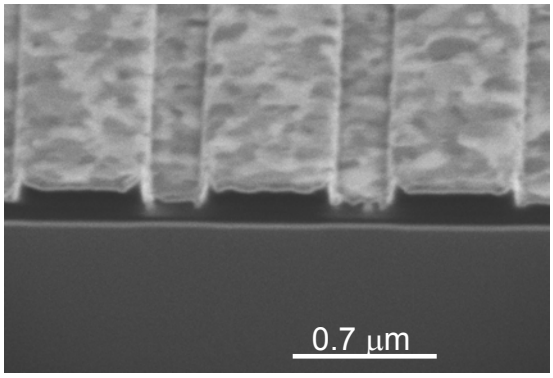

Fig. 5.10a Typical damascene structure

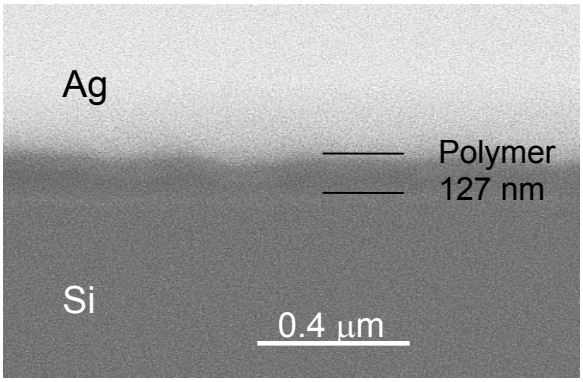

Fig. 5.10b Cross section of polymer with Ag top layer

It is generally accepted that polymers are soft, prone to scratching and structural damage due to deformation. Therefore a middle speed and low pressure were chosen throughout this experiment. Alkali-based slurry with polishing particles (CeO_2) smaller than 200 nm was used. After polishing for 5 min the polymer surface showed more roughness than the initial surface (Fig.5.11 a,b). In the middle, the film was slightly stronger polished than on the edge. It can be readily explained by abraded segments which were not immediately removed with the slurry and eroded the surface together with the polishing particles. In a second step a thin silver layer (100 nm) was sputtered on the polymer surface to investigate the adhesion between polymer and silver during the polishing process (Fig. 5.11 c-d). The images of Fig. 5.11 c-d show that after 5 minutes polishing the silver layer was not removed evenly. Also, the polymer film was not scoured. It can be suggested, that either, because of

the hardness of Ag, our polishing condition was too soft or the alkalinity of the slurry insufficient to chemically attack the silver film. On the other hand the adhesion between polymer and Ag layer also showed influence on the polishing process. The composite film based on silicalite-1 502/1 with 60.1 wt% was polished for 2 minutes under the same conditions as the polymer film. The homogenous distribution of nanoparticles in the composite surface before CMP can clearly be distinguished in the SEM micrographs (Fig. 5.11 e). After polishing all positions, where nanoparticles had been standing out before, were completely flattened. A smooth, although scratched, polymer matrix was observed as a homogenous layer. This clearly demonstrates that composite films can be planarized by CMP.

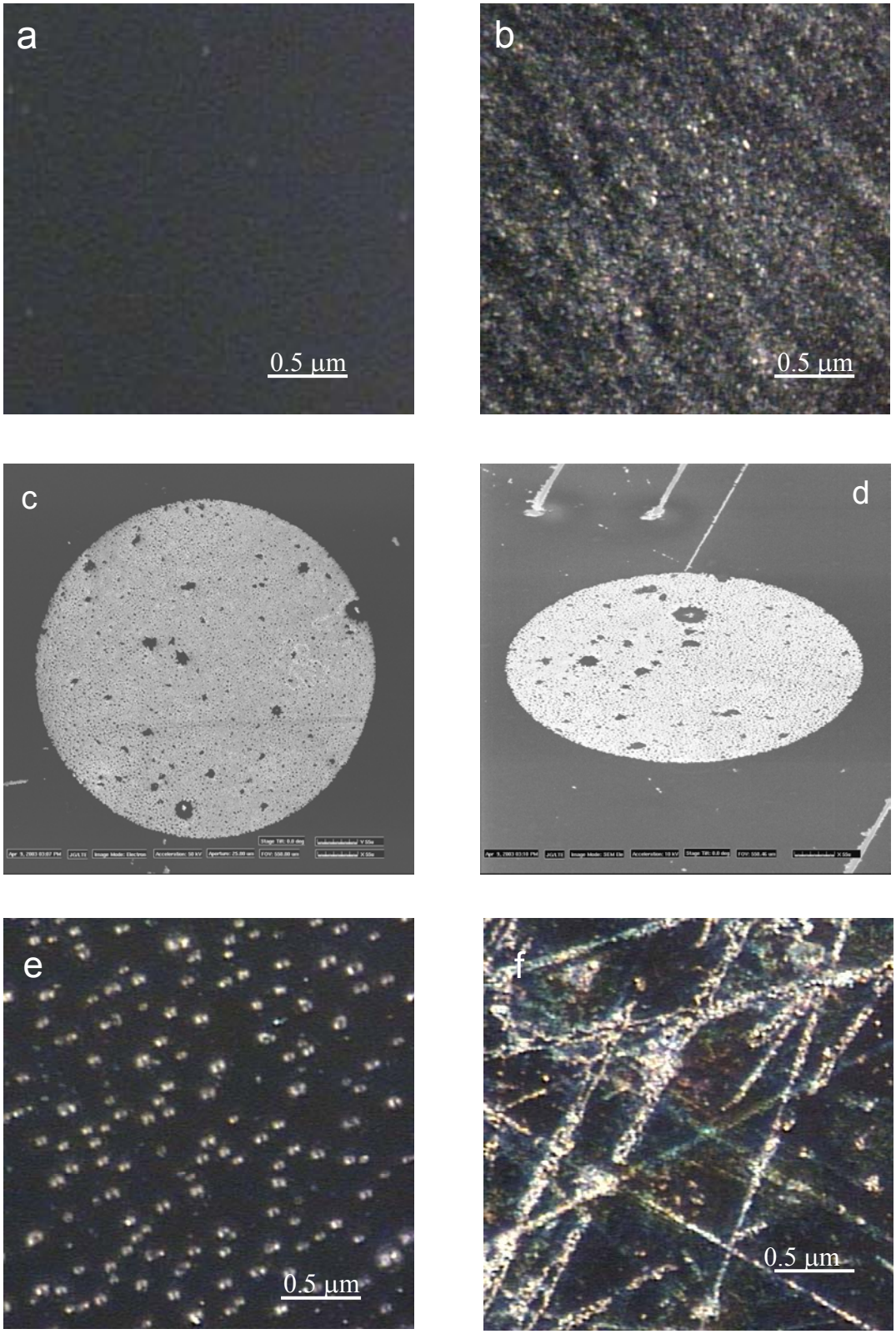

Fig. 5.11 Light micrographs a) polymer matrix before polishing, b) polymer surface after polishing; c)-d) polymer with 100 nm Ag layer after polishing; e) composite film before polishing; f) composite film after polishing

5.3 Experimental

Materials and techniques

Polymeric materials were prepared in an atmosphere of dry nitrogen using standard Schlenk techniques. Toluene (Aldrich, dry, ≤ 0.2% H_2O) was distilled from sodium under nitrogen. Triblock copolymers $EO_xPO_yEO_x$ and TEAOH were obtained from Aldrich and used as received. TEOS, HCl, H_3PO_4, H_2O_2, and Ethanol were purchased from Merck, TPAOH from Chempur and TBAOH from Lancaster. The preparation of the silsesquioxane polymers and the nanoparticles of mesoporous SBA-15, microcrystalline silicalite-1 and silicalite-2 are described in further detail in the Chapters 2 and 4.

General synthesis of silsesquioxane polymer

$[(EtO)_3Si(CH_2)_2]_8Si_8O_{12}$ was prepared by reacting of triethoxyvinylsilane and hydrido silsesquioxanes ($H_8Si_8O_{12}$) using platinum sponge as catalyst in toluene. After the reaction platinum was completely removed by filtration. Polycondensation of $[(EtO)_3Si(CH_2)_2]_8Si_8O_{12}$ occurred opening the flask and reaction with the moisture in air.

General synthesis of silicalite-1, silicalite-2 and SBA-15

Colloidal silicalite-1 was synthesized under mild hydrothermal conditions (100°C) from a clear TPAOH/TEAOH–H_2O–TEOS precursor sol. Silicalite-2 was prepared using a TBAOH–H_2O–TEOS precursor sol. After reaction the sample was washed with distilled water several times, freeze-dried and calcined at 550 °C.

In our preparation of SBA-15, tetraethyl orthosilicate (TEOS) as silicate source was added under stirring to a homogenous mixture of the triblock copolymer (see Chapter 4a), hydrochloric acid and distilled water. The resulting clear solution was heated to 100 °C for three days. After the reaction the surfactant templates were removed by calcination at 190°C or UV/O_3 (H_2O_2) treatment.

Preparation of composite films

A solution of $[(EtO)_3Si(CH_2)_2]_8Si_8O_{12}$ in toluene (30 cm^3) was mixed with a suspension of silicalite-1 in ethanol (10 cm^3) and heated to reflux (111°C) for 24 hours under nitrogen (quantities see Table 1 and 2). The flask was then opened to ambient air and stirred for another 2 h allowing the monomer to react with moisture at the room temperature. Partial removal of the solvent provided a viscous gel. Prior to their use Steel plates and Si-wavers

were first placed in a toluene solution for 10 minutes, rinsed with distilled water and dried. Coating films were prepared by spin coating the viscous gel on the steel plates using a RC Spin Coater CT 62C101 (Karl Suss France S. A.). All thin films were spin coated at a speed of 2500 - 3500 rpm for 10-15 seconds. Subsequently, the film was heated at 130°C for 120 min in air to remove any residual solvent.

CMP experiment

CMP experiments were carried out on a custom build polisher (Lehrstuhl für Technische Elektronik) as shown in the Scheme in Figure 5.12. The polymer or composite film was prepared on 1×1 cm silicon wafer as described above and placed in the sample holder. A "DD-Dac" pad with adhesive back was used as polishing pad. The slurry used for this test was SF1 alkali solution (Logitech Materials & Engineer) containing polishing particles smaller than 200 nm and was diluted 1:1 with distilled water. The slurry was dispensed at a rate of 50 ml/min. A medium speed and low pressure were used throughout this experiment. The down force pressure was set to 5 N. Wafer carrier and platens were both rotated at 30 rpm during the polishing. The polishing time was varied between 2-5 minutes. All wafers were cleaned using distilled water and dried under flowing N_2.

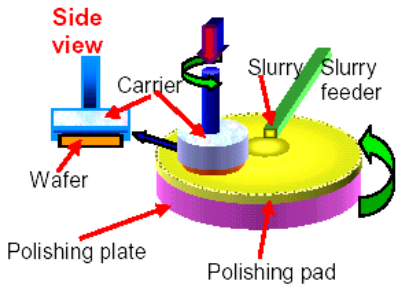

Fig. 5.12 Scheme of CMP processing

Characterization

The electric capacitance was voltage measured with a HP 4284 A Precision LCR Meter at 1 MHz frequency. The breakdown was measured on the same sample with a Brandburg PS 1008 for high Voltage Unit. The thickness of the composite films was subsequently measured with electron microscopy (SEM, JSM – 5900) after cutting the plate. The hardness of the coating films was determined with a Fischerscope H - 100 interfaced with a PC using Win - HCU software to collect the data. The morphology of the film with embedded nanoparticles was studied by TEM (JEOL 2010) and Atomic Force Microscopy AMF (Multi Mode™ Digital Instruments, Incorporated), respectively.

5.4 Conclusions

This chapter provides an overview on the new composite material prepared by us on the basis of embedded micro/mesoporous silica nanoparticles (silicalite-1, silicalite-2 and SBA-15) in silsesquioxane polymer matrices $([(O)_{3/2}Si(CH_2)_2]_8Si_8O_{12})_n$. A chemical connection between nanoparticles and silsesquioxane was obtained by condensation of hydroxyl groups on the silica surface with ethoxysilyl side groups of the silsesquioxane. In a second step, the polymer matrix was formed by condensation with added water. The physical and electric properties of thin films were characterised and the film morphology was studied in detail. In a series of composite films using silicalite-1 and silicalite-2 it was observed, that increasing contents of nanoparticles led to reduction of the dielectric constant. The composite films with 502/1 had a slightly lower dielectric constant (κ = 1.70 - 2.09) in comparison with composite films which were obtained with other silicalite nanoparticles. It can be suggested that the uniform small particles size of 16 nm and the large surface area of 597 m^2/g account for this observation. The same tendency was also found in the series of composite films with mesoporous SBA-15 nanoparticles. Here, the composite with sample 902/1 (56±5nm, 730 m^2/g) showed the lowest dielectric constant in the range of 1.62 to 2.01. Due to a large surface area and larger pore size the composite films using SBA-15 generally showed lower κ values than those using silicalite-1 or silicalite-2. It became also clear that properties like breakdown voltage and hardness were little affected by the increasing porosity of the composite materials.

Further we have tested integration of composite films in the most important integration process, chemical mechanical polishing (CMP). The experiment was carried out directly on a homogeneous film surface without underlying structures. After CMP, the pure polymer matrices showed an evenly polished surface, whereas the composite surface was rather rough because of complete removal of nanoparticles. Obviously, the polishing conditions were not sufficiently optimised for the combination of a composite having a soft polymer matrix with relatively hard nanoparticles and need to be optimised in further work.

5.5 References

[1] M. Fayolle, G. Passemard, O. Louveau, F. Fusalbal and J. Cluzel, *Microelectr. Engineering*, **2003**, *70*, 255.

[2] K. Mosig, T. Jacobs, K. Brennab, M. Rasco and R. Augur, *Microelectr. Engineering*, **2002**, *64*, 11.

[3] H. Treichel, G. Ruhl, P. Ansmann, R. Würl, C. Müller and M. Dietlmeier, *Microelectr. Engineering*, **1998**, *40*, 1.

[4] a) L. Hrubesh, F. Stucki, T. BaumannL. Niemayer, R.Strümpler, B. Zeigler and M. Mielke, *Appl. Phys. A*. **1993**, *57*, 329.

b) N. Hüsing and U. Schubert, *Angew. Chem. Int. Ed*., **1998**, *37*, 22.

c) C.J. Brinker and G.W. Scherer, *Sol-Gel Science: The Phyics and Chemistry of Sol-Gel Processing*, **1990**, Academic Press, San Diego.

[5] S. Baskaran, J. Liu, K. Domansky, N. Kohle, X. Li, G. Fryxell, S. Thevuthasan and R.E. Williford, *Adv. Mater*., **2000**, *12*, 291.

[6] Y.F. Lu, H.Y. Fan, D. Loy, R. Assink, D. LaVan and C.J. Brinker, *J. Am. Chem. Soc*., **2000**, *122*, 5258.

[7] G. Wirnsberger, P. Yang, B.J. Scott, B. Chmelka and G. Stucky, *Spectrochim Acta A*, **2001**, *57*, 2049.

[8] S. Seraj, Y. Wu, M. Forbess, S.J. Limmer, T. Chou and G.Z. Cao, *Adv. Mater*. **2000**, *12(22)*, 1695.

[9] S. Baskaran, J. Liu, K. Domansky N. Kohle, C. Coyle, S. Thevuthasan and R.E. Williford, *Adv. Mater*. **2000**, *12(4)*, 291.

[10] P. Liu, T.C. Chang, K.C. Hsu, T.Y. Tseng, L.M. Chen, C.J. Wang and S.M. Sze, *Thin Solid Films*, **2002**, *414*, 1.

[11] J. Wang, H.K. Kim, F.G. Shi, B. Zhao and T.G. Nieh. *Thin Solid Films*, **2000**, *377–378*, 413.

[12] S. Lu and K. Zeng, *Microelectr. Engineering*, **2004**, *71/2*, 221.

[13] L.H. Chang and N.C. Saha, *Thin Solid Films,* **1994**, *253(1-2)*, 430.

[14] X. Zhang, S. Dabral, C. Chiang, J. F. McDonald and B. Wang, *Thin Solid Films,* **1995**, *270(1-2*), 508.

[15] H. Treichel, G. Ruhl, P. Ansmann, R. Würl, C. Müller and M. Dietlmeier, *Microelectr. Engineering,* **1998**, *40*, 1.

[16] C. Maisonobe, G. Passemard, C. Lacour, Lecornec, P. Motte, P. Noël and J. Torres, *Microelectronic Engineering,* **2000**, *50*, 25.

[17] K. Ishizu, K. Toyoda, T. Furukawa and S. Uchida, *J. Colloid Interface Sci,* **2003**, *261(2)*, 552.

[18] C. Zhang, F.Babonneau, C. Bonhomme, R.M. Laine, C. L.Soles, H.H. Aristov and A. F. Yee, *J. Am. Chem. Soc.* **199**8, *12*0, 8380.

[19] R. D. Miller, J. L. Hedrick, D. Y. Yoon, R. F. Cook, J. P. Hummel, *MRS Bulletin* **1997**, *22*, 44.

[20] C. Nguyen, C. J. Hawker, R. D.Miller, E. Huang, J. L. Hedrick, R. Gauderon, J.G. Hilborn, *Macromolecules* **2000**, *33*, 4281.

[21] C. J. Hawker, A. W. Bosman, E. Harth, *Chem. Rev.* **2001**, *101*, 3661.

[22] T. C. Chung, P. T. Liu, Y. S. Mor, S. M. Sze, Y. L. Yang, M. S. Feng, F. M. Pan, B. T. Dai, and C. Y. Chang, *J. Electrochem. Soc.,* **1999,** *146*, 3802.

[23] A. Grill and V. Patel, *Appl. Phys. Lett.,* **2001**, *79*, 803.

[24] S. Yang, P.A. Mirau, C. Pai, Omkaram Nalamasu, Elsa Reichmanis, Janice C. Pai, Yaw S. Obeng, Joko Seputro, Eric K. Lin, Hae-Jeong Lee, Jianing Sun, and David W. Gidley, *Chem. Mater*.; **2002;** *14(1)*, 369.

[25] D.T. Price, R.J. Gutman and S.P. Murarka, Thin solid film, 1997, 308-309, 523.

[26] Y. Morand, *Microelectronic Engineering,* **2000**, *50*, 391.

[27] P. Singer, Semicond. Int., **1999**, *22(9)*, 68.

[28] C. Maddalon, K. Barla, E. Denis, E. Lous, E. Perrin, S. Lis, C. Lair and E. Dehan, *Microelectronic Engineering,* **2000**, *50(1-4)*, 33.

[29] T. C. Chang, T. M. Tsai, P. T. Liu, C. W. Chen, S. T. Yan, H. Aoki, Y. C. Chang and T. Y. Tseng, *Thin Solid Films,* 2004, *447-448*, 524.

[30] F. Küchenmeister, U. Schubert and C. Wenzel, *Microelectronic Engineering,* **2000**, *50 (1-4)*, 47.

Chapter 6

Summary

In this chapter, the general summary of this thesis is presented.

Summary

Integrated circuits (IC) have achieved progressively higher device densities and speeds over the past 30 years, which Moore's Law predicts as a doubling in device density every 18 months. As transistors shrink and the total amount of interconnect wiring increases, delays in that wiring are more and more important to circuit performance. The need to reduce the RC delay has driven both the introduction of copper wiring and the transition to dielectrics lower than silicon dioxide (SiO_2). The SiO_2 interlayer dielectric is being replaced by new low κ spin-on or vapour-deposited silicate or organic materials. These materials will need to become porous to achieve the continued reductions in κ as the roadmap progresses. The development of these new materials and processes and their integration into semiconductor chip fabrication represents a large opportunity for nanoscale structures. At this time, there is intensive effort in the industry to develop Cu / low–κ interconnect with porous dielectric with κ<2.2. While the need for low–κ dielectrics for improving the performance and density of advanced interconnects is essential, the progress in implementation of low–κ materials has been slower than anticipated. To meet the requirements of the semiconductor manufacturers, especially for high-speed devices, the implementation of copper as interconnect in conjunction with the ultra low–κ as interlevel dielectrics (ILDs) in the fabrication of microelectronic devices has been a main stream topic of research in the semiconductor community worldwide.

Finding a porous ultra low–κ material that simultaneously meets the electric, mechanical, chemical and thermal requirements is not easy. Thermal properties of the dielectric are of particular importance and they must be consistent with subsequent processing temperatures and thermal conductivity requirements for heat transfer in a chip. The dielectrics should be able to withstand repeated temperature cycling to high temperatures, preferably up to 450°C, without appreciable weight loss and shrinkage. High thermal conductivity is required, since shrinking feature dimension will lead to increased current densities and higher temperatures of operation. Good adhesion, low stress, high hardness and low surface roughness are other important mechanical requirements. For integration of the low–κ materials in a real process, high aspect ratio (height/width) structures will be required. Dual damascene processes, in conjunction with copper metallization, involve etching a pattern in the dielectric, blanket deposition of copper and subsequent planarization by chemical mechanical polishing

(CMP). This imposes considerable external forces that the multilayer structure must sustain. Therefore, the ILD must be compatible with copper CMP.

In this thesis we present a two-step concept to evolve porous material with ultra-low dielectric constant. Firstly a series of non-polar matrices were synthesized based on silsesquioxanes. Latter have the empirical formula $R_8Si_8O_{12}$, where R is alkyl, alkylene, aryl, arylene, or corresponding organo-functional derivates. On account of a well defined three-dimensional network the new silsesquioxane polymers promised good mechanical strength, high thermal stability and lower dielectric constant κ. It is well known that air gaps have the lowest κ value at close to 1. Thus, further reduction in dielectric constant can be obtained by incorporating the preformed, uniform nanopore system of nanocrystalline silicalite and mesoporous SBA-15 into these polymer matrices to introduce material porosity without detrimentally affecting the other material properties.

In Chapter 2 we have reported that new silsesquioxane polymers can be formed from sol-gel polymerisation using cubic $R_8Si_8O_{12}$ octamers with 4, 4' cage structure. Important synthetic goals are the controlled catalytic hydrosilylation of $H_8Si_8O_{12}$, T_8^H, $(HSiMe_2O)_8Si_8O_{12}$, $Q_8M_8^H$ with 1,5-hexadiene and hydrolytic condensation of monomers, such as $[(EtO)_3Si(CH_2)_2]_8Si_8O_{12}$, T_8^R and $[(EtO)_3Si(CH_2)_2SiMe_2O]_8Si_8O_{12}$, $Q_8M_8^R$ in a clean chemical reaction, which gives few side products and occurs under mild reaction conditions, i.e., at room temperature. The silsesquioxane polymer films were prepared using spin coating techniques. The material properties of the coating films were fully characterised including chemical composition, film thickness, dielectric constant κ, adhesion, hardness, breakdown voltage, morphology and thermal stability. Chemical properties were analysed by EA, IR and NMR. The result of dielectric measurement showed that the dielectric constant κ of the polymer films was between 2.1 - 2.7 which was low compared to literature data, where values in the range of 3.0-3.7 are typically reported. The breakdown voltage and hardness measurement suggest that these physical properties of films are closely associated with the length of the chain between the silsesquioxane cubes, i.e., a long linker between the silsesquioxane cubes led to an increase in these properties. The thickness of polymer films was uniform and in a narrow range between 22 - 28 μm. To test the adhesion of the film to the substrate, a cross cutting test was carried out and all polymer films showed excellent quality in this test. The film morphology was studied using scanning electron microscopy (SEM) and all polymer films were planar and flat. Thermal analysis (TGA/DSC) indicated that the new polymer materials were thermally stable to at least 400 °C.

Chapter 3 dealt with a new approach to prepare ultra-low-κ porous material based on organic/inorganic hybrid silsesquioxane polymers $([(EtO)_3Si(CH_2)_2]_8Si_8O_{12})_n$ and micro-crystalline nanoparticles of silicalite-1. In order to reduce the κ value relative to that of SiO_2, it was necessary either to incorporate atoms and chemical bonds that have a lower polarizability, or else to lower the atom density in the material, or both. Our silsesquioxane polymers had a dielectric constant between 2.1-2.7 which was increasing with the length of the alkyl chains that connect the silsesquioxane cages. Moreover, the material density of the polymer was very low (ρ=1.2 g/cm^3). To obtain a dielectric material with κ value smaller than 2.0 it could only be managed with adding porosity in the dense matrices. Silicalite-1 is a aluminium-free zeolite of the MFI type with uniform molecular pores of 5.5-6.5 Å. The as-synthesized silicalite-1 with particle size of 50 nm has large BET surface area of 568 m^2/g. The composite material was prepared by polycondensation of surface hydroxyl groups with ethoxysilyl side groups of silsesquioxane in a sol-gel process. The composite films could be formed easily using spin-coating techniques. The results of characterization showed, that the nanoporous composite films had κ values in the range of 2.1 - 1.7 which is much lower than that of the corresponding polymer film (κ = 2.4). Increasing amount of silicalite-1 in the composite films led to decrease of the dielectric constant, as the material density concurrently decreased to between 1.06 and 0.83 g/cm^3. Because of the very high thermal stability of silicalite-1 (up to 800 °C) the composite films with embedded silicalite-1 particles in the silsesquioxane polymer matrices show also good stability, although other material properties like mechanical strength and breakdown voltage were affected on account of the increased porosity.

In Chapter 4 nanoparticles of silicalite-1, silicalite-2 and SBA-15 were characterized in detail. Colloidal silicalite-1 with MFI framework topologies is typically synthesized under mild conditions at 100°C using a precusor sol of template-H_2O-silica source. Tetraethylorthosilicate (TEOS) was used as silica source. As surfactant templates we have chosen (1) tetrapropyl ammonium hydroxide (TPAOH) with the molar composition 9 TPAOH : 25 SiO_2 : 425 H_2O : 100 EtOH and (2) tetraethylammonium hydroxide (TEAOH) with PO_4^{3-} as promoter. In this case, the composition of the reaction mixture was 9 TEAOH : 11.5 SiO_2 : 1.3 P_2O_5 : 414 H_2O : 46 EtOH. Colloidal silicalite-2 (MEL type) was prepared in the presence of a binary mixture of templates containing TBAOH and TEAOH with the molar composition 9 TBAOH : 76.5 SiO_2 : 22.5 TEAOH : 630 H_2O : 306 EtOH. The silicalite-1, silicalite-2 nanoparticles obtained were characterized with XRD, N_2 adsorption, SEM and TEM. The silicalite-1 sample 501/2, obtained with the TEOS-TPAOH-H_2O system, had the

smallest particle size (16 nm from DLS). Sample 601/1 prepared with the TEAOH-H_2O system with added PO_3^{4-} had also a very small particle size of 15-50 nm. Silicalite-2 sample 802/1 had a particle size between 25 and 65 nm. Additionally all calcined samples of silicalite-1 and silicalite-2 showed a very high BET surface area.

Well-ordered mesoporous silica structures of SBA-15 were synthesized using a templating scheme where an aqueous acidic solution (HCl) containing the amphiphilic triblock copolymer $EO_xPO_yEO_x$ (TCP) is reacted with tetraethoxysilicate (TEOS) as silicate source. The reactions were carried out at two pH values of 0.6 and 0.9 using TCPs with different EO/PO ratios. It was observed that TCP 2 (EO/PO ratio of 0.6) and TCP 3 (EO/PO ratio of 1.4) resulted in the formation of hexagonal structures whereas the use of TCP 1 with a larger EO/PO ratio (5.3) favored the formation of a cubic structure. The particle size formed at two different pH values was in the same range for TCP 1 and TCP 3 as template, while with TCP 2 the particle size was relatively larger at pH = 0.6 than at pH = 0.9. The sample 901/2 prepared with TCP1 showed the smallest particle size (56 ± 5 nm) and a narrow size distribution. As the TCP are oxidized easily, as-synthesized SBA-15 samples can be calcined only at 190°C to remove the template. However, even at this low temperature the particles had a tendency to agglomerate. To provide efficient alternatives for removing the surfactant template, mild oxidation methods employing UV-light to generate O_3 from O_2 or $OH^{\bullet}$ radicals from H_2O_2 were investigated. The main advantage of the UV-treatment with O_3 and $OH^{\bullet}$ radicals is the non-thermal processing. While solid samples are required for calcination and UV/O_3 treatment, the UV/H_2O_2 treatment was carried out in aqueous suspension. The EA analysis showed that UV/H_2O_2 was the most effective method to remove TCP template in comparison. It was also observed that UV treated samples have a larger BET surface area than calcined samples. In particular, the pore size of the UV/H_2O_2 treated samples was considerably larger than that of the calcined and UV/O_3 treated samples.

In Chapter 5 the work was focused on characterization of low-κ composite films which were prepared by embedding nanoparticles of microcrystalline silicalite-1(2) or mesoporous SBA-15 in silsesquioxane polymer matrices. Due to outstanding characteristics, such as thermal stability, strong hydrophobicity as well as low dielectric constant ($\kappa = 2.4$), the silsesquioxane polymer $([(O)_{3/2}Si(CH_2)_2]_8Si_8O_{12})_n$ was chosen as matrix. Composite films were prepared in a two-step process. First, the surface hydroxyl groups of microporous silicalite-1(2) and mesoporous SBA-15 were linked with the side groups of the monomer $[(EtO)_3Si(CH_2)_2]_8Si_8O_{12}$. In a second step, the remaining ethoxysilyl groups of the monomer were polycondensed with water to give a highly viscous suspension, which was used for spin

coating. Characterization of the composite films showed that reduction of the dielectric constant correlated almost linearly with the increasing content of nanoparticles in the polymer matrix. Particle size and surface area have some influence on the dielectric constant. The composite films with silicalite-1 sample 502/1 have the lowest dielectric constant in the range of 1.70 – 2.09. In comparison with other embedded silcalite-1(2) particles (301/6, 601/1 and 802/1) the particle size of 502/1 was very uniform and small (16 nm) with a large surface area of 597 m^2/g. The same tendency was also observed for the series of composite films with mesoporous SBA-15 nanoparticles. The composite films with the SBA-15 sample 902/1 had κ values between 1.62 and 2.01, which is lower than of films that with embedded samples 702/2 and 702/3. In comparison, the sample 902/1 had the smallest particle size (56 ± 5 nm) and the largest surface area of 735 m^2/g. Generally, the dielectric constant of composite films with embedded SBA-15 was lower than with the same weight content of silicalite-1(2) nanoparticles. The reason was probably the larger surface area and lower density of SBA-15. Further, we have tested integration of composite films in the most important process of microchip fabrication, chemical mechanical polishing (CMP). The experiments were carried out directly on polymer (composite) film surfaces without underlying structures. After CMP, the pure polymer films showed an evenly polished surface, whereas the composite surface was rather rough because of complete removal of nanoparticles. Obviously, the polishing conditions were not suitable for the combination of a soft polymer matrix with relatively hard nanoparticles. The conditions for CMP need to be optimised in further work.

In summary, we have developed a new, chemically well-defined, polymer for application as low-κ material in the semiconductor industry. The properties can be modified and significantly improved by embedding porous nanoparticles in the polymer matrix. The composite materials have not only an ultra-low dielectric constant, but also can be readily spin coated as thin films as required in the fabrication of integrated microchips.